

2005

An investigation of the thread and under-head coefficients of friction on clamp-load in the bolted joint

Michael P. Oliver
University of Dayton

Follow this and additional works at: https://ecommons.udayton.edu/graduate_theses

Recommended Citation

Oliver, Michael P., "An investigation of the thread and under-head coefficients of friction on clamp-load in the bolted joint" (2005). *Graduate Theses and Dissertations*. 4752.
https://ecommons.udayton.edu/graduate_theses/4752

This Dissertation is brought to you for free and open access by the Theses and Dissertations at eCommons. It has been accepted for inclusion in Graduate Theses and Dissertations by an authorized administrator of eCommons. For more information, please contact mschlange1@udayton.edu, ecommons@udayton.edu.

**AN INVESTIGATION OF THE THREAD AND UNDER-HEAD
COEFFICIENTS OF FRICTION
ON CLAMP-LOAD IN THE BOLTED JOINT**

A Dissertation

Submitted to

The School of Engineering

UNIVERSITY OF DAYTON

In Partial Fulfillment of the Requirements for

the Degree of

Doctor of Philosophy in Mechanical Engineering

by

Michael P. Oliver

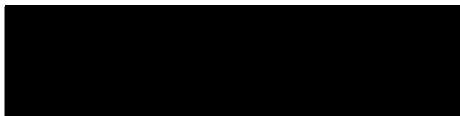
UNIVERSITY OF DAYTON

Dayton, Ohio

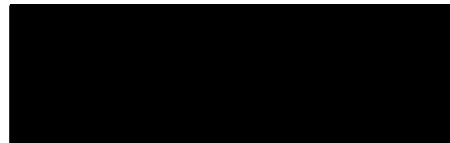
December 2005

AN INVESTIGATION OF THE THREAD AND UNDER-HEAD COEFFICIENTS OF FRICTION ON CLAMP-LOAD IN THE BOLTED JOINT

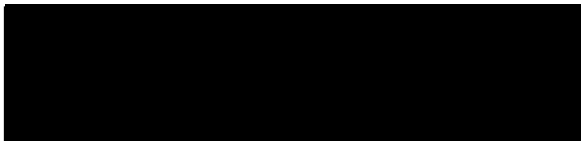
APPROVED BY:



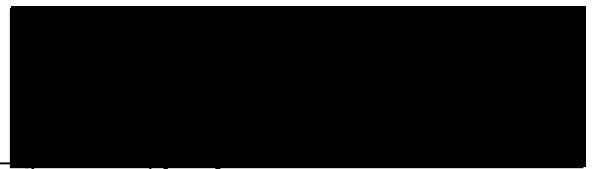
Vinod K. Jain, Ph.D.
Advisory Committee Chairman
Professor, Mechanical and Aerospace
Engineering Department



Shankar Mall, Ph.D.
Committee Member
Professor, Department of Aeronautic
and Astronautic, Air Force Institute
of Technology



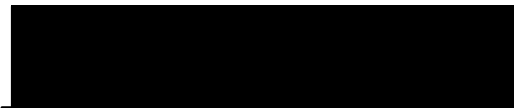
Reza Kashani, Ph.D.
Committee Member
Associate Professor, Mechanical and
Aerospace Engineering Department



Gerald J. Shaughnessy
Committee Member
Associate Professor, Mathematics
Department, College of Arts and
Science



Donald L. Moon, Ph.D.
Associate Dean
Graduate Engineering Programs and
Research, School of Engineering



Joseph E. Saliba, Ph.D., P.E.
Dean
School of Engineering

ABSTRACT

AN INVESTIGATION OF THE THREAD AND UNDER-HEAD COEFFICIENTS FRICTION ON CLAMP LOAD IN THE BOLTED JOINT

Name: Michael P. Oliver
University of Dayton

Advisor: Vinod K. Jain

The coefficient of friction (CoF) has a dominant effect on the clamp load in a bolted joint. Friction occurs at threads as well as in the under-head region of the bolt-head or nut. Tests were conducted to determine the effect of lubrication, tightening speed, flange diameter, length of engagement, and the nut, bolt, and washer hardnesses on clamp load and thread and under-head CoFs. In most cases a tightening torque of 45 N-m was used. A finite element analysis model of an experimental bolted joint was developed to determine the clamp load on individual threads, flank pressure, and bolt elongation. The bolt in the model was tightened dynamically by applying a torque at the flats of the hexagonal head.

The results indicate that the flange size has a pronounced effect on the clamp load as compared to the length of thread engagement; as the flange diameter increased, the magnitude of the clamp-load also increased. A medium hardness bolt coupled with a high hardness washer produced higher clamp-load compared to any other material hardness

combination. The thread and under-head coefficient of friction decrease with the tightening speed. The under-head CoF has a more pronounced effect on the clamp load than the thread CoF. The load distribution on different threads was also obtained from the FEA model and compared with the previous analytical and FEA (static) models. The 1st thread was found to support the largest portion of the clamp load while the last thread the smallest portion. However, the percentage of the load carried by the 1st thread was different from those of the static models. The FEA results were also compared with the experimental results. There was a difference of about 5.2% between the FEA computed and experimentally determined clamp load. The experimental thread torque data was coupled with the FEA results to obtain the thread coefficient of friction values on each of the engaged threads. The coefficient of friction at the 1st thread was largest and decreased with the thread number.

ACKNOWLEDGEMENTS

The author would also like to thank Dr. Vinod Jain. Through his guidance, patients, suggestions, and support; this dissertation has finally come to a close. Dr. Jain pushed for answers to questions I had not thought of as well as pushed my level of understanding of friction. I would also like to thank Drs. Kashani, Mall, and Shaughnessy for their valuable guidance from time to time. I would also like to thank Dr. Kevin Hallinan, chair person, Mechanical and Aerospace Engineering Department for his guidance and support.

I would like to thank Dr. Gunther Hartmann for his knowledge and experience of fasteners. His guidance helped make this dissertation possible. The machinists at Ultrapunch machine shop deserve much praise. They worked extremely hard and in a few cases, performed the impossible to machine parts for the thread torque fixture. This fixture was truly a nice piece of machining. The machinists in the Model Shop in the Kettering Operations of Delphi also deserve thanks. Through the use of laser cutting, a precision part for the thread torque fixture was created in mere minutes. Delphi, my employer, also deserves thanks. They paid the tuition as well as provided the lab facilities in which all experimental research was conducted.

Paul Copeland of Engineering Methods, an ANSYS distributor, offered extremely helpful guidance on getting the dynamic FEA model to do what it was intended to do.

Finally, the author would like to first and foremost thank his wife for her undying support and love. Her encouragement lasted through the boasts of crankiness, depression, and frustration. Without her, this paragraph, nor the document it is attached to, would ever have been completed. This degree is for her.

TABLE OF CONTENTS

LIST OF FIGURES.....	x
LIST OF TABLES.....	xv
NOMENCLATURE.....	xvii
CHAPTER 1: INTRODUCTION AND LITERATURE SEARCH.....	1
1.0 Introduction.....	1
1.1 Evolution of Threads and Threaded Fasteners.....	1
1.2 Thread Manufacturing.....	2
1.3 Classification of Fasteners.....	3
1.4 Primer of a Bolted Joint.....	5
1.5 Thread Load Distribution.....	6
1.6 Friction.....	8
1.7 Current Frictional Testing.....	10
1.8 Summary.....	11
CHAPTER 2: EXPERIMENTAL.....	20
2.0 Torque Equations.....	20
2.1 Thread Toque Equations.....	20
2.2 Under-Head Torque Equations.....	22
2.3 Total Toque Equations.....	22
2.4 Fixture to Determine Thread and Under-Head CoF.....	24
2.5 Friction Experiments on a Bolted Joint.....	26
2.5.1 Effect of Under-Head Area and Length of Thread Engagement on Clamp-Load.....	27
2.5.2 Effect of Tightening Speed on Clamp-Load.....	29
2.5.3 Effect of Bolt, Washer, and Nut Material Hardness on Thread and Under-Head CoF.....	30

2.5.4	Effect Minimizing Under-Head CoF on the Magnitude of Thread CoF.....	30
2.6	Thread Torque Measurement Experiment.....	31
2.7	FEA Model Joint Experiment.....	35
CHAPTER 3: DEVELOPMENT OF THE FINITE ELEMENT ANALYSIS		
	MODEL.....	51
3.1	Model Creation.....	51
3.2	Model Execution.....	56
3.3	Load Distribution on the Threads.....	57
3.4	FEA Model for the Seven Thread Engagement.....	59
CHAPTER 4: RESULTS AND DISCUSSION.....		
4.1	Experimental Research.....	82
4.1.1	Effect of Under-Head Area and Length of Engagement on Clamp- Load.....	82
4.1.2	Effect of Tightening Speed on Clamp-Load.....	84
4.1.3	Effect of Bolt, Washer, and Nut Material Hardness on Thread and Under-Head CoF.....	86
4.1.4	Effect of Minimizing the Under-Head CoF on Thread CoF.....	87
4.2	FEA Model Joint Experiment.....	89
4.3	Thread Torque Measurement.....	90
4.4	Finite Element Analysis.....	91
4.4.1	Finite Element Analysis of the Bolted Joint.....	91
4.4.2	Load Distribution.....	91
4.4.3	Direct Comparison to Static Research.....	94
4.5	Thread CoF	95
CHAPTER 5: CONCLUSIONS AND RECOMMENDATIONS FOR FUTURE		
	WORK.....	125
5.1	Conclusions.....	125
5.2	Future Research.....	128
APPENDIX I.....		
		129

REFERENCES.....	136
------------------------	------------

LIST OF FIGURES

Figure 1.1	Artist's rendering of an Egyptian using Archimedes screw to lift water for irrigation purposes.....	12
Figure 1.2	Drawing showing a profile of an external thread with appropriate terminology.....	13
Figure 1.3	Schematic of the basic profile of the internal and external threads.....	14
Figure 1.4	Drawing comparing a bolted joint to a series of springs.....	15
Figure 1.5	Schematic of a bolted joint showing compression in the jointed members and tension in the bolt.....	16
Figure 1.6	Ishikawa diagram showing the factors that contribute to the development of clamp-load.....	16
Figure 1.7	Analytical and FEA load distribution data.....	17
Figure 1.8	Photograph of a nut showing the start of the internal threads.....	18
Figure 1.9	Relationship between kinetic and static CoF.....	19
Figure 2.1	Free body diagram of a section of the thread flank. Not shown is the included half angle.....	37
Figure 2.2	Variation of applied torque, developed clamp-load (tension), and thread and under-head CoF plotted with time	38
Figure 2.3	Schematic of cross-section of a torque/tension load-cell (the configuration shown is for the development of thread torque)	38
Figure 2.4	Side view of torque/tension load-cell.....	39
Figure 2.5	Front view of torque/tension load-cell showing the puck on the inside....	40
Figure 2.6	Back view of torque/tension load-cell showing the plate.....	40
Figure 2.7	Side view of the strain gauged housing of the load-cell. Area 1 shows the gauges.....	41
Figure 2.8	Magnified and rotated view of Area 1 from Figure 2.7. Area A shows the torque gauges and Area B shows the tension gauges.....	41

Figure 2.9	Bolt flange diameters.....	42
Figure 2.10	Nut heights (length of engagement).....	42
Figure 2.11	Schematic of the fixture holding the blades and threaded washers	43
Figure 2.12	Blade and the threaded washer indicating how thread torque is generated torque is generated.....	44
Figure 2.13	Drawing of blade used to measure thread torque.....	44
Figure 2.14	Photograph of the Thread Torque Fixture.....	45
Figure 2.15	Schematic of the signal connections between and computers, data acquisition units, torque transducer, load-cell, fixture, and DC trigger unit.....	46
Figure 2.16	Photograph of the ground non-threaded spacer used as a bearing surface for all calibrated threaded washers.....	47
Figure 2.17	Photograph of the ground square and non-threaded washers.....	47
Figure 2.18	Drawing of the bolt and nut-block used for the FEA modeling as well as machining the actual joint.....	48
Figure 2.19	Photograph of the bolt used in the FEA model investigation. The ultrasonic sensor is located at the end of the bolt	49
Figure 3.1	Locations of the key points used to establish both the internal and external thread profiles	61
Figure 3.2	ANSYS surface image of the 1 st pitch of internal threads.....	62
Figure 3.3	ANSYS surface image of the 1 st pitch of external threads.....	63
Figure 3.4	ANSYS surface image of the internal threads after copying and slicing at the top and bottom.....	64
Figure 3.5	ANSYS surface image of the external threads after copying and slicing at the top and bottom	65
Figure 3.6	ANSYS solid image of the internal threads before (a) and after (b) removal of the top and bottom parts	66
Figure 3.7	ANSYS image of the two solids creating the internal threads of the model. The solid in (b) is the bottom of the nut-block	67

Figure 3.8	ANSYS image of two solids used to create the external threads of the model. Image (a) shows the threaded hollow cylinder and (b) the final solid cylinder	68
Figure 3.9	ANSYS image of the bolt.....	69
Figure 3.10	ANSYS image of the solids creating the entire nut-block assembly.....	70
Figure 3.11	ANSYS FEA model of the external threads (a) and the internal threads (b) created using the SOLID186 elements	71
Figure 3.12	Axisymmetric image of the entire joint. Areas A and B indicate the contact regions of the model.....	72
Figure 3.13	Axisymmetric image of the joint showing the contact between the internal and external threads. The upper portion of the image represents the internal thread	73
Figure 3.14	Axisymmetric image of the M10 x 1.0 minimum contact model. Note the difference between the flank area and the area of contact. The upper part of the image is the internal thread	74
Figure 3.15	Axisymmetric image of the M10 x 1.0 nominal contact model. The upper area of the image is the internal thread.....	75
Figure 3.16	Axisymmetric plot of the M10 x 1.0 maximum contact model. Note that the root radius of the external thread has been altered. This was done so that no contact occurs between the root radius and the minor diameter of the internal thread (as happens in a real joint). The upper area of the image is the internal thread.....	76
Figure 3.17	Areas of the flanks of the nut that were in contact with the flanks of the bolt. Area numbers correspond to those of Table 3.6. Thread No. 1 is closest to the head of the bolt. Threads shown are from the 1.5mm pitch at maximum contact level.....	77
Figure 3.18	Total area of contact between the internal and external threads for the minimum, nominal, and maximum contact levels grouped by pitch size ...	78
Figure 3.19	Area of contact between the internal and external threads for the 1 st engaged thread for minimum, nominal, and maximum contact levels grouped by pitch size	78

Figure 3.20	Cross-sectional areas of the bolt for the models created for the minimum, nominal, and maximum contact levels grouped by pitch size	79
Figure 4.1	Plot of clamp-load Vs flange diameter. Data includes all nut heights.....	97
Figure 4.2	Plot of under-head and thread CoF Vs flange diameter. Data includes all nut heights.....	97
Figure 4.3	Plot of clamp-load Vs length of engagement. Data includes all flange diameter.....	98
Figure 4.4	Plot of under-head and thread CoF Vs nut height. Data includes all flange diameters.....	98
Figure 4.5	Thread CoF Vs tightening speed. A logarithmic trend line was fitted to the data.....	99
Figure 4.6	Under-Head CoF Vs tightening speed. A logarithmic trend line was fitted to the data.....	99
Figure 4.7	Clamp-load Vs tightening speed. A logarithmic trend line was fitted to the data.....	100
Figure 4.8	Thread and under-head CoF Vs tightening speed for dry experiment. A logarithmic trend line was fitted to the data.....	100
Figure 4.9	Clamp-Load Vs tightening speed for dry experiment (no lubrication was present). A logarithmic trend line was fitted to the data.....	101
Figure 4.10	Run-down plot of applied torque, under-head, and thread torque Vs time. Applied torque: 45 N-m.....	101
Figure 4.11	Run-down plot of clamp-load, thread and under-head CoF Vs time. Applied torque: 45 N-m.....	103
Figure 4.12	Plot of thread torque Vs seven engaged threads.....	104
Figure 4.13	Plot of thread torque Vs six engaged threads.....	104
Figure 4.14	Plot of thread torque Vs five engaged threads.....	105
Figure 4.15	Plot of thread torque Vs four engaged threads.....	105
Figure 4.16	Plot of thread torque Vs three engaged threads.....	106
Figure 4.17	Plot of thread torque Vs two engaged threads.....	106
Figure 4.18	Plot of thread torque Vs one engaged thread.....	107

Figure 4.19	Plot of results from both the FEA modeling and the experiment for clamp-load and bolt elongation.....	108
Figure 4.20	Bar chart showing the clamp-load for the minimum, nominal, and maximum contact levels, grouped by thread pitch.....	109
Figure 4.21	Bar chart showing the % of total clamp load on the 1 st thread for the minimum, nominal, and maximum contact levels, grouped by pitch.....	109
Figure 4.22	Bar chart showing the contact area at the 1 st thread for the minimum, nominal, and maximum contact levels, grouped by pitch.....	110
Figure 4.23	Plot of the load carried by different threads for an eight-thread engagement for the minimum contact level, grouped by pitch.....	110
Figure 4.24	Plot of the load carried by different threads for an eight-thread engagement for the nominal contact level, grouped by pitch.....	111
Figure 4.25	Plot of the load carried by different threads for an eight-thread engagement for the maximum contact level, grouped by pitch.....	111
Figure 4.26	Plot of the contact pressure distribution across eight thread-engagement for the minimum contact level, grouped by pitch.....	112
Figure 4.27	Plot of the contact pressure distribution across eight-thread engagement for the nominal contact level, grouped by pitch.....	112
Figure 4.28	Plot of the contact pressure distribution across eight-thread engagement for the maximum contact level, grouped by pitch.....	113
Figure 4.29	Plot of the contact area for the 1 st thread on the 1.25mm pitch, minimum contact.	114
Figure 4.30	Plot of the contact area for the 1 st thread on the 1.25mm pitch, maximum contact.	115
Figure 4.31	Plot of the load distribution for a 1 in 16 TPI bolt from Chen et al [15] using a static 3D model as well as the maximum contact level for the 1.0mm, 1.25mm, 1.5mm, and 1.75mm pitch.....	116
Figure 4.32	Plot of the thread CoF based on experimental thread torque data and FEA based clamp-load results.....	117

LIST OF TABLES

Table 1.1	Common thread types and their respective included angle.....	19
Table 2.1	Contact areas of the threads and under-head regions for the M10 x 1.5 threads calculated from geometric dimensions.....	50
Table 2.2	Programmed Vs actual tightening speed at the target torque of 28 N-m.....	50
Table 2.3	Experiment of different material hardness in two hardness levels for the washer and nut, one hardness level for the bolt from Section 2.5.3.	51
Table 2.4	Experiment of different material hardness in three hardness levels for each factor from Section 2.5.4.....	51
Table 3.1	Element and Node Data for the Model of Section 3.1.....	80
Table 3.2	Thread and under-head CoF values for the model of Section 3.1.....	80
Table 4.1	P-Value convention.....	118
Table 4.2	Averages for three replications on each of the six nut heights and four flange diameters with respect to flange diameter.....	118
Table 4.3	Averages for three replications on each of the six nut heights and four flange diameters with respect to nut height.....	118
Table 4.4	Effect of material hardness on clamp load parameters.....	119
Table 4.5	Effect of minimizing under-head CoF on clamp load parameters.....	120
Table 4.6	Effect of thread and under-head CoF on clamp load parameters	120
Table 4.7	Clamp-load and CoF data for 15 N-m of applied torque for FEA model joint	120
Table 4.8	Clamp-load and CoF data for 30 N-m of applied torque for FEA model	121
Table 4.9	Clamp-load and CoF data for 45 N-m of applied torque for FEA model joint	121

Table 4.10	Clamp-load and bolt elongation at various torques	121
Table 4.11	Thread torque and adjustment for 7 engaged threads	122
Table 4.12	Thread torque and adjustment for 6 engaged threads	122
Table 4.13	Thread torque and adjustment for 5 engaged thread.....	122
Table 4.14	Thread torque and adjustment for 4 engaged.....	123
Table 4.15	Thread torque and adjustment for 3 engaged threads.....	123
Table 4.16	Thread torque and adjustment for 2 engaged threads.....	123
Table 4.17	Thread torque and adjustment for 1 engaged thread.....	123
Table 4.18	Addition of measured thread torque values from Section 2.7.6 to the FEA results from Section 3.4 and discussed in Section 4.5.....	124

NOMENCLATURE

d	Nominal or major bolt diameter
d_h	Joint clearance hole diameter
D_{km}	Equivalent diameter
d_m	Mean thread diameter of the bolt
d_p	Nominal pitch diameter of the bolt
$d_{p \min}$	Minimum pitch diameter of the bolt
d_r	Minor or root diameter of thread
d_w	Bolt under-head diameter
F_{Friction}	Frictional force
F_t	Tangential force
k	Nut factor
N	Normal force
p	Thread pitch
P	Clamp-load
τ	Shear stress
T_{in}	Torque in or applied torque
T_{thd}	Thread torque
T_{und}	Under-head torque
α	Included half angle of thread
η	Efficiency
λ	Lead or pitch angle of thread
μ	Coefficient of friction (CoF)
μ_{thd}	Thread coefficient of friction
μ_{und}	Under-head coefficient of friction
σ	Stress

CHAPTER I

INTRODUCTION AND LITERATURE SEARCH

1.0 Introduction

1.1 Evolution of Threads and Threaded Fasteners

The idea of threads pre-dates the use of the modern threaded fastener. The invention of threads can be traced back to Archytas, 428-350 B.C. [1]. He has been referred to as the founder of mechanics and was a contemporary of Plato. Archytas' threads were used to extract juice from grapes and the oil from olives. Archimedes, a Greek mathematician 237-212 B.C. [2], used a thread to remove water from the hull of boats as well as for irrigation purposes by advancing a thread helix, as seen in Figure 1.1. The evolution of the thread continued with the innovation of equipping a lathe with a screw drive which allowed a tool carriage to be moved longitudinally and semi-automatically by Thiout [1] around 1750.

The ability to cut threads on a fastener was introduced by Wyatt and Wyatt in 1760 [1]. Ramsden [1], in 1770 made the first satisfactory screw-cutting lathe. Whitworth [1] was credited with introducing the first standardized thread with a 55° included angle as well as standardizing the number of threads per inch to a specified diameter. Whitworth's standards were adapted by the British (United Kingdom) in the 1860's. In the United States, Sellers [1] independently proposed a standard which was based on a 60° included angle, with specific threads per inch, which were also associated with specified fastener diameters. Sellers' standards were adapted as a US Standard and

subsequently developed into the American Standard Coarse (UNC) and American Standard Fine (UNF) series [1]. This thread had flat roots and crests, which made it easier to machine compared to the Whitworth's thread. During the same period, the metric thread standards were being developed and adapted through out Europe; however, each standard had a different included angle. The Germans had an included angle of 53.13° and the Swiss had an included angle of 47.5° . An international thread standard was eventually adapted, and was based on a 60° included angle with flat crests and rounded roots [1].

There is a large variety of threads to make fasteners today and Table 1.1 shows some of the basic thread types along with the included angle. Not included in this table are the other types of threads used in wood screws, sheet metal screws, and threads on glass and plastic containers. The most widely used thread in Europe is the International Standards Organization (ISO) metric series. The United States uses the ISO metric series as well as the UNC and UNF series. Figure 1.2 shows a drawing of an external thread with basic terminology [3]. Figure 1.3 shows the schematic of the basic metric thread profile from an industry standard [4]. There is also a type of thread that contains multiple starts. This series has 2 – 4 separate and distinct threads that form the helix. The advantage of this type of thread is that it can be engaged quickly and easily and improves efficiency by reducing the required torque to advance the screw.

1.2 Thread Manufacturing

Rolling and cutting are the two main methods for creating threads on a fastener. In the cutting method, the thread profile is created by machining (for either internal or external), tapping (internal thread), or using a die (external thread). The thread rolling can

be used for either internal or external threads. The external threads are produced by rolling the bolt blank between two parallel plates which have the desired major and minor diameters. Internal threads are produced much the same way using a tapered rod which moves relative to the nut. In rolling, the material is cold worked which causes the root of the thread to be stronger compared to that of the machined thread. The cold working introduces compressive residual stresses, which is good for fatigue resistance. Another advantage is that the threads are created much faster in the rolling process compared to the machining process. The main disadvantage of rolling the threads is cost: the roll dies have to be machined and that there is a volume requirement in order for this process to be economically feasible. The main advantage of using the machining process is thread creation at a lower initial cost.

1.3 Classification of Fasteners

There are two types of external threaded fasteners, the bolt and the screw. It used to be that if the fastener had threads to its head; it was a screw. If the threads stopped midway to the head; it was a bolt. The current convention is that a bolt is used with a nut and a screw is used in a blind threaded hole or creates its own threads such as a wood screw or self-tapping screw.

The shape of the commonly used nuts and bolts is diverse. The head of the bolt or screw is designed to perform two functions; establish a bearing surface or clamping surface at the parts in the joint and provide the means for the bolt to be driven or torqued. The two most common head shapes used in the automotive sector are the internal/external hexagonal and the internal/external Torx type [5]. The advantage of both these drives is the ease of getting the socket or drive either into or on the head. Hexagonal

screws/bolts can be classified as hex flange, heavy hex flange, or hex head. The principal difference between the two flange heads is the thickness and diameter of the flange. The hex head does not have a flange. The flange dimensions in the heavy hex are larger than that in the plain hex head. The heavy hex is used in applications requiring larger bearing area, stiffness, and strength.

The drive portion of the nut is mostly hexagonal in shape. The two most common shapes of nuts is the flanged (either heavy hex flange or hex flange) or non-flanged. The heavy hex flanged nut is used for designs requiring an increased bearing area compared to that of the hex flange nut. The non-flanged nut is used in low load applications. Some of the nuts can have a physical attribute what is called a locking device. This feature requires additional torque to simply turn the nut. It is used as a means of keeping the nut from falling off the bolt even if the clamp-load or tension is lost. The locking feature can be a ring or patch made from either nylon or an epoxy adhesive. The nut could also have a mechanical feature which means the top of the nut has been crushed so that a “tight” fit could be established between the nut and the bolt. The coating or plating used on the fasteners is based mainly on cost and performance requirements. The latter includes corrosion resistance and a specific friction range.

The automotive industry uses mainly the ISO series fasteners with coarse, fine, and super fine threads. Approximately 1,600 fasteners are required to assemble an average vehicle [6]. In 2002, approximately 41 million vehicles were produced worldwide which in-turn required 6.56 trillion fasteners [7]. This only represents a small number of fasteners used in industry and does not include the other sectors such as the consumer appliance and aerospace industries. Thus, the rationale for studying the initial

tightening behavior of fasteners can be justified based on the quantity of fasteners used in the automotive industry alone.

1.4 Primer of a Bolted Joint

A bolted joint can be thought of as a series of springs: one spring for the bolt and one spring for each for jointed members. Figure 1.4 shows how this set of springs works. As the bolt is tightened, the spring of the bolt elongates, which in-turn compresses the springs of the joint members. If the joint were disassembled, the springs (fastener and members) would return to their original position. Thus, when the bolt is tightened to a prescribed torque, tension (clamp-load) is developed in the bolt and compression in the joint members. An example of this is shown in Figure 1.5. The tension creates contact pressure on the flanks of the threads as well as in the under-head region of the bolt.

Friction, along with numerous other factors, affect the generation of clamp-load in a joint. Three major contributors to the development of clamp-load are the applied torque, elastic properties of the bolt and nut, and the coefficient of friction (CoF) in both the thread and under-head contact regions of the joint. However, the CoF in both the thread and under-head regions is a function of the developed clamp-load and pressure. As the clamp-load increases, the friction in both contact regions will change because of its dependence on pressure. The magnitude of the friction depends on the magnitude of the thread and under-head CoF due to the applied coating/plating (or lack of) and the contact pressure.

The Ishikawa diagram shown in Figure 1.6 illustrates the complexity involved in determining the magnitude of clamp-load in a bolted joint [8]. The Ishikawa diagram is a statistical flow chart; that the right side of the diagram shows the parameters responsible for the development of clamp-load and the possible reasons for its development on the

left. The diagram also illustrates all the factors that need to be addressed in designing and assembling a threaded joint. There are numerous simple equations to estimate this torque and clamp-load relationship. Equation 1.1 is one such equation where k is called a “nut factor”, P is the clamp-load developed, and d is the nominal diameter of the bolt.

$$\text{Torque} = k d P \quad (1.1)$$

1.5 Thread Load Distribution

Several analytical and empirical models had been proposed to determine the static load distribution in the threads of a bolt. These models examined the pressure distribution along the flank of the threads due to clamp-load. Analytical models from Sopwith [9], Goodier [10], and Yamamoto [11] provided a detailed analysis of load distribution in threaded fasteners. These models considered an eight-thread engagement where the nut height is equal to eight pitches of a 1.0 inch diameter bolt with 8 threads/inch (1in – 8TPI). The results of these models indicated that the 1st thread supports nearly 29% of the total load while the 8th thread supports approximately 2% of the total load. The Sopwith [9] model is based on the contribution of strains produced by the bending of the thread, axial recession of the bolt due to radial compression, and expansion of the nut caused by radial pressure of the joints. The Goodier [10] model showed that the load distribution was governed by stretching of the bolt, compression in the nut, and bending of the threads. The Yamamoto [11] model was based on bending and shearing of the threads, radial contraction and expansion of the bolt and nut, and the assumption of plane strain in the thread region. These analytical models applied the load at the thread flank at the pitch diameter, and did not uniformly distribute the load across the flanks as would happen in reality.

Kenny et al. [12] studied the load distribution in two and three dimensions (2D and 3D) using photo-elastic analysis of clamped joints. Even though the models were static in nature, they created a realistic model in three-dimension for research. Their results correlated with Sopwith's [9] model. Experimental work from D' Eramo et al. [13] used strain gauges placed on the outer surface of the nut and examined the stress distribution on the 1st four threads of the total engagement. The strain gauge data were used as an input to their finite element analysis (FEA) model. They found that their results were 28% different from the theoretical models [9-11] on the 1st loaded thread. No explanation about the difference was given from the researchers, but one rationale is actual experimental results versus analytical data; the experimental data contained manufactured parts which were not perfect as compared to the analytical model which was.

The most recent research on threaded fasteners had been performed utilizing FEA. A number of assumptions were made to develop the FEA model and make the computation time reasonable. The FEA analysis only computed the axial force on the joint, neglecting the torsional shear stress produced during tightening, and analyzed the eight and ten-thread engagements. Englund et al. [14] created an axisymmetric model with 4-node quadrilateral elements. This ANSYS model made no allowance for the helical nature of the threads. They did, however, use non-linear contact elements, which allowed the flanks of the mating threads to maintain or break physical contact and slide relative to each other. The results of their work indicated that the thread CoF does not significantly affect the load distribution along the length of engagement in the assembled condition (static loading). The friction coefficient was there simply to allow for radial

sliding of the flanks of the threads during axial loading, and not for torsional/axial sliding which would have taken place during a dynamic rotation.

Chen et al. [15] used both 2D and 3D modeling for their research. They used ABAQUS which allowed non-linear sliding contact between flanks of the mating threads (in the axial direction). The results of their work indicated that there was no significant contribution of thread helix to the FEA solution to warrant the use of a 3D based code instead of axisymmetric code. Figure 1.7 shows the results of the FEA and analytical models listed above.

The models discussed above used full and complete flanks and major and minor diameters on all eight internal and external threads. However, this approach is not an actual representation of internal or external threads and only represents the joint in the assembled or static condition. An actual nut and bolt would have truncated threads, especially on the nut (the first and last threads of the nut tapers off). Figure 1.8 shows a photograph of the location where the threads start in an actual nut. The above literature survey shows that no FEA analysis considered the physical tightening of the bolt into the nut. In addition, rotational shear stresses as well as torsional wind-up of the bolt (twisting of the bolt due to the head rotating slightly more than the threads) were not addressed in the static models.

1.6 Friction

Friction is defined as the resistance to motion that exists when a solid object is moved with respect to a surface that it touches [16]. There are three generally accepted laws of friction:

1. The friction force is proportional to the normal force. The constant of proportionality is

called the coefficient of friction (CoF) as is depicted by Equation 1.2.

$$F_{friction} = \mu N \quad (1.2)$$

2. The friction force is independent of the apparent area of contact (two objects with vastly different surface areas could have the same frictional force).
3. The friction force is independent of the sliding velocity (this implies that the force required to initiate sliding is the same as the force required to maintain sliding).

The above laws were proposed by Coulomb. Exceptions to the 1st law involve very hard and very soft materials like diamond and Teflon, respectively or diminutive loads, such as those in the milligram range [17]. A second example of the deviation from the 1st law involves a thin/hard layer on a softer substrate. At low loads, the hard layer's frictional properties predominate. At high loads the hard layer is compromised and the frictional properties of the substrate predominate.

Exceptions to the 2nd law involve very clean and smooth surfaces placed in contact with each other in a vacuum. Here, the friction is independent of the load and a chemical bond is actually created between the two materials. The apparent area is the actual area of contact.

Exceptions to the 3rd law are vast. It is well known that there are two CoF values: static and kinetic (dynamic) as shown in Figure 1.9. Generally, the static CoF is higher than the dynamic CoF. Velocity is an important factor in describing the nature of dynamic friction and that the friction decreases with increasing velocity past the point of a few millimeters in distance. The exception to this rule is when a slip-stick phenomenon occurs, called chatter. Several researchers Persson et al. [18], Shi et al. [19], and Rabinowicz [20] concluded that Coulomb's laws do not fully describe dynamic behavior

of friction.

Friction is affected by a material's bulk and surface properties, which include:

Bulk Properties

- Yield strength
- Hardness
- Modulus of elasticity
- Crystalline structure

Surface Properties

- Chemical reactivity
- Adsorption properties
- Surface energy

1.7 Current Frictional Testing

There is little work available to understand the friction developed in the threads and under-head region of a bolt. Most experiments conducted in the field of tribology used a constant load to determine the CoF between mating parts. However, the load in a bolted joint is ever-increasing as the bolt is tightened. The bearing surface of the joint member and the under-head region of a bolt during tightening are in constant contact with each other. As torque is applied, the clamp-load increases. There are two mechanisms that are active in the thread area as the load increases. First, new external threads of the bolt are being exposed to previously loaded female threads of the nut; as the bolt's threads are being threaded into the nut, all of its threads are new. There will be a difference in frictional coefficients between a surface that is new versus one that had been used or loaded. Second, a pressure is created on each of the engaged threads and that the pressure is different on each thread. Since friction is a function of load, it is expected to be different on each thread as well. The experimental work of Golubev et al. [21] and Fukuoka et al. [22] supports the above views. The Golubev's work indicated that the

thread CoF decreases with increasing clamp-load. The Fukuoka's work showed that the bearing surface friction affected the development of bolt tension more than the thread friction.

According to the current understanding of the relationship between the under-head and thread coefficients of friction, as documented in several fastener-related text, Bickford [23] and Shoberg [24], the two values are relatively the same. They further indicate that of the total energy consumed in tightening a bolted joint, 90% is lost due to friction and the remaining 10% goes to developing clamp-load. Results from the author's experiments indicate that the energy loss due to friction can range from approximately 77% to 95%. The loss is dependent on the CoF in both the thread and under-head region.

1.8 Summary

The purpose of the research was to address the physical phenomenon of tightening a bolt into a nut. Experimental research for the first time measured the amount of thread torque developed on each engaged thread of a seven-thread engagement. In addition, a FEA model was developed to allow the dynamic tightening of a bolt into a nut. The dynamic model was patterned after an actual bolt and nut joint so that results from the model could be compared with the experimental results of the actual joint. Experiments were conducted to determine the thread and under-head CoF values for an actual joint which were then used as inputs for the model. This allowed for an accurate modeling of a bolted joint.

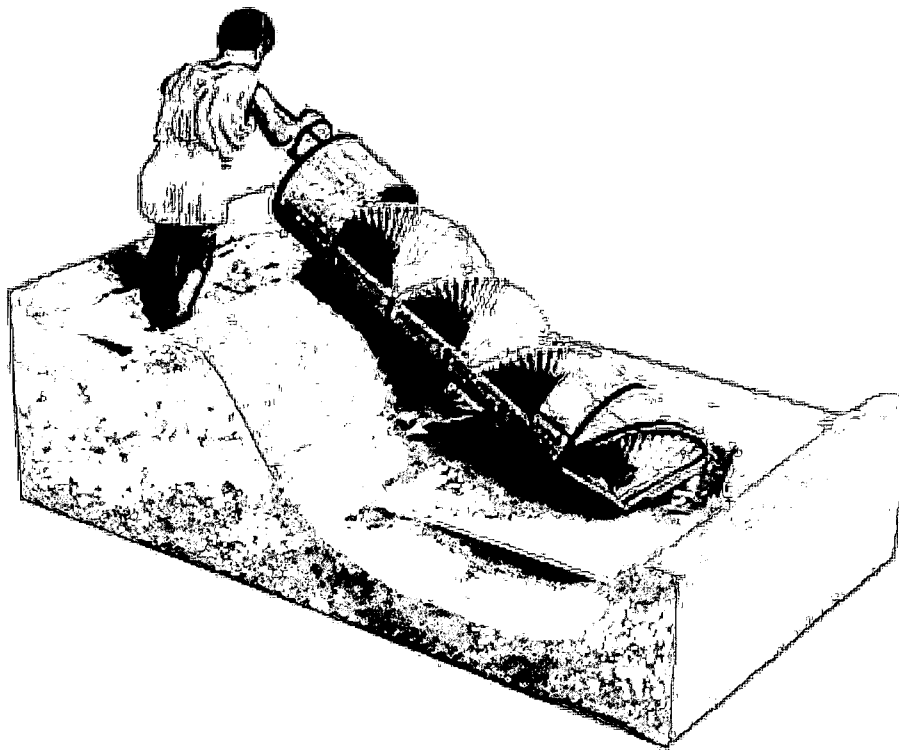


Figure 1.1 Artist's rendering of an Egyptian using Archimedes screw to lift water for irrigation purposes [1].

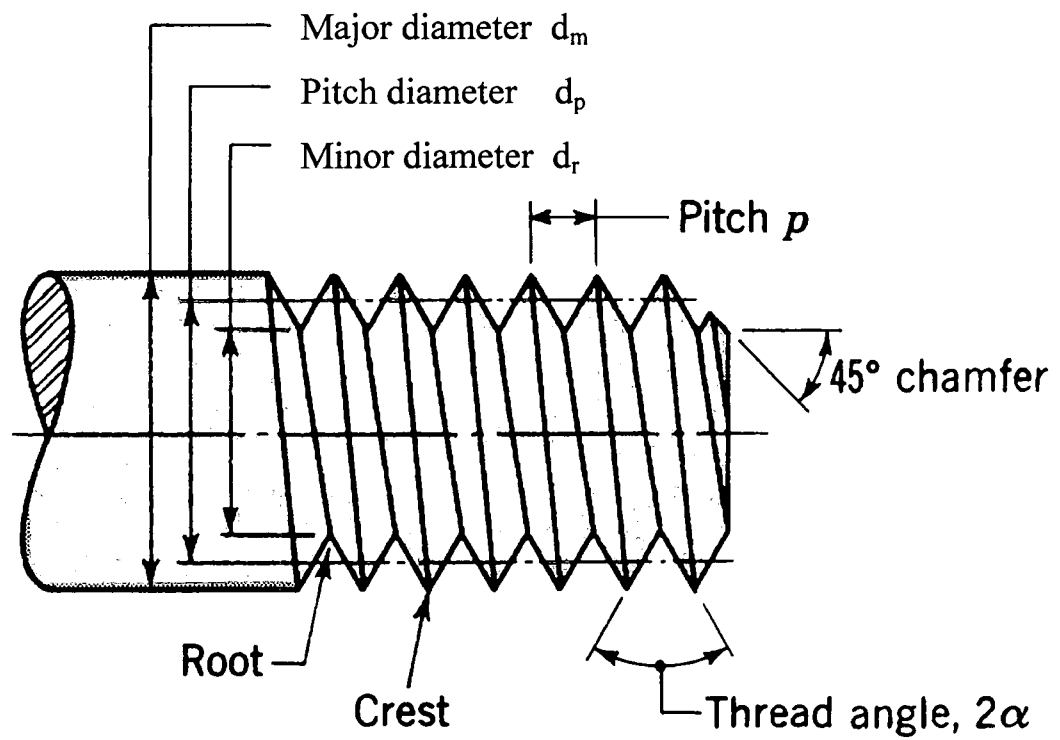


Figure 1.2 Drawing showing a profile of an external thread with appropriate terminology [3].

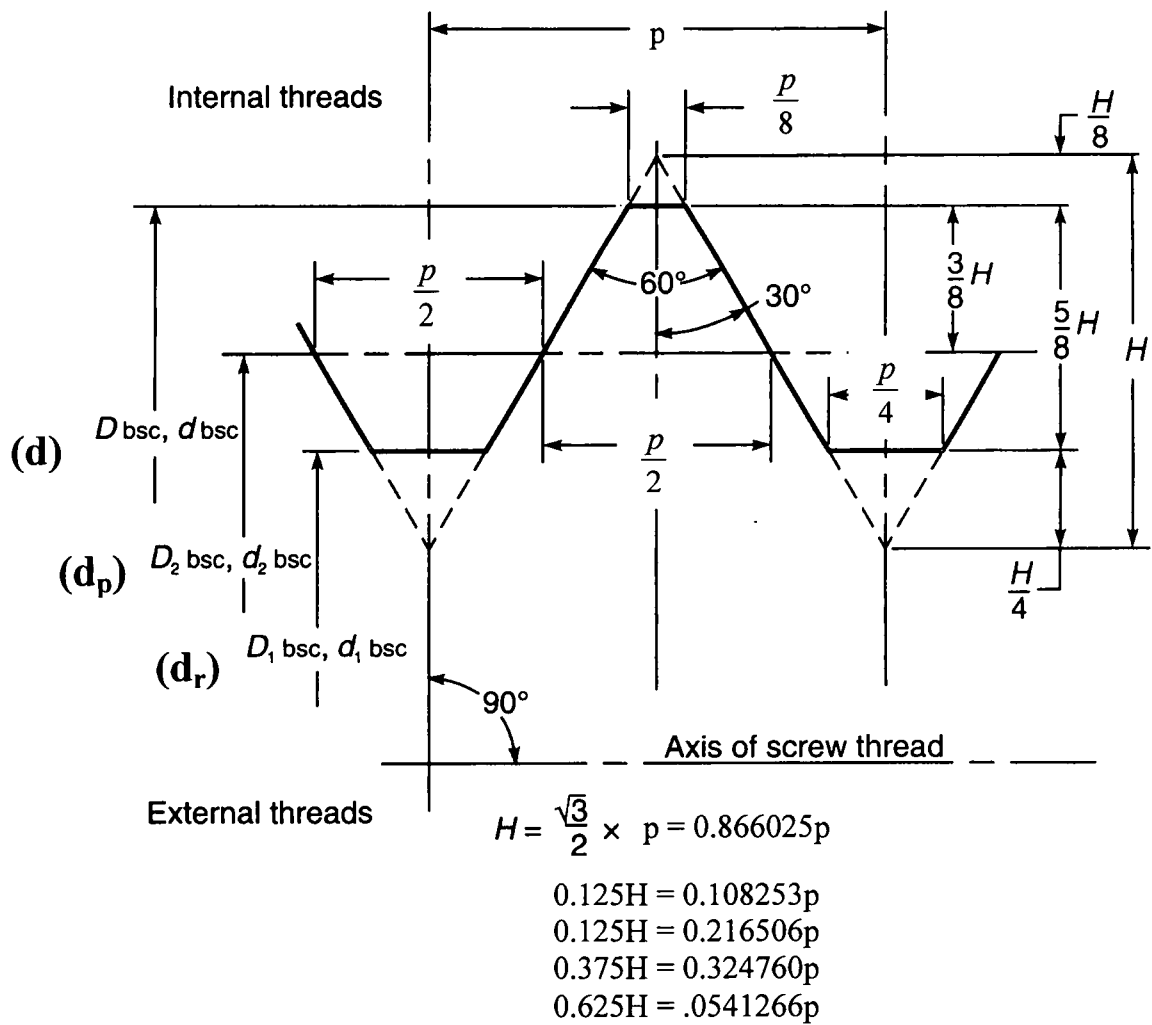


Figure 1.3 Schematic of the basic profile of the internal and external threads [4].

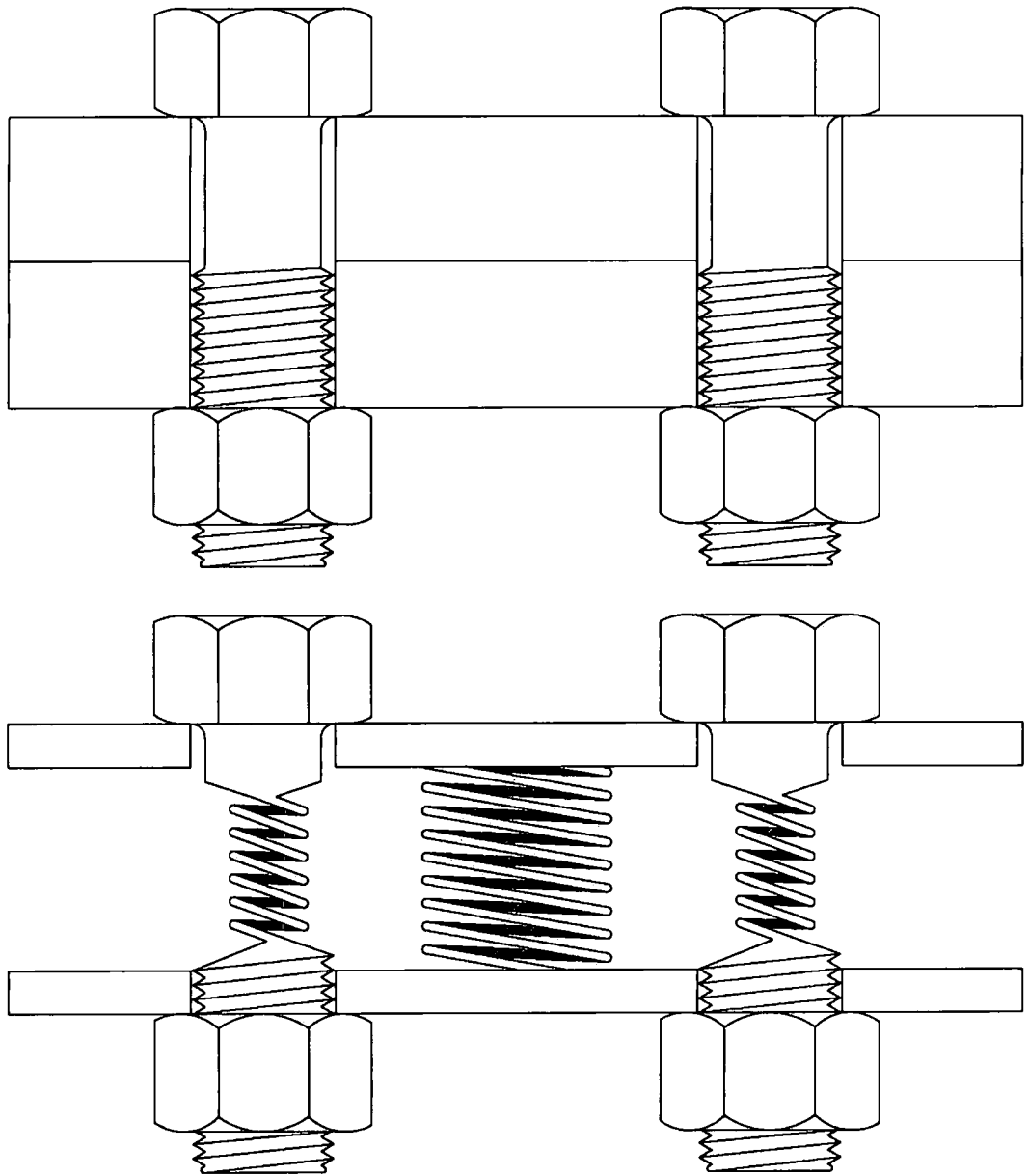


Figure 1.4 Drawing simulating a bolted joint to a series of springs.

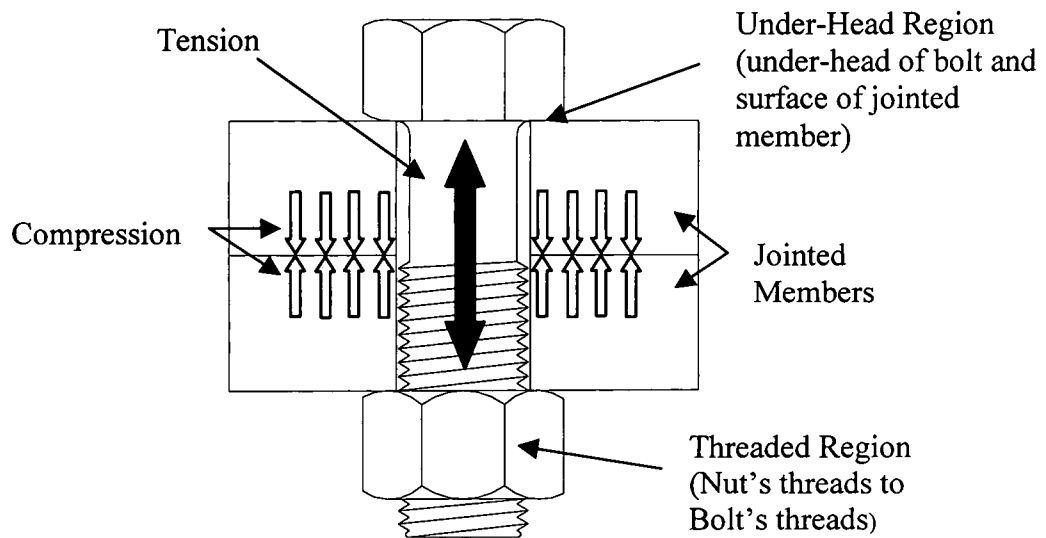


Figure 1.5 Schematic of a bolted joint showing compression in the jointed members and tension in the bolt.

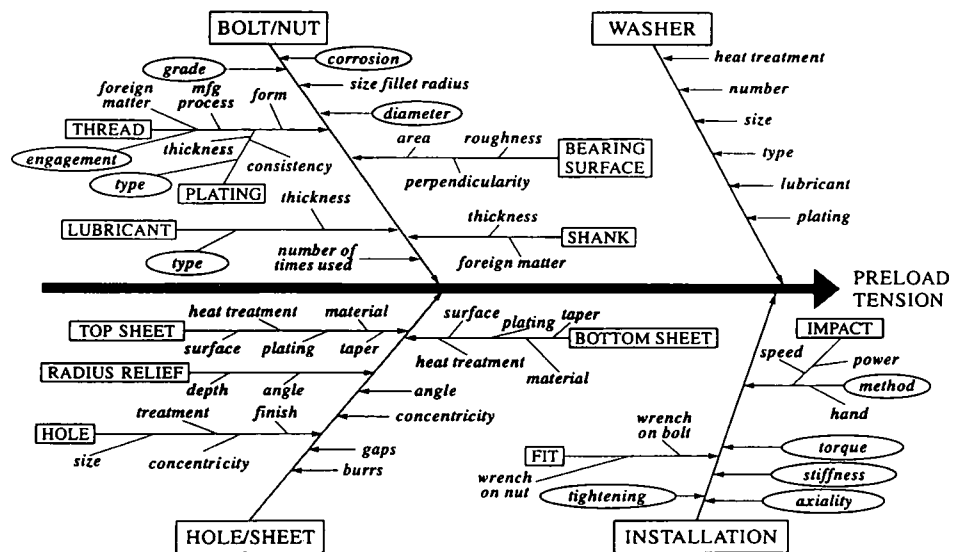


Figure 1.6 Ishikawa diagram showing the factors that contribute to the development of clamp-load [8].

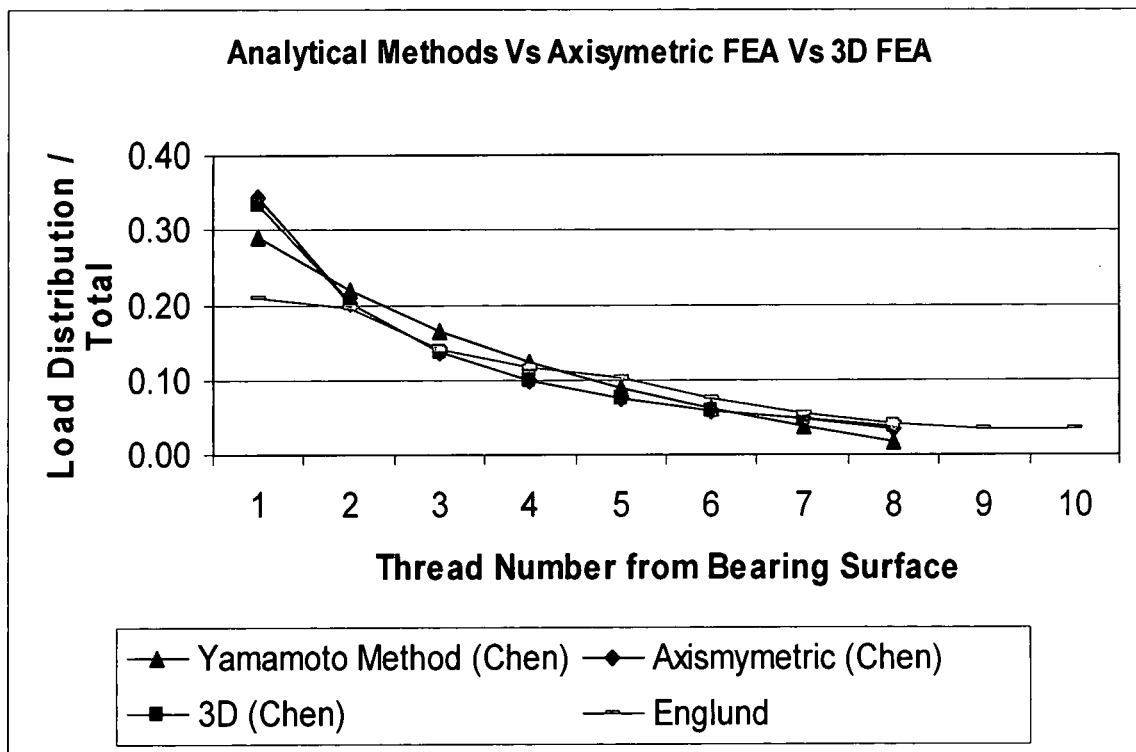


Figure 1.7 Analytical and FEA Load Distribution Data.

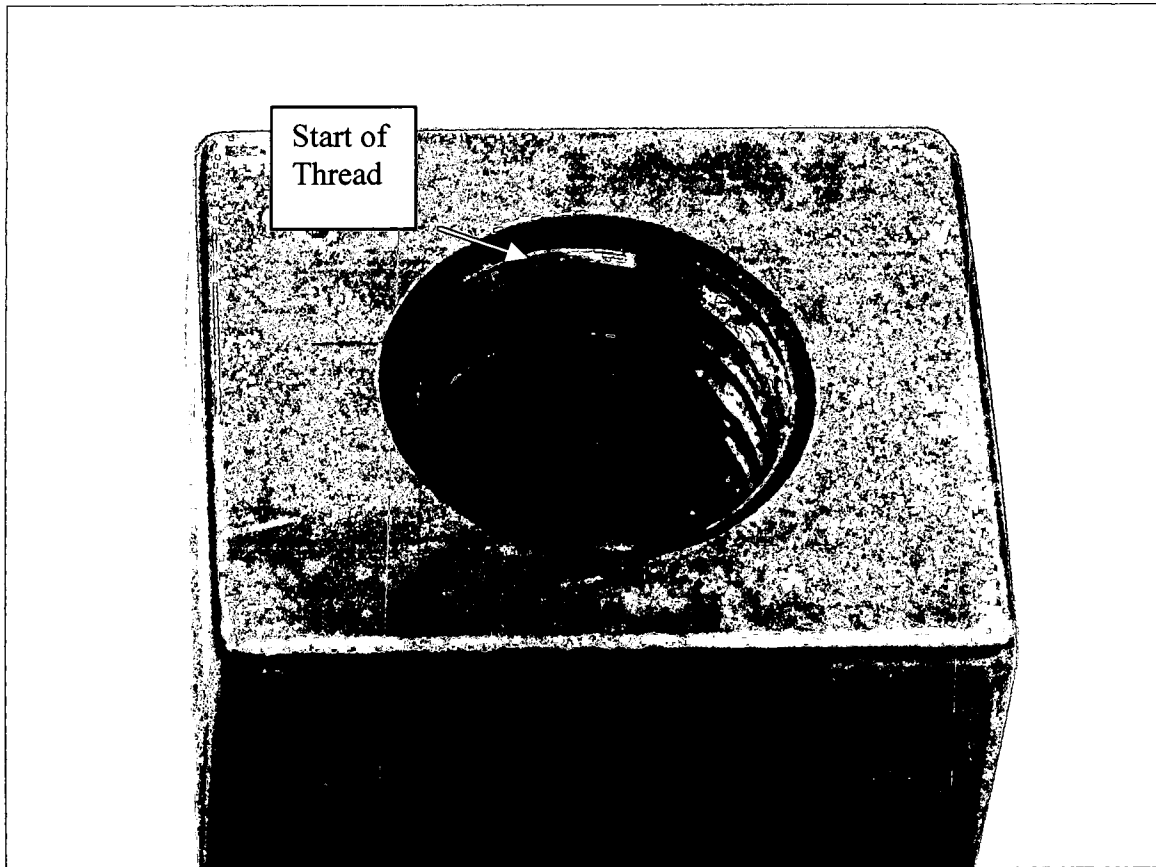


Figure 1.8 Photograph of a nut showing the start of an internal thread.

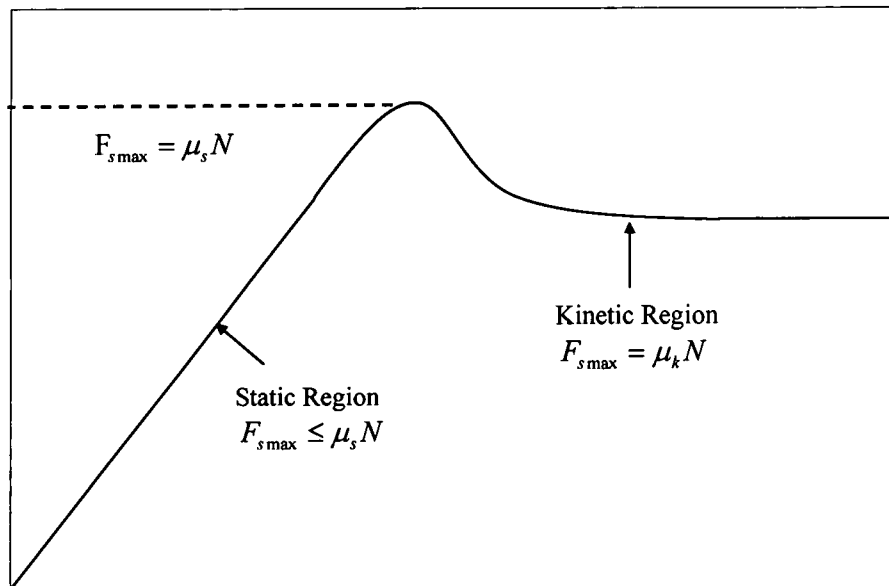


Figure 1.9 Relationship between the kinetic and static coefficient of friction.

Table 1.1 Common thread types and their respective included angle	
Thread Type	Thread Included Angle
Unified Coarse Thread (UNC)	60°
Unified Fine Thread (UNF)	60°
Unified Extra Fine (UNFF)	60°
Metric M Profile (ISO)	60°
Metric MJ Profile (ISO)	60° with Rounded root
Acme Screw Thread	29°
Buttress Thread	10°
British Standard Whitworth Thread (BSW)	55°
British Standard Fine Thread (BSF)	55°
British Standard Pipe Threads (BSP)	55°
British Association Thread (BA)	47.5°
Square Thread	90°

CHAPTER II

EXPERIMENTAL

2.0 Torque Equations

The equations used to determine the bolt tightening torque are given in text books and design standards. They are developed based on clamp-load, coefficient of friction (CoF), and geometry of the thread and under-head region of a bolted joint. These equations are then modified to determine the friction in both the thread and under-head regions separately. The thread and under-head torque equations are derived in the following sections.

2.1 Thread Torque Equations

Figure 2.1 shows a single developed thread of a square threaded screw. The angle λ is known as the lead or pitch angle and represents the angle that the helix of the thread makes with the plane of rotation, P is the clamp-load, N is the normal force, μ_t is the thread CoF, and F_t is the tangential force. A horizontal force (F_t) is applied to move the clamp-load (P) on this inclined plane. Summing the forces in the x and y directions:

$$\sum F_y = P + \mu_{thd} N \sin(\lambda) - N \cos(\lambda) = 0 \quad (2.1)$$

$$\sum F_x = F_t - N \sin(\lambda) - \mu_{thd} N \cos(\lambda) = 0 \quad (2.2)$$

Solving Equation 2.1 and 2.2 gives

$$N = \frac{F_t}{\sin(\lambda) + \mu_{thd} \cos(\lambda)} = \frac{P}{\cos(\lambda) - \mu_{thd} \sin(\lambda)}$$

$$F_t = \frac{P(\sin(\lambda) + \mu_{thd} \cos(\lambda))}{(\cos(\lambda) - \mu_{thd} \sin(\lambda))} \quad (2.3)$$

Torque is defined by,

$$T = \text{Force} \times \text{Distance}$$

Re-writing this equation for thread torque (T_{thd}) and using the mean radius as the distance.

$$T_{thd} = \frac{F_t d_m}{2} \quad (2.4)$$

Substitution of Equation 2.3 into Equation 2.4 gives

$$T_{thd} = \frac{P d_m (\sin(\lambda) + \mu_{thd} \cos(\lambda))}{2 [\cos(\lambda) - \mu_{thd} \sin(\lambda)]} \quad (2.5)$$

To simplify Equation 2.5, divide both the numerator and denominator by $\cos(\lambda)$.

$$T_{thd} = \frac{P d_m (\tan(\lambda) + \mu_{thd})}{2 (1 - \mu_{thd} \tan(\lambda))} \quad (2.6)$$

The lead angle λ is given by

$$\tan(\lambda) = \frac{P}{d_m \pi}$$

Substituting this relationship into Equation 2.6 gives

$$T_{thd} = \frac{P d_m \left(\frac{P}{d_m \pi} + \mu_{thd} \right)}{2 \left(1 - \frac{\mu_{thd} P}{d_m \pi} \right)}$$

Further simplification gives the thread torque Equation 2.7, which matches with those in most design text books [25, 26] for a square threaded power screw raising a load P.

$$T_{thd} = \frac{P d_m}{2} \left(\frac{p + d_m \pi \mu_{thd}}{d_m \pi - \mu_{thd} p} \right) \quad (2.7)$$

The effect of the included angle (2α) is to increase the frictional force due to a wedging action on the flank of the threads. Therefore, the frictional term in Equation 2.7 must be divided by $\cos(\alpha)$ to consider the effect of this angle. Thus the torque needed to tighten a bolt is given by:

$$T_{thd} = \frac{Pd_m}{2} \left(\frac{p + d_m \pi \mu_{thd} \sec(\alpha)}{d_m \pi - \mu_{thd} p \sec(\alpha)} \right) \quad (2.8)$$

2.2 Under-Head Torque Equations

The under-head torque can be calculated by considering the rubbing between two disks. The equivalent frictional force (F_t) is equal to the clamp-load (P) times the coefficient of friction between the bolt head and the joint member (μ_{und}).

$$F_t = P\mu_{und} \quad (2.9)$$

The torque needed to overcome the under-head friction is given by

$$T_{und} = \frac{F_t D_{km}}{2} \quad (2.10)$$

where D_{km} is the equivalent diameter and is defined as the average of the bearing surface through-hole diameter (d_h) and the flange diameter of the bolt (d_w).

$$D_{km} = \frac{(d_w + d_h)}{2}$$

Substituting Equation 2.9 into Equation 2.10 gives the under-head torque as

$$T_{und} = P\mu_{und} \frac{(d_w + d_h)}{4} \quad (2.11)$$

2.3 Total Torque Equation

The total torque (T_{in}) needed to tighten a bolt in a joint is equal to the sum of the thread torque and the under-head torque:

$$T_{in} = T_{thd} + T_{und} \quad (2.12)$$

Substituting Equations 2.8 and 2.11 into Equation 2.12 gives

$$T_{in} = \frac{P d_m}{2} \left(\frac{p + d_m \pi \mu_{thd} \sec(\alpha)}{d_m \pi - \mu_{thd} p \sec(\alpha)} \right) + P \mu_{und} \frac{(d_w + d_h)}{4} \quad (2.13)$$

The torque Equations 2.8, 2.11, and 2.13 are the same as that found in the text books.

International standards organizations such as DIN946 [27] and ISO16047 [28] depict the equations differently. Both organizations divide the thread torque into two components, the pitch torque (T_{pitch}) and the thread frictional torque ($T_{thread\ friction}$).

$$T_{thd} = T_{pitch} + T_{thread\ friction} \quad (2.14)$$

The pitch torque (T_{pitch}) can now be found by setting μ_{thd} equal to zero in Equation 2.8.

$$T_{pitch} = 0.159(P)p \quad (2.15)$$

The μ_{thd} is acting along the face of the flank. Resolving the clamp-load onto the flank, multiplied by distance (half the mean diameter) gives the thread friction torque ($T_{thread\ friction}$), Equation 2.18.

$$T_{thread\ friction} = 0.578 P d_m \mu_{thd} \quad (2.16)$$

Substituting Equations 2.17 and 2.18 into Equation 2.13 gives the resulting thread torque (T_{thd}) of Equation 2.19. This final equation is the equation for torque that is found in both the DIN and ISO specifications. The under-head torque is given by Equation 2.10 which is the same as that found in both the standards.

$$T_{thd} = P(0.159 p + 0.578 d_m \mu_{thd}) \quad (2.17)$$

To find the Thread CoF, solve Equation 2.19 for μ_{thd} .

$$\mu_{thd} = \frac{\left(\frac{T_{thd}}{P}\right) - 0.159 p}{0.578 d_m} \quad (2.18)$$

The Under-Head CoF can be obtained from Equation 2.11.

$$\mu_{und} = 2 \left(\frac{T_{und}}{PD_{km}} \right) \quad (2.19)$$

The Equation for the total torque in (T_{in}) is given by Equation 2.22. The results from this equation will match those obtained from Equation 2.13.

$$T_{in} = P \left(0.159 p + 0.578 d_m \mu_{thd} + \mu_{und} \frac{(d_w + d_h)}{4} \right) \quad (2.20)$$

2.4 Fixture to Determine Thread and Under-Head CoF

The current method of determining the CoF in both the threaded and under-head regions involves the measurement of three physical parameters: clamp-load, under-head torque, and applied tightening torque. These parameters are measured during tightening of the bolt. These values are then used with the appropriate equations to determine the thread and under-head CoF values. Note that this method assumes a constant CoF at the threads. The research by the author indicates that friction changes as the load increases. As the fastener is tightened, clamp-load increases and the under-head and thread CoF change. Figure 2.2 shows the variation of applied torque, clamp load, under-head CoF, and thread CoF with time for tightening a M10 x 1.5 mm fastener at 28 N-m. Here the

thread and under-head CoF curves were generated with equations found in industry specifications [28]. The equations are embedded in the data acquisition software that was used in all the experiments reported in this research. Note the relative difference between under-head and thread CoF values as well as the transient behavior of both friction values as well as the clamp-load. The figure indicates that the CoF in both regions is not constant.

The thread and under-head CoF values are calculated from the analytical Equations 2.20 and 2.21. In order to determine the values of the two CoF's, a bolted joint must be tightened in a torque/tension load-cell (Figure 2.3). The load-cell measures both tension and either thread or under-head torque (the type of torque will depend on which side of the load cell is used to tighten the bolt). Figures 2.4, 2.5, and 2.6 show the side, front, and back views, respectively, of the load-cell. The puck is shown in Figure 2.5 and the plate is shown in Figure 2.6. If the fastener is tightened on the inside of the cell, Figure 2.5, under-head torque will be measured. If the fastener is tightened on the backside of the cell, Figure 2.6, then thread torque will be measured.

The torque/tension load-cell has two sets of strain gauges connected in a wheat-stone bridge: one set for measuring torque and the other for measuring tension. The gauges for measuring tension are mounted perpendicular to the plate and puck while the gauges for measuring torque are mounted parallel to the puck and plate, Figures 2.7 and 2.8. When the fastener is tightened: 1) Clamp-load is developed by the puck and plate is compressed towards each-other with respect to the frame of the cell; this action compresses the strain gauges that are mounted in the perpendicular direction - gauges depicted by Area B in Figure 2.9. 2) Torsion is developed from the puck with respect to

the frame of the cell (this places a torsional force on the strain gauges that are mounted in the parallel direction, regardless of which side of the fastener is tightened; gauges depicted by Area A in Figure 2.9. The view of the load-cell body, Figure 2.5, shows a square counter-bore in the center of the puck.

The output of the load-cell is torque and clamp-load. The manufacturer calibrates these two signal channels separately. This calibration is performed in order to ensure that a phenomenon called “cross-talk” does not occur between the two channels. The cross-talk is described by the manufacturer of the load-cell as an effect of one channel onto the other channel. If a torsional force is placed on the cell without applying tension, then tension should be zero. If tension is not zero, then cross-talk is occurring. Note that the total torque is equal to the sum of the thread torque and under-head torque. Since applied torque and under-head torque are both physically measured, the thread torque can then be determined. The torque and clamp-load values can also be inserted into the appropriate equations to determine the under-head and thread CoF values from Equations 2.20 and 2.21.

2.5 Friction Experiments on a Bolted Joint

Five experiments were conducted to examine the possible relationships of the thread and under-head contact regions in a bolted joint. All experiments were conducted in a laboratory environment using both machined and forged materials for the bolt joint.

The following experiments were conducted:

1. Effect of bolt under-head area on under-head CoF and clamp-load
2. Effect of the length of engagement on thread CoF and clamp-load
3. Effect of tightening speed on clamp-load
4. Effect of bolt, washer, and nut material hardness on thread and under-head CoF
5. Effect of minimizing the under-head CoF on the magnitude of thread CoF

The materials used for the joint members in most the experiments, were either A2 or 4140 steel. These materials were used because of their ability to be heat treated to a wide range of hardness as well as their physical availability during the time of the experiments. The lubricants used were the compounds of moly-disulfide, graphite, sulfur, or Teflon. The moly-disulfide and graphite based lubricant was Moly-Lit (10-30% moly-disulfide, 15-25% lead-monoxide, 10-25% graphite, and 50-80% petroleum oil) and the graphite based lubricant was N-5000 (55-60% mineral oil, 15-20% nickel, 10-15% graphite, 10-15% oxygenated aliphatic hydrocarbon, 3-5% lithium soap, and 1-3% aluminum). These two lubricants were anti-seize compounds that have a low CoF. The sulfur based anti-seize compound TS-74 (phosphorous and sulfur based inorganic compound which contains neither graphite nor moly-disulfide) has a characteristic of supporting very large pressures without flowing. The teflon based lubricant was applied in liquid form and dried. This allowed for a minimal build-up of Teflon.

2.5.1 Effect of Under-Head Area and Length of Thread Engagement on Clamp-Load

The 1st two experiments were conducted at the same time. A randomized 2-factorial experiment with 3 replications was created to examine the relationship between the thread and under-head CoF. The under-head size of the bolts varied from 18 to 21 mm in diameter and the length of engagements of the nut varied from 5.5 to 13 mm. Figures 2.9 and 2.10 illustrate the different sizes of the head diameter as well as the different lengths of engagement.

The bolts used were M10 x 1.5 6g6g 65 mm long hex head flange bolts and machined from A2 steel and heat treated to a hardness of 34-38 HRC. Here, the number “6” represents the tolerance range, maximum to minimum value. The letter “g” is the

magnitude of the allowance is the deviation from the basic profile of the internal threads, which is the minimum condition of the internal threads. The nut and washer were also produced from the same A2 material and hardness. The nuts were held fixed in the plate of the load-cell and the bolt was tightened against a washer inside the puck of the load-cell. There were four bolts representing each of the four head sizes and six nuts representing each of the six different nut heights. The same washer was used for all run-downs. The experiment consisted of running each of the four head sizes with each of the six different nut heights. Since there were three replications of each, a total of 72 joints were tested. Before each run-down, the bearing surface of the under-head and thread regions were coated with Moly-Lit anti-seize compound.

The contact areas for all combinations in both the head as well as the thread regions are shown in Table 2.1. The under-head areas were calculated from the flange dimensions. The thread contact area was calculated based on the calculus of surface revolution and is based on actual measurements of the thread dimensions.

The anti-seize paste was applied to the thread and under-head regions of the bolt prior to each tightening. The joints were assembled into the torque-tension load-cell and then an electric torque gun was used to tighten the bolts to a torque of 45 N-m at a speed of 100 rpm. The nut and washer were held fixed while the bolt rotated. A data acquisition system collected and then stored the under-head torque and clamp-load data from the load-cell, and the applied torque, speed, and angle of rotation from the torque transducer. The algorithm in the acquisition system automatically calculated the necessary parameters to obtain the thread and under-head CoF values based on the equations of torque and friction discussed previously. Following the tightening, the graphical data was

analyzed at 40 N-m.

2.5.2 Effect of Tightening Speed on Clamp-Load

The 3rd experiment examined the relationship between run-down speed, thread and under-head CoF, and clamp-load. There were actually four separate experiments conducted in this section. The 1st three consisted of applying the three different types of anti-seize lubricants on the threads and under-head regions. The 4th experiment consisted of using dry fasteners. The same bolt, washer, and nut were used for each run-down on the 1st three experiments and all hardware were machined from A2 tool steel hardened to 34-38 HRC. The M10 x 1.5 6g6g bolt was 65 mm long and had a 20 mm under-head flange. The nut used had a height of 10mm. Moly-Lit, N-5000, and TS-74 anti-seize compounds were used for the 1st, 2nd, and 3rd set of experiments respectively. All lubricants were used one at a time and applied to the threads and bearing surface before each individual run. There were three replications for each of the 15 different speeds; these three replications at the 15 different speeds were conducted for each of the three different lubricants. Table 2.2 shows the programmed versus actual speed at the targeted torque. The dry portion of the experiment had to be suspended prematurely due to the onset of galling which occurred in the under-head region. This was expected due to the plain finished materials in contact with each-other.

The joints were assembled into the torque-tension load-cell and then an electric torque gun was used to tighten the bolts to a torque value of 30 N-m at the various speeds. The same test procedure as described in Section 2.5.1 was used. Following the tightening, the graphical data was analyzed at 28 N-m.

2.5.3 Effect of Bolt, Washer, and Nut Material Hardness on Thread and Under-Head CoF

Here, the investigation on material hardness, examined the affect of bolt, washer, and nut hardness on the thread and under-head CoF values. It was a 3^3 factorial experiment with three replications and a total of 81 run-downs were performed. There were three hardness levels for the M10 x 1.5 6g6g bolt (65mm long), with a 20 mm diameter flange. Three different washers, as well as three different nuts of different hardness levels were used and all nuts and washers were machined to the same dimensions. The length of engagement of both nuts was 10 mm and the thickness of the washers was 2 mm. The material used for all test pieces was 4140 steel. Table 2.3 lists the hardness ranges for each bolt, washer, and nut. The anti-seize paste was applied to the thread and under-head regions of the bolt prior to each tightening. The joints were assembled into the torque-tension load-cell and then an electric torque gun was used to tighten the bolts to a torque value of 45 N-m at a speed of 100 rpm. Following the tightening, the graphical data was analyzed at 40 N-m.

2.5.4 Effect of Minimizing Under-Head CoF on the Magnitude of Thread CoF

The 5th set of experiments examined the effect of minimizing the under-head CoF on a bolt as it was tightened. In this experiment, the nut was a M10 x 1.5 6H6H, Class 10 material with a hardness of 26-36HRC. The nut was bright zinc plated and 10 mm in height. The nut was driven and the bolt, a 9.8 property class M10 x 1.5 6g6g bolt (60mm long) and plain finished, was held fixed. The bearing surface for the nut was either an assembly of 10 mm thrust bearing sandwiched between two hardened and yellow zinc plated washers or a plain finished washer, heat treated to 56HRC. The N-5000 lubricant

was applied to all bearing surfaces prior to each run. The experiment was a 2^2 factorial with three replications and a total of 12 run-downs were performed. The same bolt and nut were used for all 12 run-downs. The same plain finished washer and the same thrust bearing assembly were used for each of the three replications for each condition.

A 2nd investigation was also conducted in this section of the research. The same fasteners, as above were used with the exception of no thrust washer. This investigation looked at the relationship between the thread and under-head CoF when one area was lubricated and the other was dry, compared to when both regions dry and both regions lubricated. Table 2.4 shows the experimental set-up for this section. The N-5000 anti-seize paste was applied to the thread and under-head regions of the bolt prior to each tightening when required. The joints were assembled into the torque-tension load-cell and then an electric torque gun was used to tighten the bolts to a torque value of 45 N-m at a speed of 100 rpm. Following the tightening, the graphical data was analyzed at 40 N-m.

2.6 Thread Torque Measurement Experiment

An investigation was conducted to measure the magnitude of torque developed on an individual thread basis. This thread torque measurement was made possible with a series of threaded washers where each washer contained exactly one pitch and with a series of blades that measured the torque that each washer produced (Figures 2.11 and 2.12).

The washers were machined from A-2 steel and heat-treated to 32-36HRC. The outer profile and minor diameter through hole was first cut using an electro discharge machine (EDM). The thickness of the washer stack was approximately 20 mm. The stack was then turned on its side, and the same machine then sliced each of the seven washers

to a thickness of 1.7 mm. Each washer was then ground to a final thickness of 1.5 mm, the size of the pitch for a M10 x 1.5 mm thread. The seven washers were then re-stacked into their original orientation, clamped, and tapped to create the M10 x 1.5 internal thread. Therefore, each of the seven washers contained one complete pitch or one full thread. The threads were measured using a System 22 inspection method, which measures pitch diameter, functional diameter, and minor diameter. The threads were at the upper end of the M10 x 1.5 6H6H tolerance zone.

The blades used to measure the thread torque were machined and hardened from the A-2 steel and ground to the same thickness, 1.5 mm. A 0.5 mm diameter through hole and a 1.13 mm counter-bore was drilled at the end of the blade using the EDM, as seen in Figure 2.13. A fiber optic strain gauge was then placed into the hole and secured with epoxy (M Bond 10). This type of strain gauge is a glass fiber that has a set of mirrors bonded inside a capsule, which is secured to the end of the glass fiber. The mirrors are positioned approximately 3 mm from the end of the capsule. The end of the capsule was secured at a distance of 3 mm from the end of the "L" section of the blade. As this end of the blade is compressed, the mirrors are moved closer together and a negative strain value is registered in the BUS Module, manufactured by FISO, that converts the light signal, from the gauge, to a voltage.

Figure 2.14 shows the completed fixture which is attached to a torque/tension load-cell, similar to that shown in Figures 2.4 through 2.6. There were 10 separate data channels and therefore required the use of two computers and two data acquisition systems to collect the data. The schematic for the connections of the systems and fixture are shown in Figure 2.15. Time was the basis or common denominator between the two

computers and data acquisition systems. A DC voltage generator device, capable to delivering 10 V DC to both acquisition systems, is also shown in the schematic. When a 10 V signal was generated, both systems started collecting and storing data simultaneously. Following the testing, the data could all be compiled onto one graph for analysis.

This experiment was started by first calibrating the seven individual blades, independently of each. The 1st washer, which is adjacent to the fixture itself, was calibrated first. Triflow, a Teflon based lubricant, was applied to the surfaces and threads of all washers. A bolt was torqued into the threads of the 1st washer to a value of 10 N-m. The thread torque data from the torque/tension load-cell was plotted against the strain from the 1st blade. Six run-downs were performed to create an average calibration curve of thread torque to blade strain. The 2nd washer was calibrated in a similar manner, but with the exception of a non-threaded washer being placed in front of this threaded washer Figure 2.16. The 3rd through 7th washers were calibrated using this same procedure. The 7th washer had five ground square spacers and the one non-threaded washer placed in front of it during the calibrations, as seen in Figure 2.17. Appendix I contains the resulting calibration curves that were created with the use of shareware software called LAB Fit. This code examines the collected data and then recommends a best-fit curve based on 208 mathematical equations using 2nd, 3rd, or 4th order equations. All equations used for the seven average calibrations were 2nd order and are shown on the plots of the curves along with the associated R^2 value.

During the developmental phases of this investigation, it was discovered that the 2nd through 7th washers created additional thread torque to the 1st washer when all seven

were tightened. Due to this discovery, an additional experiment was conducted to determine what the contribution of the torque was. This experiment was performed by placing a washer with no threads (Figure 2.16) in the 1st washer's place and then adding the normal threaded washers to the joint. The first run-down had a thread-less washer in the 1st position and a threaded in the 2nd position. The second run-down added the threaded washer to the 3rd position and so on. As the bolt was tightened into the series of washers, the 1st washer supported both the developed clamp-load and resulting torque from the washers stacked on top of it.

With calibration complete and the contribution of the 1st washer accounted for, the actual experiment was conducted. All seven washers or 1st seven threads were used in the first test (two run-downs were performed for each condition). This was followed by the first six washers or 1st six threads, then the first five and so on. The last test used only the 1st washer or thread alone.

Data from the testing was analyzed at a thread torque value of 4.5 N-m, which was the thread torque measurement from the torque/tension load-cell. The data was pulled at the time of each run-down and was determined from the computer and acquisition unit that collected the applied torque, tension, and under-head torque (Computer #1). This time reference was then applied to the computer and acquisition unit that collected the strain from the blades (Computer #2). The corresponding strain values were then pulled and entered into a spreadsheet with the appropriate calibration equations for each blade.

The seven individual thread torque values were then summed according Equation 2.15. $T_{\text{Thread } n}$ represents the thread torque on each of the seven threads.

$$T_{Thd} = \sum_1^7 T_{Thread.n} \quad (2.21)$$

2.7 FEA Model Joint Experiment

A joint was created in the laboratory for the sole purpose of validating the FEA model presented and discussed in the next chapter. This joint was created with a bolt and a nut-block, Figure 2.18. The nut-block was 30 mm in length and had 18 mm of non-threaded counter-bore and 12 mm of threads. The threads were created with a tap of size M10 x 1.5 6H6H. The bolt in the joint had a 20 mm diameter flange, 16.5 mm of threads, and 15 mm long shank (Figure 2.18). The threads of the bolt were ground to the upper end of the M10 x 1.5 6g6g range. The under-side of the flange was also ground to ensure that the flange's lower surface was perpendicular to the bolt shank. The material used for the nut-block was 4140 steel heat-treated to 32-36HRC. The major diameter of the bolt was 9.3921 mm and the pitch diameter 8.968 mm.

A 2 mm thick, 25.4 mm square washer was then machined from the nut-block material. The resulting nut and washer were required to perform friction measurements for input into the FEA model of the next chapter. The frictional testing was performed with the aide of a torque-tension load-cell (similar testing discussed in Sections 2.2.1 through 2.2.4. Triflow was applied to the under-head the bolt and nut and threads. This lubricant was used due to its superior adhesion properties on the bare steel and it does not create a thick film. The joint was assembled into the load-cell and the bolt was torqued to 45 N-m. Frictional analysis was performed on the plots at 15 N-m, 30 N-m, and 45 N-m of applied torque.

The top of the hex head and the threaded end of the bolt used above were ground flat and parallel to each-other. An ultrasonic clamp-load measuring device, Figure 2.19,

was glued to the top of the bolt head. The clamp-load measuring device is a piezoelectric sensor that oscillates up and down (in the axial direction) when a DC voltage is applied to it. The instrumented bolt was then tightened into a nut-block, represented by the Figure 2.18, three times. A target torque of 48 N-m was used. The applied torque and developed ultrasonic clamp-load data was then analyzed at applied torques of 15 N-m, 30 N-m, and 45 N-m.

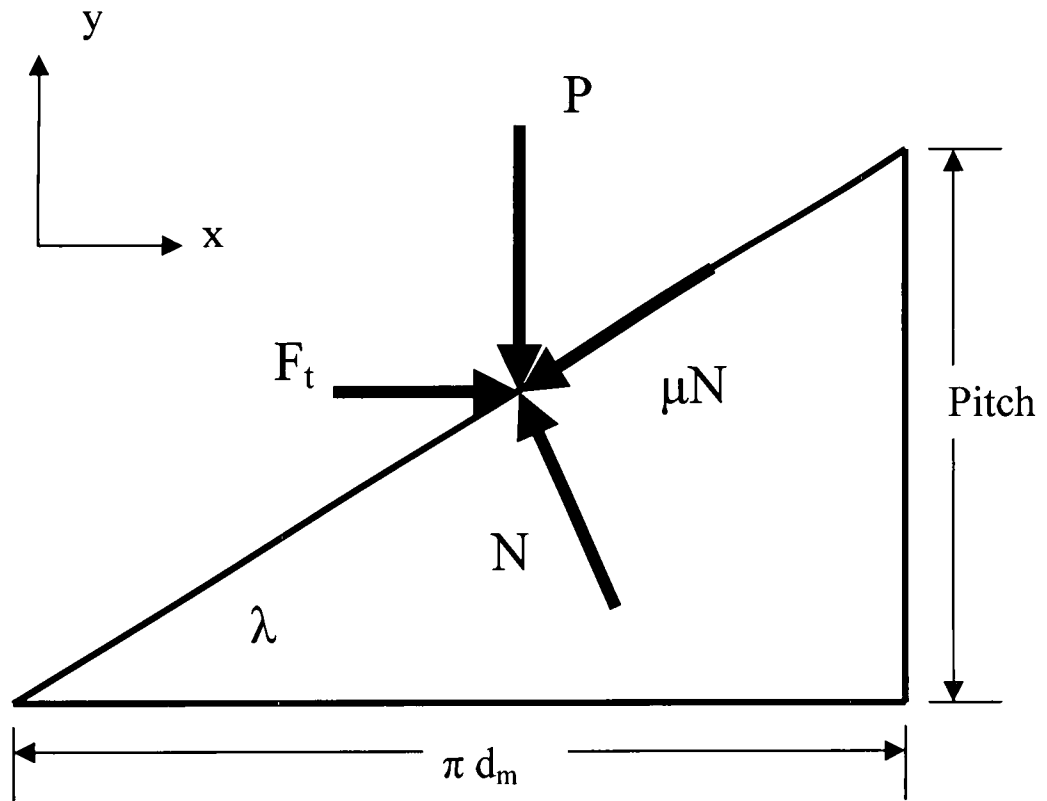


Figure 2.1 Free body diagram of a section of the thread flank. Not shown is the included half angle.

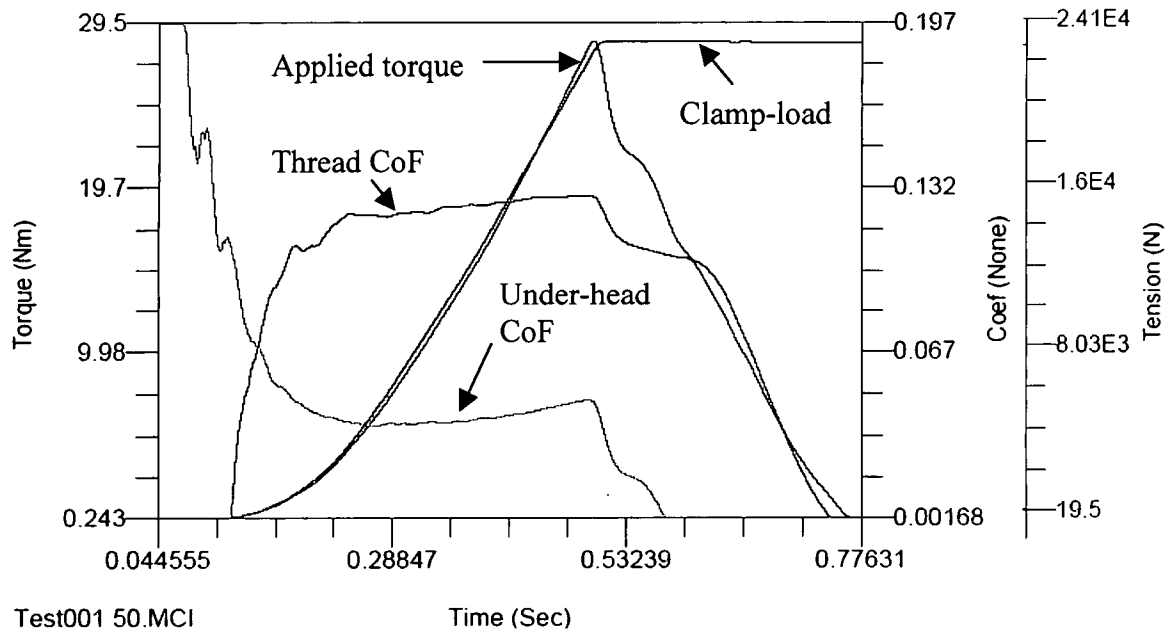


Figure 2.2 Variation of applied torque, developed clamp-load (tension), and thread and under-head CoF plotted with time.

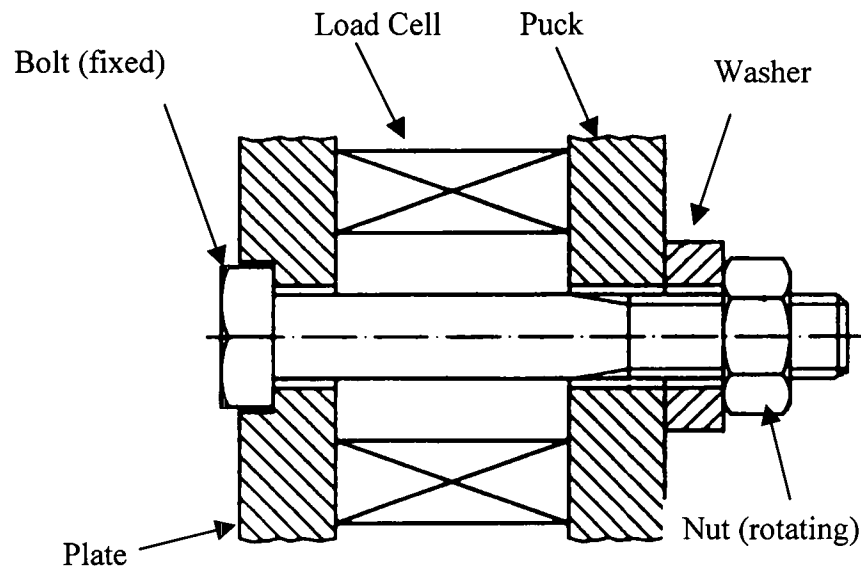


Figure 2.3 Schematic of cross-section of a torque/tension load-cell (the configuration shown is for the development of thread torque).

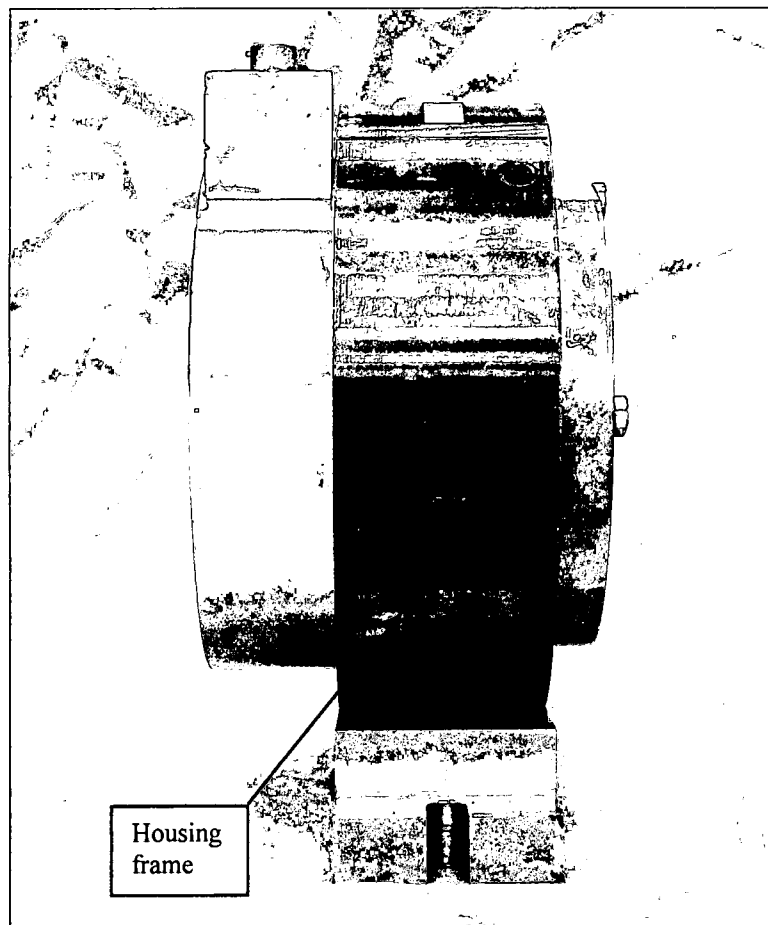


Figure 2.4 Side view of torque/tension load-cell.

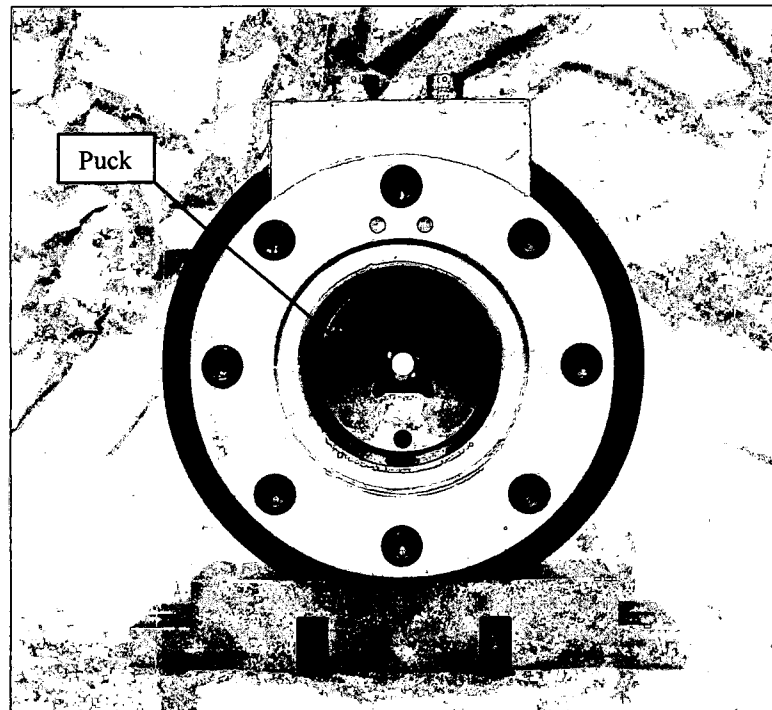


Figure 2.5 Front view of torque/tension load-cell showing the puck on the inside.

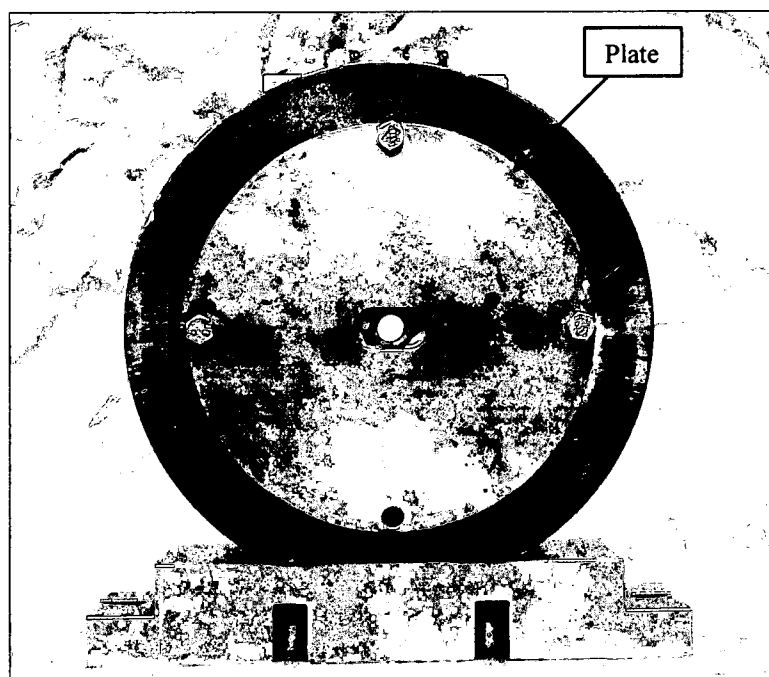


Figure 2.6 Back view of torque/tension load-cell showing the plate.

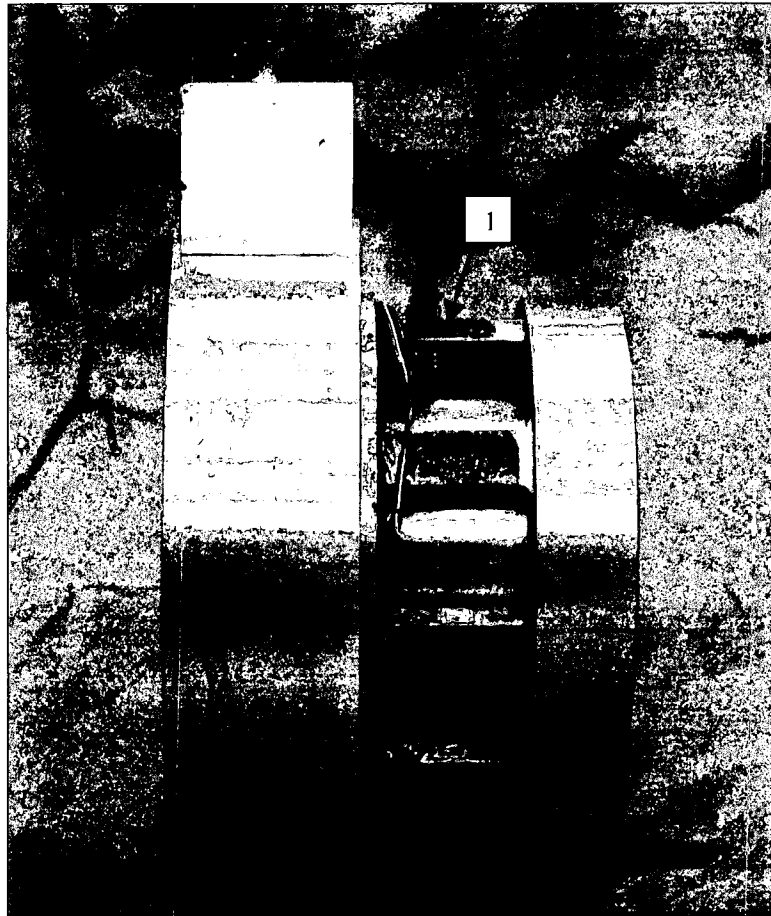


Figure 2.7 Side view of the strain gauged housing of the load-cell. Area 1 shows the gauges.

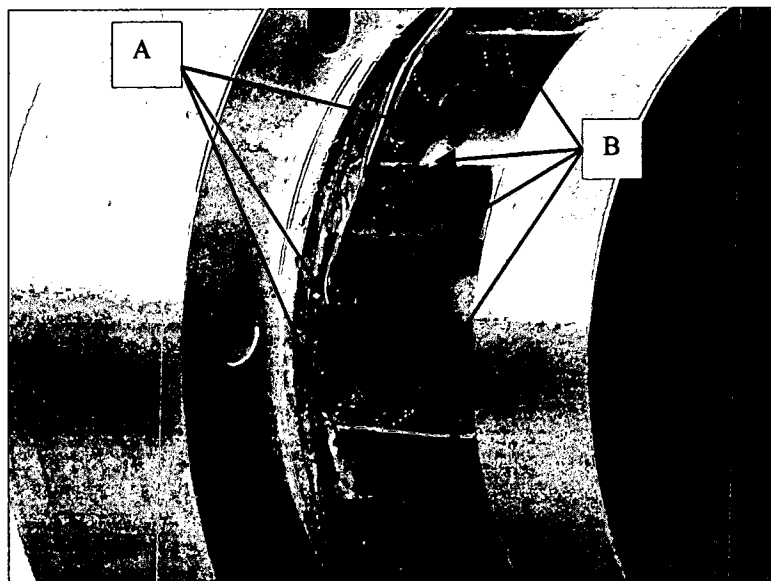


Figure 2.8 Magnified and rotated view of Area 1 from Figure 2.7. Area A shows the torque gauges and Area B shows the tension gauges.

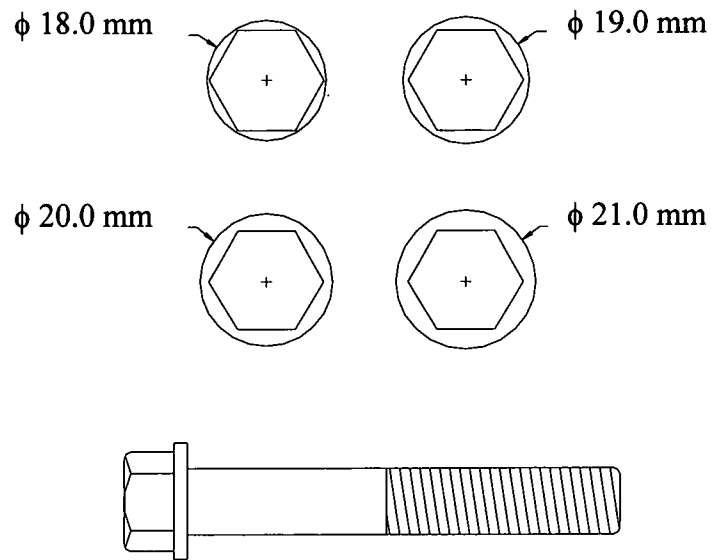


Figure 2.9 Bolt flange diameters.

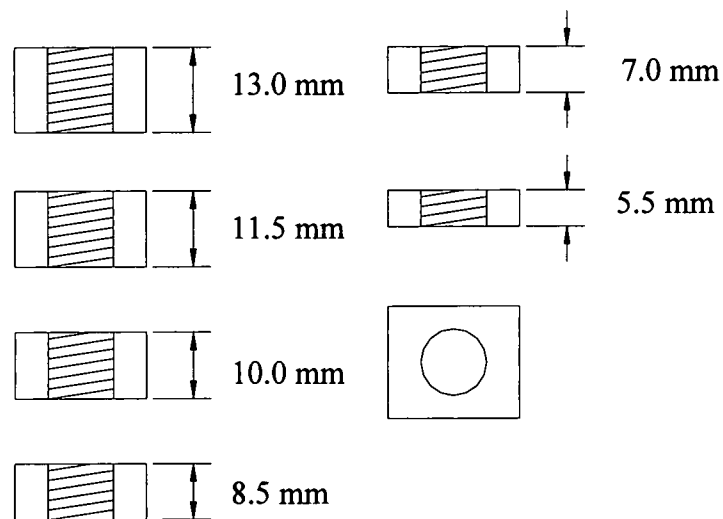


Figure 2.10 Nut heights (length of engagement).

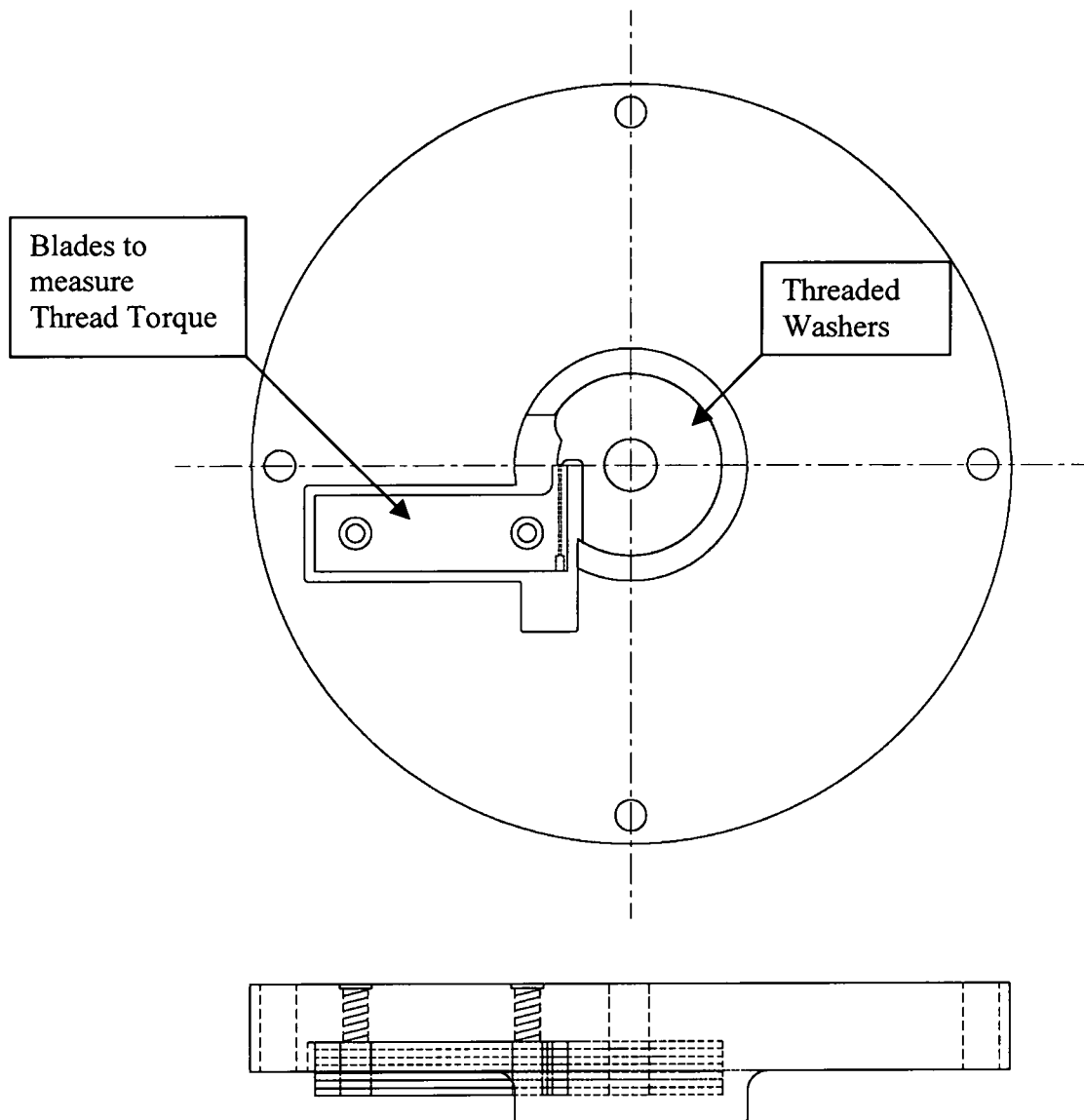


Figure 2.11 Schematic of the fixture holding the blades and threaded washers.

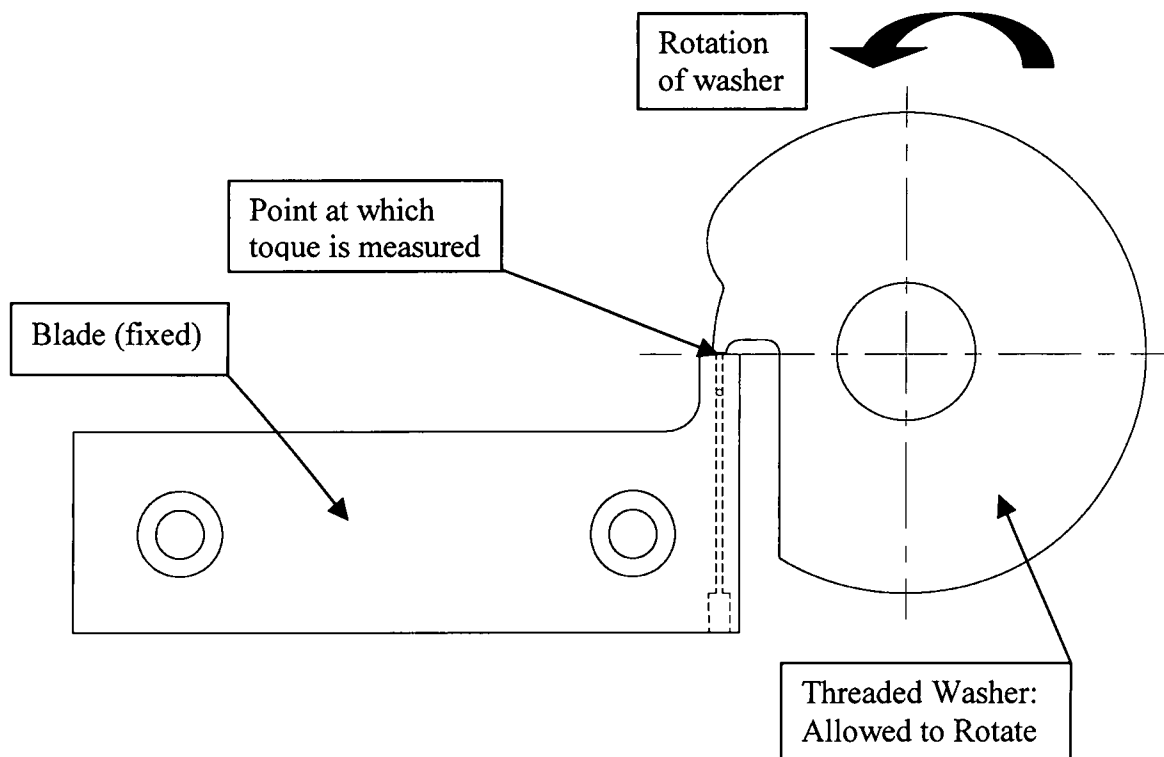


Figure 2.12 Blade and the threaded washer indicating how thread torque is generated.

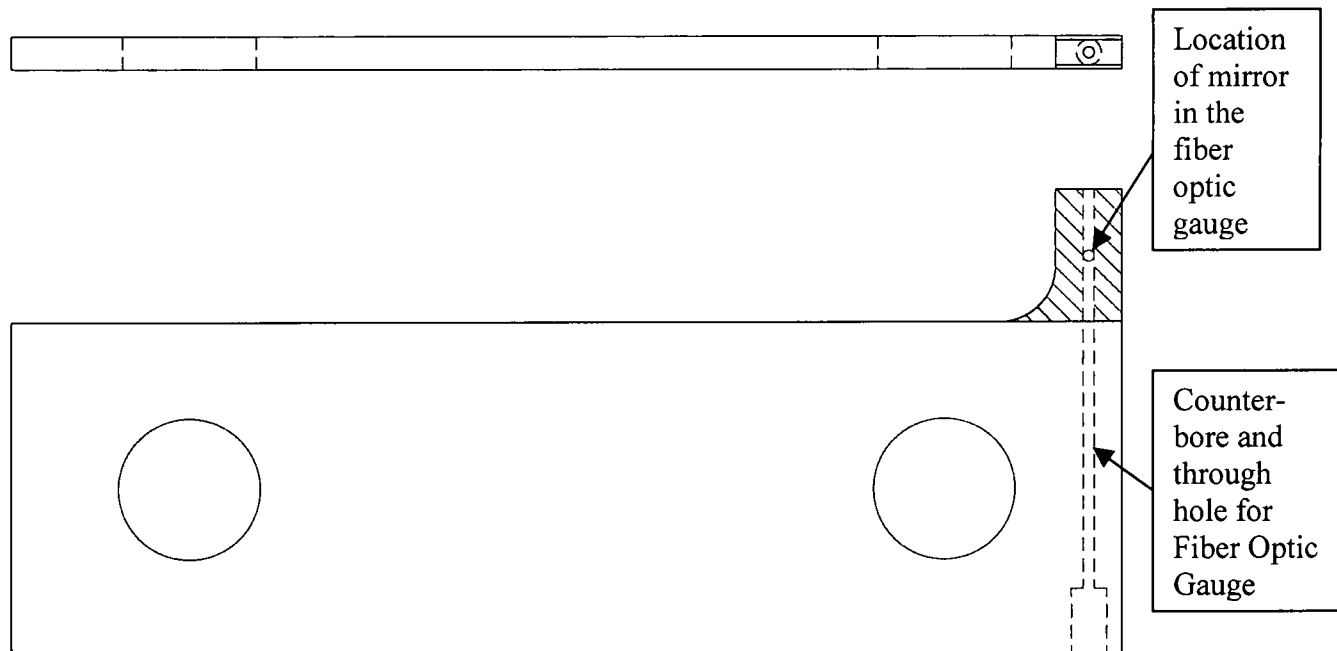


Figure 2.13 Drawing of blade used to measure thread torque.

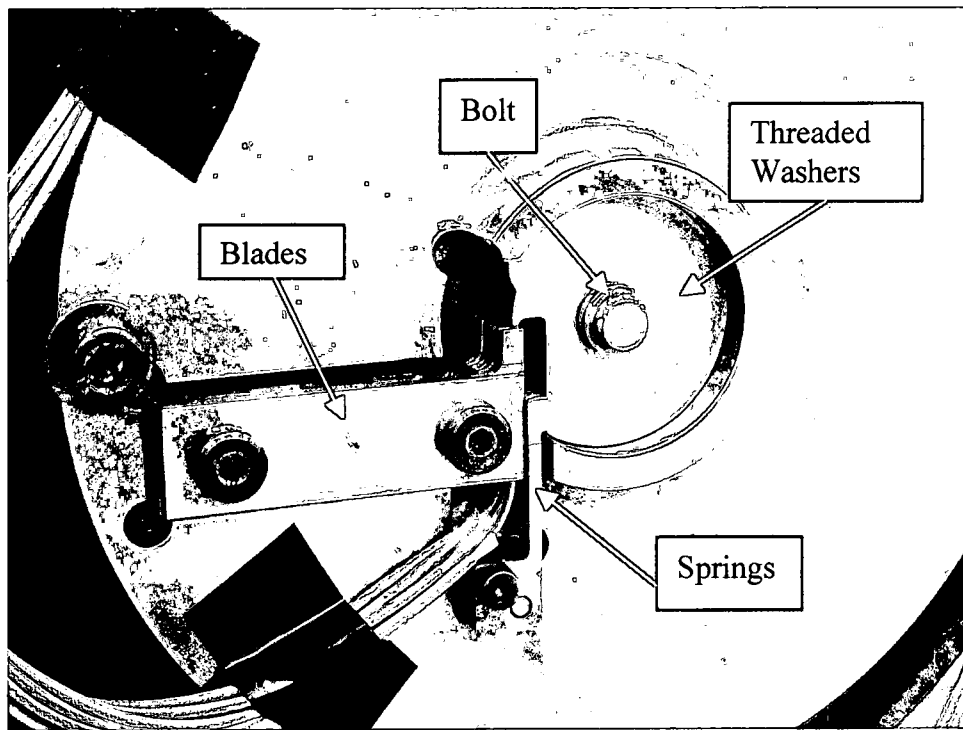


Figure 2.14 Photograph of the thread torque fixture.

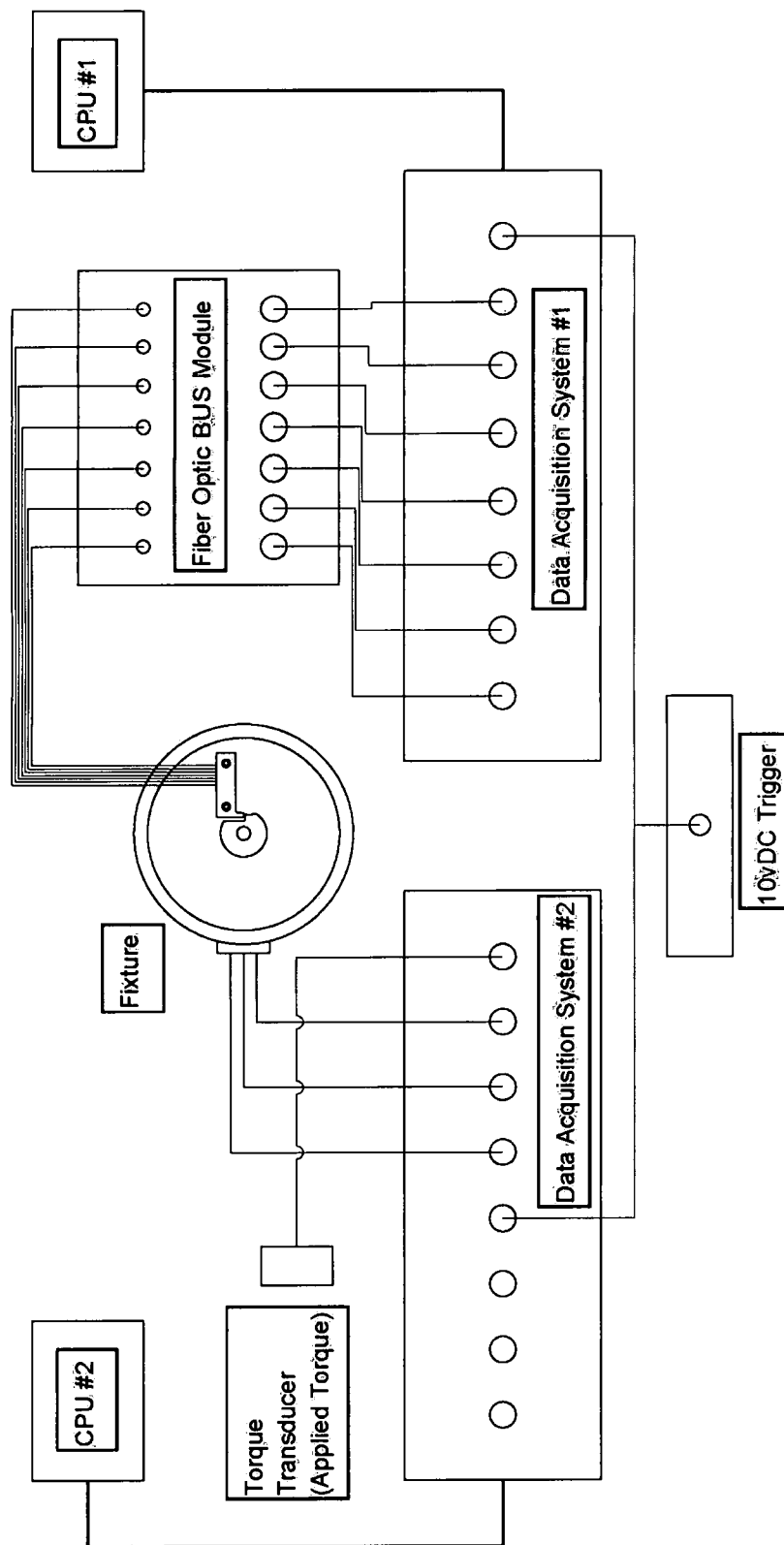


Figure 2.15 Schematic of the signal connections between and computers, data acquisition units, torque transducer, load-cell, fixture, and DC trigger unit.



Figure 2.16 Photograph of the ground non-threaded spacer used as a bearing surface for all calibrated threaded washers.

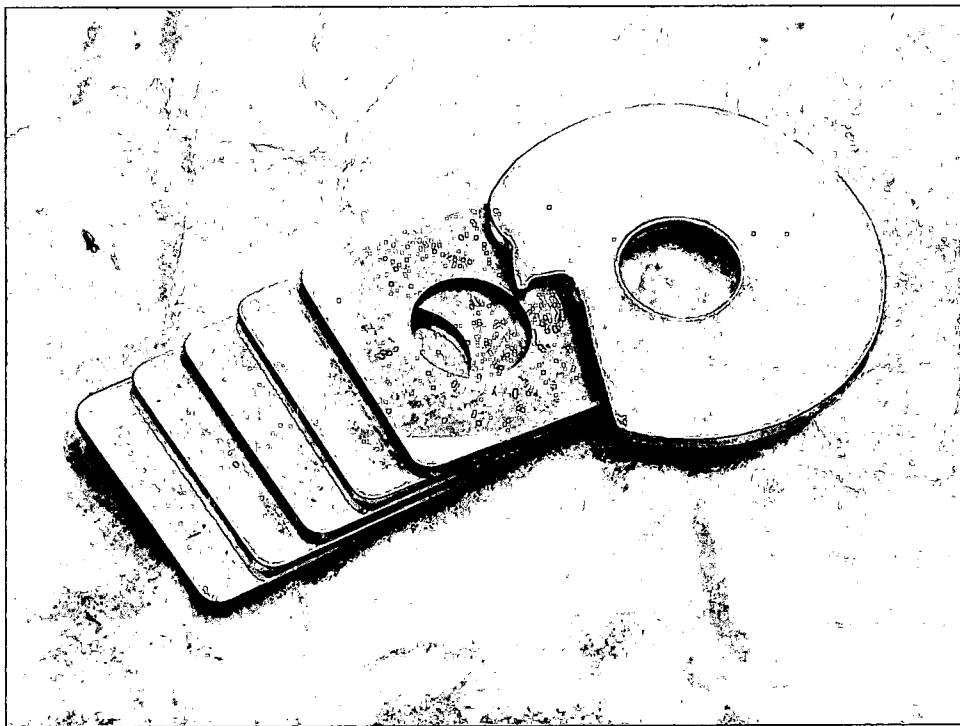


Figure 2.17 Photograph of the ground square and non-threaded washers.

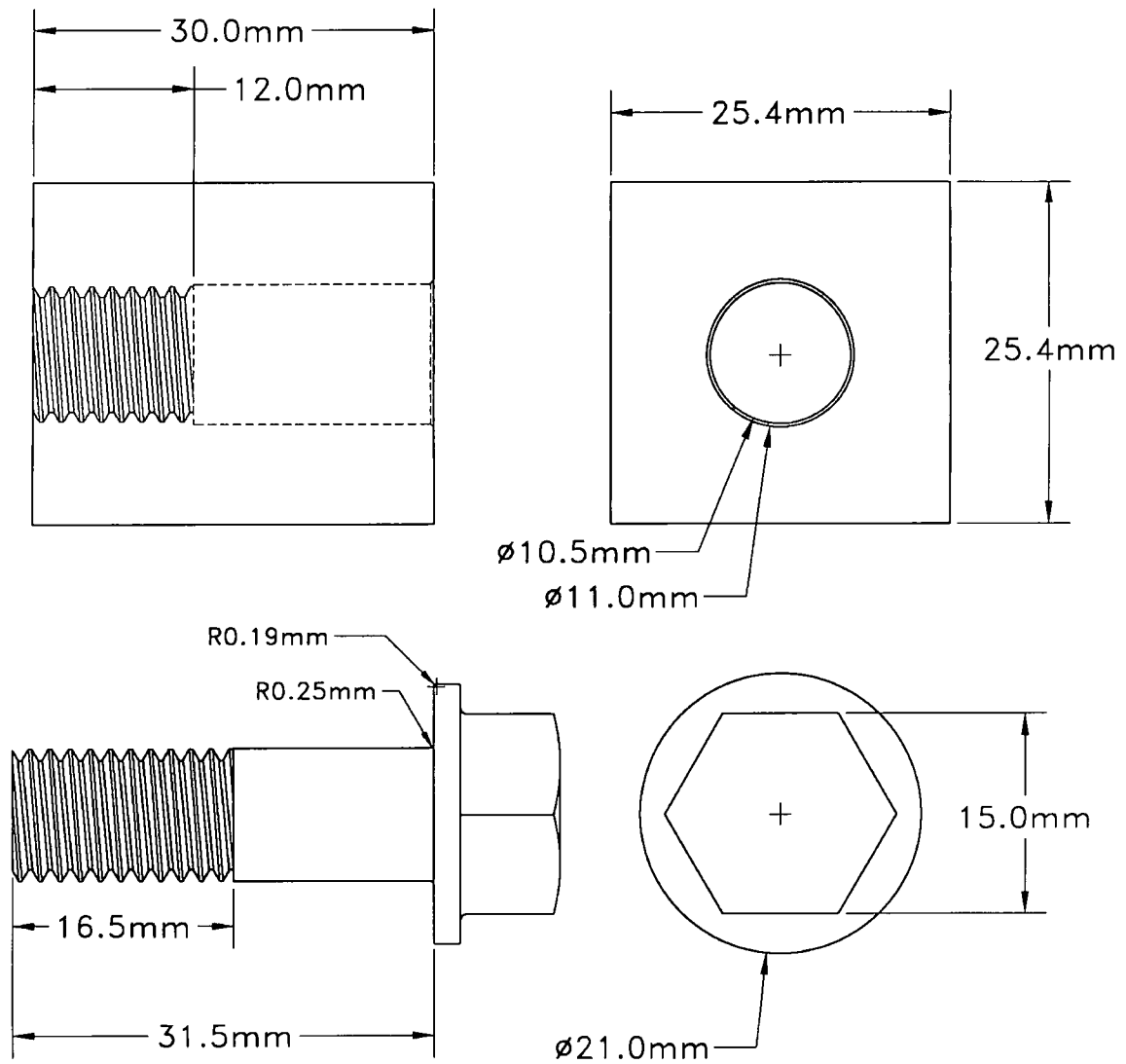


Figure 2.18 Drawing of the bolt and nut-block used for the FEA modeling as well as machining the actual joint.

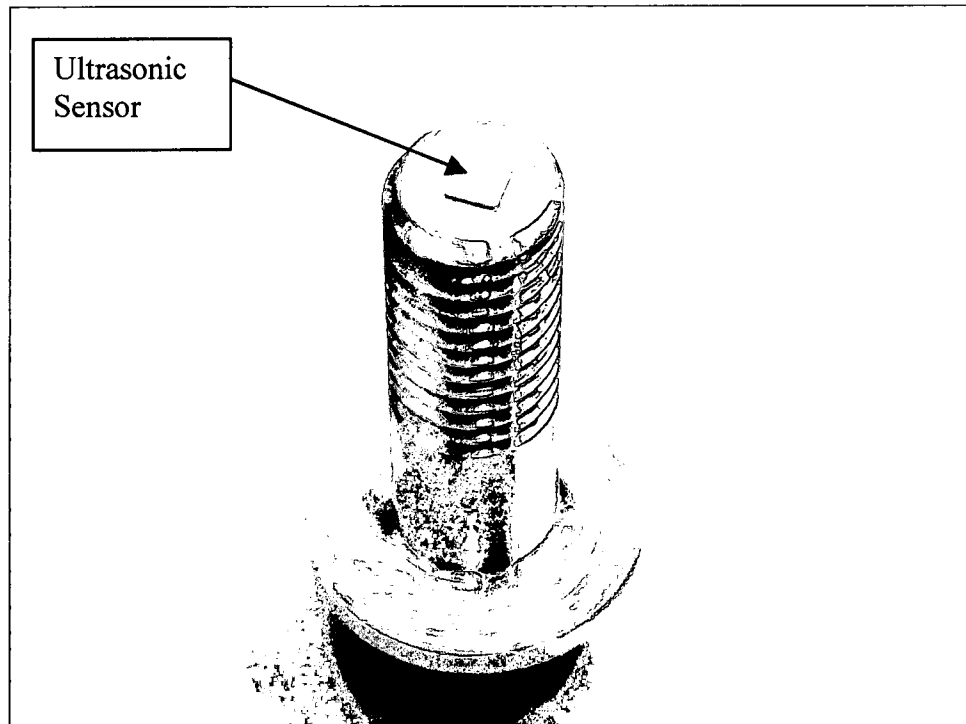


Figure 2.19 Photograph of the bolt used in the FEA model investigation. The ultrasonic sensor is located at the end of the bolt.

Table 2.1 Contact areas of the threads and under-head regions for the M10 x 1.5 threads calculated from geometric dimensions			
Nut Height (mm)	Thread Engagement Area (mm²)	Under-Head Diameter (mm)	Under-Head Area (mm²)
13	131.4	21	80.1
11.5	116.2	20	65
10	101.1	19	51.5
8.5	85.9	18	39.6
7	70.7		
5.5	55.6		

Table 2.2 Programmed Vs actual tightening speed at the target torque of 28N-m	
Programmed Speed (rpm)	Actual Speed (rpm)
25	12
50	20
100	51
150	85
200	92
250	140
300	143
400	35
500	47
600	147
700	224
800	314
900	394
1000	485
1200	608

Table 2.3 Experiment of different material hardness in three hardness levels for each factor from Section 2.5.3

Test Part	Hardness of Test Parts (HRC)		
Bolt	24 – 28	34 - 38	44 - 48
Washer	24 – 28	34 - 38	44 - 48
Nut	24 – 28	34 - 38	44 - 48

Table 2.4 Thread and under-head friction reduction experiment from Section 2.5.4

Test	Thread Condition	Head Condition
1	Dry	Lubricated
2	Lubricated	Dry
3	Dry	Dry
4	Lubricated	Lubricated

CHAPTER III

FINITE ELEMENT ANALYSIS

3.0 Development of the Finite Element Analysis Model

A three dimensional (3D) FEA model has been developed that allows a bolt to be dynamically tightened to a specified torque. The model was patterned after an actual joint that was discussed in Section 2.8. The dynamic coefficient of friction (CoF) values for the thread and under-head regions were measured from the physical tightening of the actual joint. These values were then inputted into the model for accuracy. The results of the model were then compared with the experimental results it was patterned after.

3.1 Model Creation

The FEA model was created using ANSYS v8.1 Mechanical. The FEA joint was patterned after an actual joint created in the laboratory so that the physical parameters and experimental results could be compared with results of the FEA model (Section 2.8). The joint (Figure 2.18) was created within the confines of the ANSYS code and the profiles of both the internal and external threads were established first. The internal threads were anchored by five key points and the external threads by six key points. These points represent the intersection of lines and curves comprising the shape of the actual threads, as per equations established by ANSI/ASME 1.13M 1983 Metric Screw Threads – M Profile [4]. The parameters of internal threads were calculated from Equations 3.1 through 3.7 for the M10 x 1.5 6H6H thread profile, and are given below:

$$\text{Minimum Major Diameter} = \text{Basic Major Diameter} + \text{Major Diameter Allowance} \quad (3.1)$$

$$\text{Minimum Pitch Diameter} = \text{Basic Major Diameter} - 0.649519(p) + \text{Pitch Diameter Allowance} \quad (3.2)$$

$$\text{Minimum Pitch Diameter} = \text{Basic Major Diameter} - 0.64951(p) + \text{Pitch Diameter Allowance} \quad (3.3)$$

$$\text{Maximum Pitch Diameter} = \text{Minimum Pitch Diameter} + \text{Pitch Diameter Tolerance} \quad (3.4)$$

$$\text{Maximum Major Diameter} = \text{Maximum Pitch Diameter} + 0.793857(p) \quad (3.5)$$

$$\text{Minimum Minor Diameter} = \text{Minimum Major Diameter} - 1.082532(p) \quad (3.6)$$

$$\text{Maximum Minor Diameter} = \text{Minimum Minor Diameter} + \text{Minor Diameter Tolerance} \quad (3.7)$$

External thread parameters were calculated using Equations 3.8 through 3.14 for the M10 x 1.5 6g6g thread profile:

$$\text{Maximum Major Diameter} = \text{Basic Major Diameter} - \text{Major Diameter Allowance} \quad (3.8)$$

$$\text{Minimum Major Diameter} = \text{Maximum Major Diameter} - \text{Major Diameter Tolerance} \quad (3.9)$$

$$\text{Maximum Pitch Diameter} = \text{Basic Major Diameter} - 0.649519(p) - \text{Pitch Diameter Allowance} \quad (3.10)$$

$$\text{Maximum Pitch Diameter} = \text{Maximum Pitch Diameter} - \text{Pitch Diameter Tolerance} \quad (3.11)$$

$$\text{Minimum Minor Diameter} = \text{Minimum Major Diameter} - 1.082532(p) \quad (3.12)$$

$$\text{Maximum Rounded Form Minor Diameter} = \text{Maximum Pitch Diameter} - A$$

$$A = \left[0.5 \left(\frac{\sqrt{3}}{2} \right) p + 2(0.125p) \left[1 - \cos \left(60^\circ - \arccos \left(1 - \frac{\text{Pitch Tolerance}}{4(0.125p)} \right) \right) \right] \right] \quad (3.13)$$

$$\text{Minimum Rounded Form Minor Diameter} = \text{Minimum Pitch Diameter} - 0.616025(\text{Pitch}) \quad (3.14)$$

The physical locations of these points are shown in Figure 3.1 for both the internal and external threads. Points A – E are for the internal threads and Points 1 – 6 are

for the external threads. The major diameter of the external threads was set at the maximum limit and minor diameter was set at the minimum limit using the 6g6g tolerance grade and position. The major and minor diameters of the internal threads were set at their respective minimum limits for the 6H6H tolerance grade and position. This created the maximum amount of flank-to-flank contact between the threads. Note that there was surface-to-surface contact between the internal and external threads prior to the execution of the analysis. This was the starting point for the application of the torque to the bolt of the model.

Following the creation of the key points of the profiles of the internal and external threads, flank surfaces of the threads were created using the major and minor diameters of both internal and external threads as shown in Figures 3.2 and 3.3, respectively. The angular extent of these surfaces was 45° along the path of the helix. Once established, they were then repeatedly copied and stacked on top of each other to create a seamless thread helix (Figures 3.4 and 3.5).

The solid portion of the internal threads was created by first adding the internal threaded surfaces to the inner diameter of a hollow cylinder. A major difference between this model and the static models discussed in Section 1.5 is that the internal threads in the current model have been truncated or cut at the top and bottom ends. This is representative of what occurs in an actual joint. Figure 3.6 shows an internal thread before (Fig. 3.6a) and after ((Fig. 3.6b) thread cutting operation was performed. Figure 3.6a represents the internal thread that was used by all the researchers of the static FEA researchers. Once the cuts were made, the internal threaded nut was created by attaching all the surfaces. The resulting solid was 12 mm in height which allowed for an eight

thread internal thread engagement. This internally threaded solid was then “glued” (ANSYS term for holding two solids together instead of adding them together) to the nut-block, Figure 3.7. Note that the internal thread was created separately from the nut-block so that the two solids could be meshed differently; higher density in the internal threads where the critical analysis was required, and lower density mesh in the nut-block, where the analysis results were less critical.

The creation of the external threads was performed by adding the external threaded surfaces to a hollow cylinder, Figure 3.8a. A solid cylinder was then added to this threaded solid, Figure 3.8b. The hollow threaded cylinder was created so that a denser mesh could be generated in the threaded region, and a coarser mesh in the center section of the attached solid cylinder, where critical analysis was not required. The threaded solid was then cut to produce 10.5 threads.

The remaining parts of the bolt such as the shank, hexagonal head, and the flange were added to the external threads (Figure 3.9). Similarly, the bearing surface of the nut-block was created then added to each other. The bearing surface was subsequently glued to the existing nut block, Figure 3.10. The parts that made up the bolt were then glued together as to prevent rigid body motion when the model is executed. The gluing versus adding is a modeling technique which allows for different mesh densities at different locations and thus the appropriate accuracy.

Each of the 25 solids that comprise the model was then meshed. The critical areas of the model, such as the internal and external threads were meshed with SOLID186, 20 node tetrahedral elements. The less critical areas were meshed with SOLID187, 10 node tetrahedral elements. Both types of elements allowed for three-dimensional linear and

non-linear movements and can be used in complex solids. The bolt's threads were meshed by evoking the SMRT 7 command at the root of the minor diameter and this command allowed the software to mesh the remaining solid of bolt thread. The internally threaded block was meshed by evoking the ESIZE 5 command with a SMRT 8 setting. The meshed portions of both the internal and external threads are shown, Figure 3.11a and b, respectively. The bolt flange was meshed with the SOLID186 elements using the SMRT 2 command and the bearing surface of the nut-block was meshed with the 186 elements using SMRT 1 command. Table 3.1 shows the number of elements as well as the number of nodes for each volume in the joint. The completed model had 310,862 elements, 455,236 nodes, and 1,366,000 degrees of freedom (DoF).

Two sets of contacts were created in the joint model; (1) contact between the internal and external threads and, (2) contact between the bearing surface of the nut-block and the flange of the bolt, as shown by the Areas A and B of Figure 3.12. Figure 3.13 shows the image of a portion of the engaged threads; here the internal threads are on the upper side. In both sets of contacts, sliding was allowed in all directions. Since the model was created with surface-to-surface contact established in the thread and under-head regions, it ensured that no gaps were present. The latter prevented the ANSYS algorithm from trying to determine where the contact pairs were located and thus unnecessarily using computer time and resources. The sides of the nut-block were constrained in the x, y, and z directions to prevent rigid body motion of the model while a torque was being applied to the bolt. The center of the torque was a pilot node (pivot point for the torque) and was located in the center of the bolt head, on the z-axis. The material used for both the bolt and the nut-block was steel with an elastic modulus and Poison's Ratio of

203,402.5 MPa and 0.295, respectively. The material properties of both parts were considered isotropic and elastic.

The assumptions made for this model were the following:

- 1) The threads were perfect; no thread form errors such as errors in pitch, included angle, taper, or out-of-roundness were present.
- 2) The flange of the bolt was perpendicular to the shank of the bolt.
- 3) The friction coefficient in the threads and under-head were experimentally measured, thus were considered dynamic; tightened at 100 rpm while developing clamp-load.
- 4) The torque applied to the sides of the hexagonal head of the bolt was uniform.

The model was created and solved on an HP x4000 Workstation which contained dual Xenon 1.2GHz processors with 2GByte of RAM. One load-step, with a minimum of 10 sub-steps, was used to solve the model.

3.2 Model Execution

Three separate analyses were conducted using this model. The difference in these analyses was the amount of the applied torque: 45 N-m, 30 N-m, and 15 N-m. These torque values were used to verify the results of the model with the experimental data. The frictional values for the two contact regions, under-head and thread, were experimentally determined in Section 2.8 for each of the torque values and are listed in Table 3.2. These values represent the changes associated with the thread pressure and speed at which the fastener was tightened. The manner in which the ANSYS solved this model was that it applied the torque all at once and there was no tightening speed, thus the bolt

immediately supported the applied torque.

Following the convergence of the model, the flanks of the internal threads that support the load were analyzed. This was accomplished by first isolating the areas on the surface of the internal thread flanks that were in contact with the external threads of the bolt. The elements and nodes associated with these internal thread flank areas were then identified. The load and elongation in the “z” or axial direction of the bolt were summed and plotted for the isolated nodes. The clamp-load and elongation of the bolt were then compared with the experimental data to determine the accuracy of the model.

3.3 Load Distribution on the Threads

A second finite element model was created to investigate the distribution of both the load and pressure on each engaged thread. Here, thread pitches; 1.5 mm, 1.25 mm, and 1.0 mm which are defined as coarse, fine, and super fine were used on an M10 diameter bolt. In addition, levels of contact between the internal and external threads: defined as maximum contact, nominal contact, and minimal contact were used for each of these pitches. This analysis was conducted to determine if the load distribution is affected not only by the thread pitch, but also by the amount of contact between the internal and external threads.

To obtain the maximum material contact, the major and minor diameters of the external threads were set to the maximum limits while the major and minor diameters of the internal threads to the minimum limits. This differs from the Section 3.1 analysis where the major diameter of the external threads was at the maximum limit and the minor diameter set at the minimum limit. Each fastener size and pitch has corresponding maximum and minimum values for the major and minor diameters. The models for the

minimum contact level required setting the major and minor diameters of the external threads to the minimum limits and the major and minor diameters of the internal threads to the maximum limits. The mean values of the major and minor diameters of both the internal and external threads were used to obtain the nominal contact conditions. Figures 3.14, 3.15, and 3.16 show images of the thread contact for each configuration level. Figure 3.14 also shows the difference between the flank area of the internal thread and the area of contact between the internal and external threads.

The flanks of the internal threads that supported the clamp-load were isolated from the joint and then grouped to obtain the total contact area for all the eight threads (Figure 3.17). Each thread is represented by a different color. To obtain the actual physical condition of the nut, the 1st and 8th threads have been machined. The image of Figure 3.17 is for the maximum contact level for the 1.5 mm pitch threads. Figure 3.18 shows a bar chart showing the total contact area for the minimum, nominal, and maximum contact levels, grouped by the pitch size. The chart represents the actual area where the internal and external threads touched one another during tightening. Note that the contact area increases with both increasing pitch size as well as contact level. Figure 3.19 shows a bar chart for the contact areas for the 1st engaged thread for all contact levels, grouped by pitch size.

As the pitch of the external thread changes, the pitch diameter and cross-sectional area of the bolt change as well. Figure 3.20 is a bar chart showing variation in the bolt's cross-sectional area for each contact level and the pitch size. The cross-sectional area was determined by Equation 3.15. [23]. Here $d_{p \min}$ is the minimum pitch diameter.

$$A_s = 0.7854(d_{p \min} - 0.268867 p)^2 \quad (3.15)$$

Note that as the pitch of the threads increases, the cross-sectional area of the bolt decreases. For the minimum contact level, the pitch diameter was established at the lowest point of the tolerance range. Similarly, for the maximum contact level, the pitch diameter was established at the upper point of the range. For the nominal contact level, the mid-point of the pitch tolerance range was used.

The load on each thread was calculated by summing the forces in the axial direction at the flanks of the internal thread that were in contact with the external threads. The load on each of the eight individual threads was summed in the axial direction in order to determine both the clamp-load carried by each of the individual threads as well as the total clamp load on all eight threads. The load on each surface was divided by the actual contact area between the internal and external threads to get the contact pressure.

A third FEA model was created in order to duplicate the results of the previously research conducted under static loading conditions. This was conducted using a 1 inch – 8TPI thread; a metric equivalent to this fastener is a M25 x 3.0 mm thread. But this size of fastener could not be created with the current model; therefore, a M10 x 1.75 mm fastener at the maximum contact level was substituted because it was the maximum allowable size that could be used with this model. Following the convergence of the model, the load distribution was calculated for each of the eight engaged threads and compared with the results with the previous research.

3.4 FEA Model for the Seven-Thread Engagement

A 4th 3D dynamic FEA model was created to match the experiments conducted in Section 2.8. Note that this was a seven-thread engagement, in which the thread torque on each individual thread was measured. This model was similar to the ones discussed in

Sections 3.1 and 3.2 with the exception the nut had seven threads instead of the eight threads. The applied torque to the bolt was 9.58 N-m and the thread and under-head CoF values were 0.143 and 0.154 respectively.

Finite element analysis was used to calculate the load carried by each thread and experimental results were then used to determine the thread torque on each thread. Using both sets of results, the thread coefficient of friction was determined from Equation 2.18.

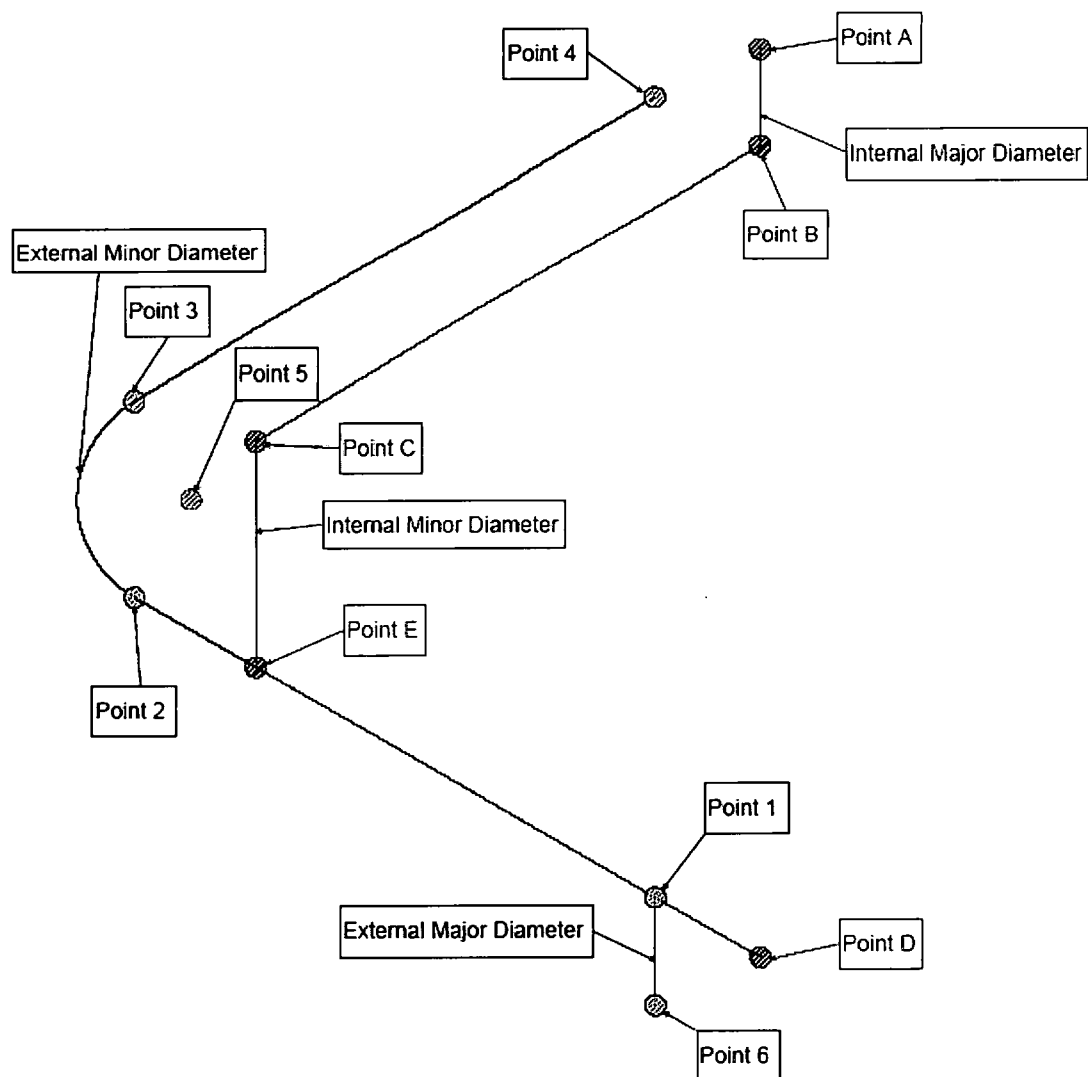


Figure 3.1 Locations of the key points used to establish both the internal and external thread profiles.

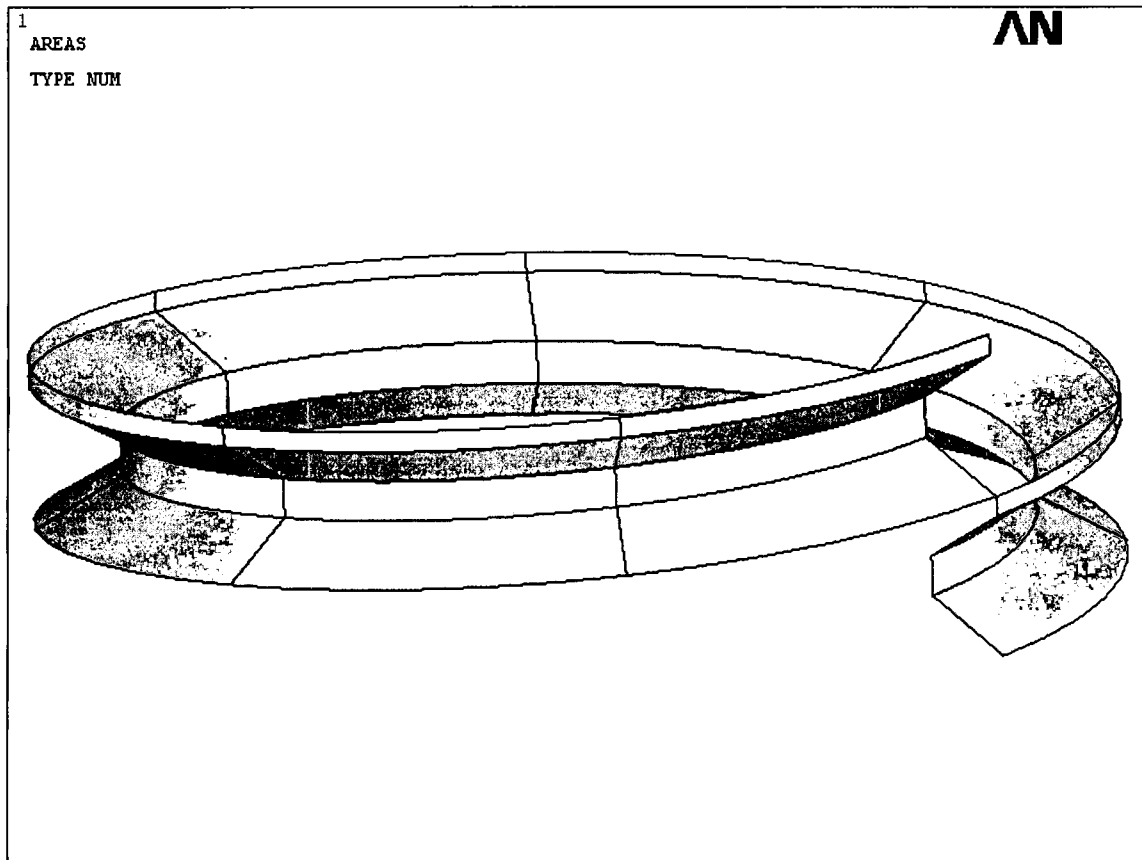


Figure 3.2 ANSYS surface image of the 1st thread of the nut block.

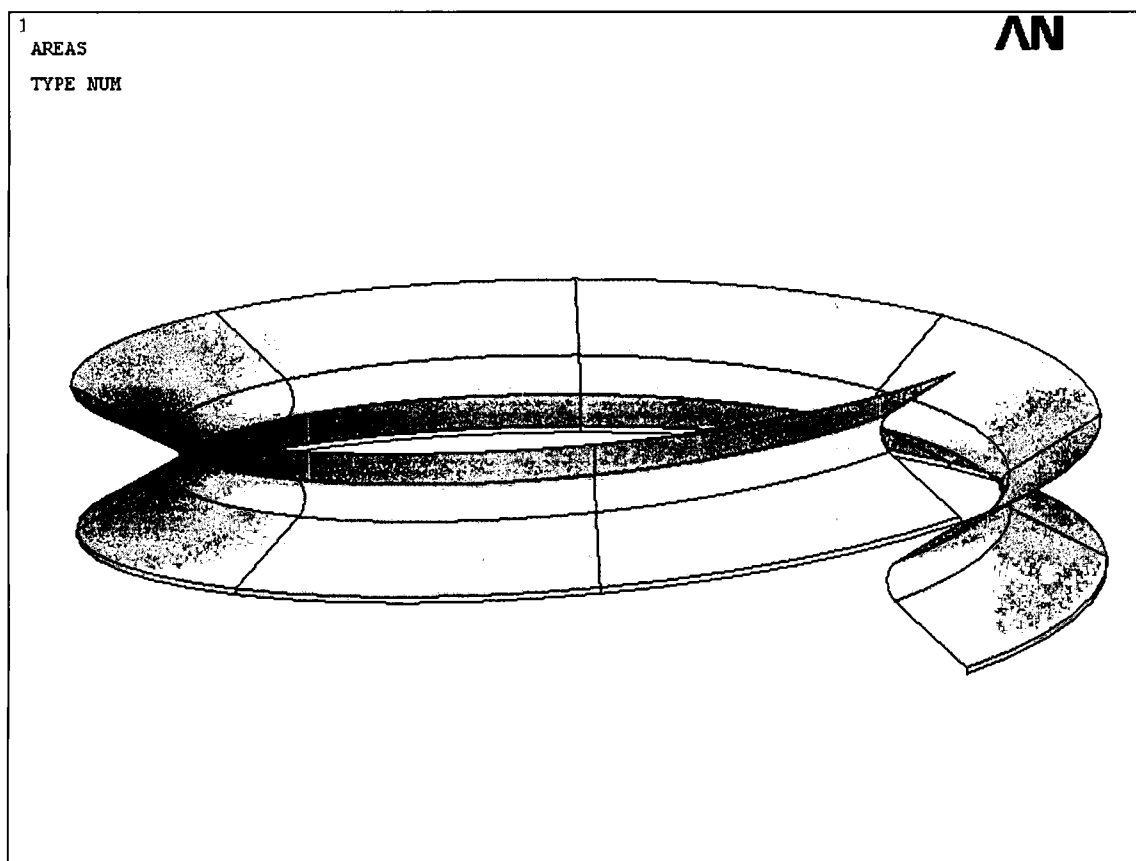


Figure 3.3 ANSYS surface image of the 1st thread of the bolt.

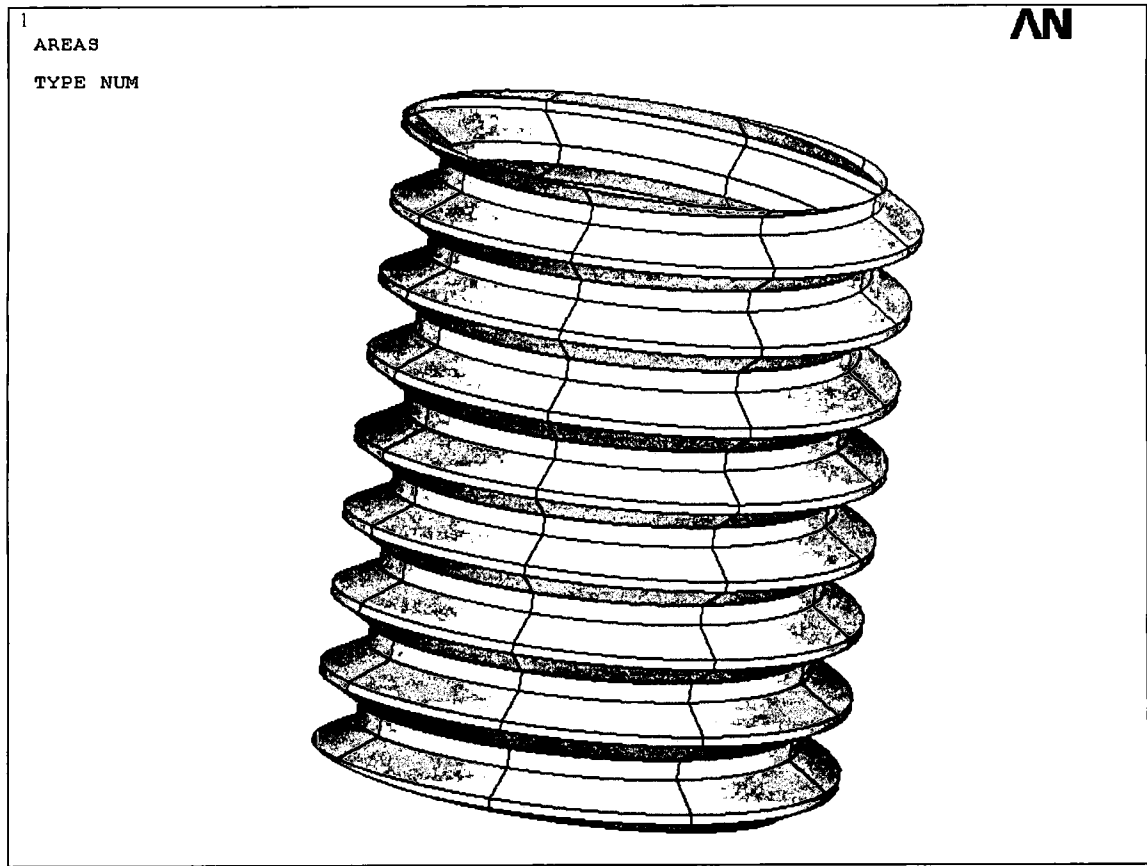


Figure 3.4 ANSYS surface image of the internal threads after copying and slicing at the top and bottom.

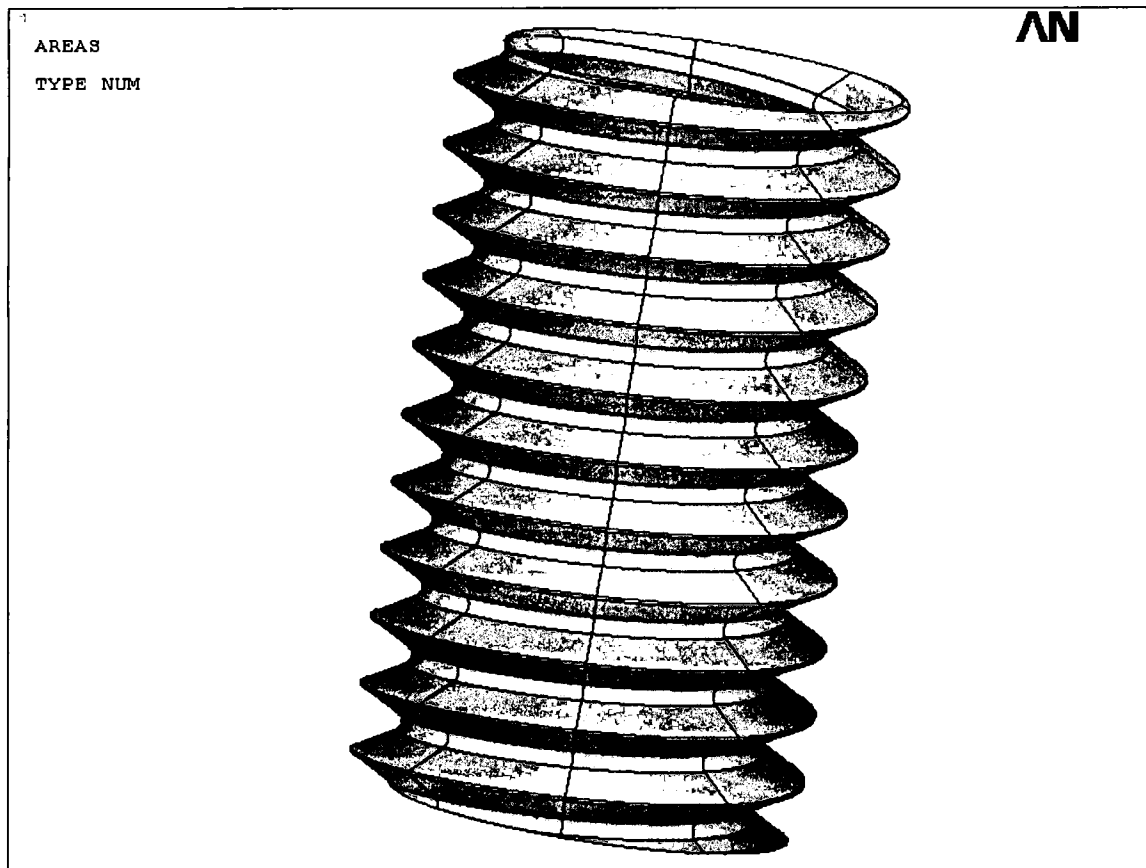


Figure 3.5 ANSYS surface image of the external threads after copying and slicing at the top and bottom.

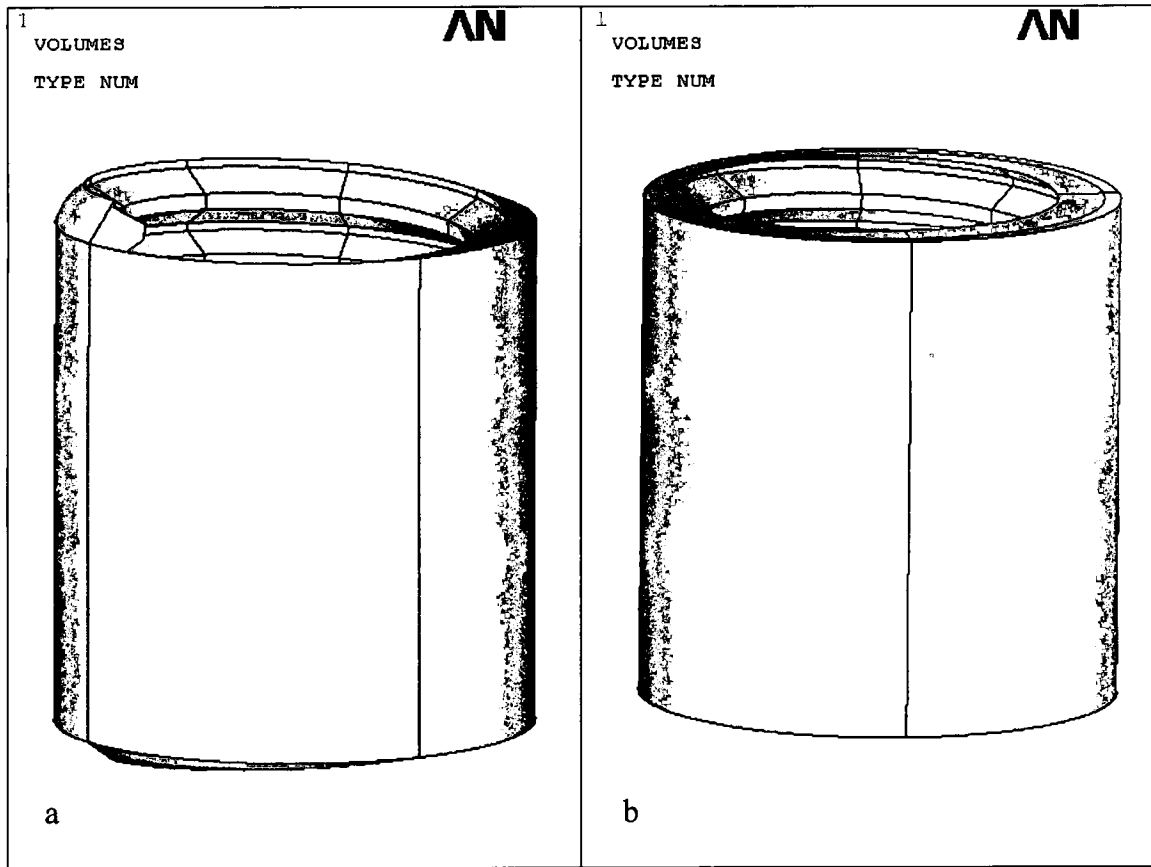


Figure 3.6 ANSYS solid image of the internal threads before (a) and after (b) removal of the top and bottom parts.

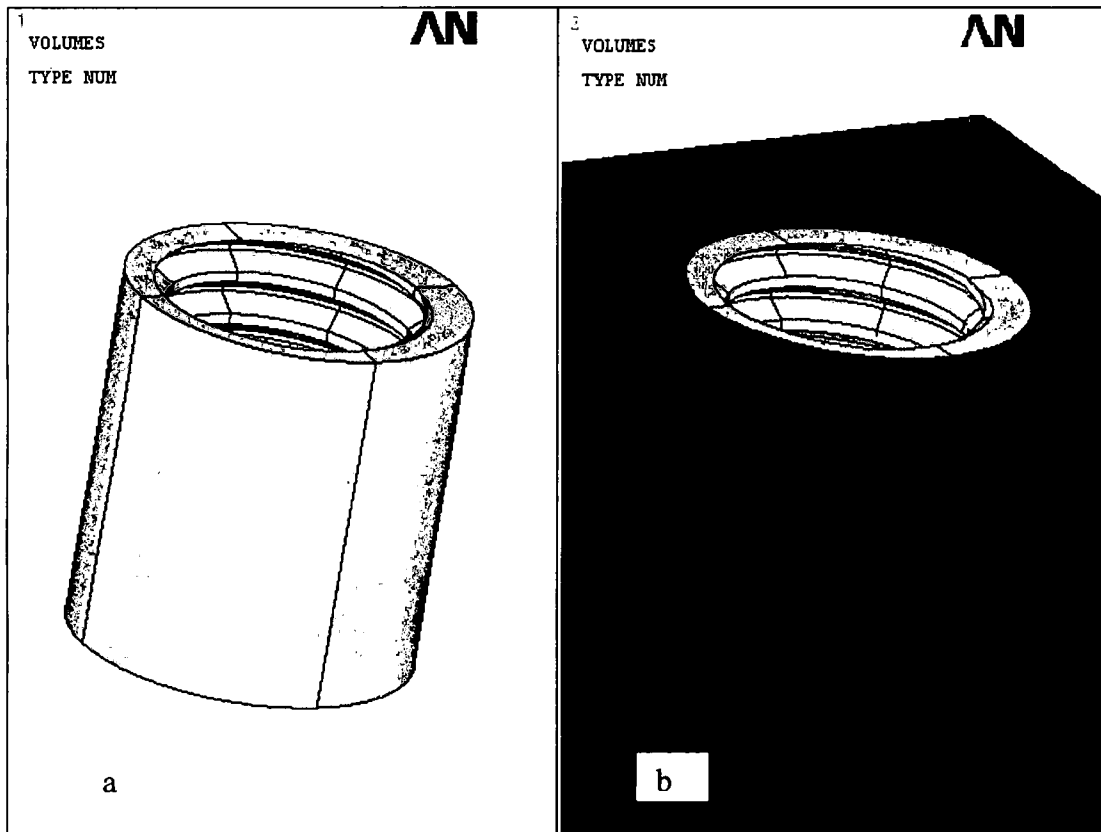


Figure 3.7 ANSYS image of the two solids creating the internal threads of the model. The solid in (b) is the bottom of the nut-block.

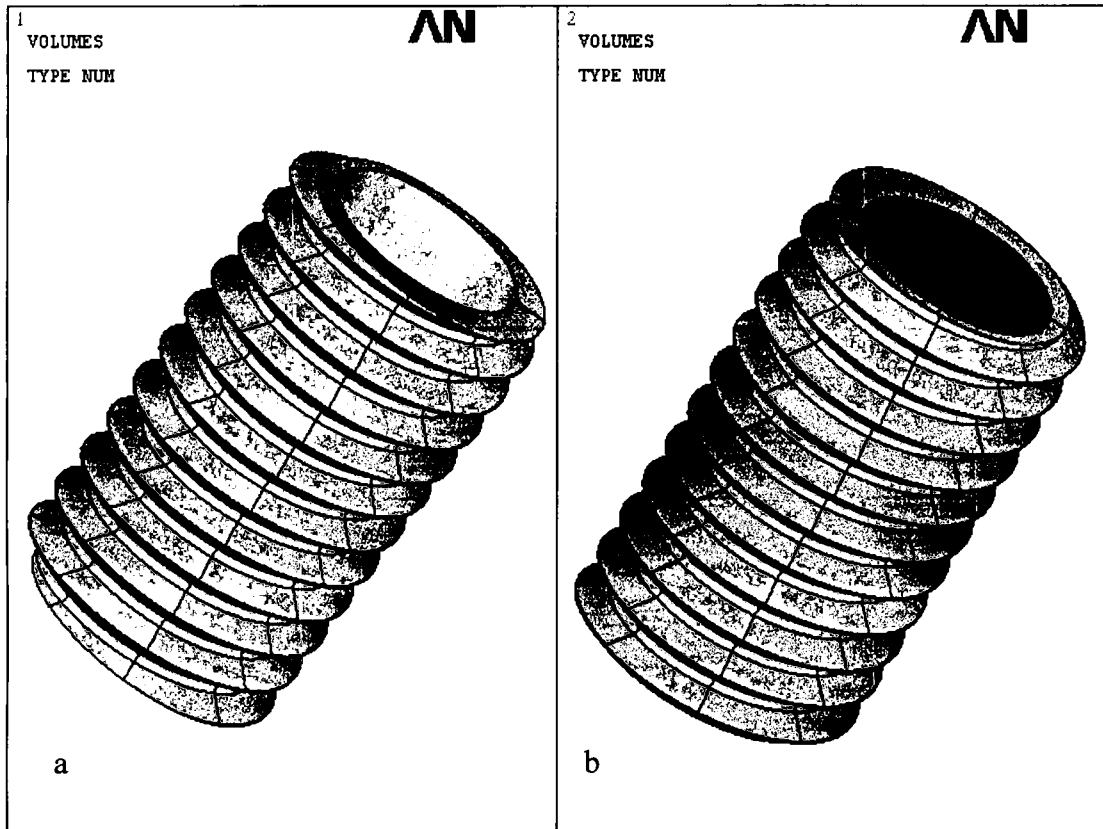


Figure 3.8 ANSYS image of two solids used to create the external threads of the model. Image (a) shows the threaded hollow cylinder and (b) the final solid cylinder.

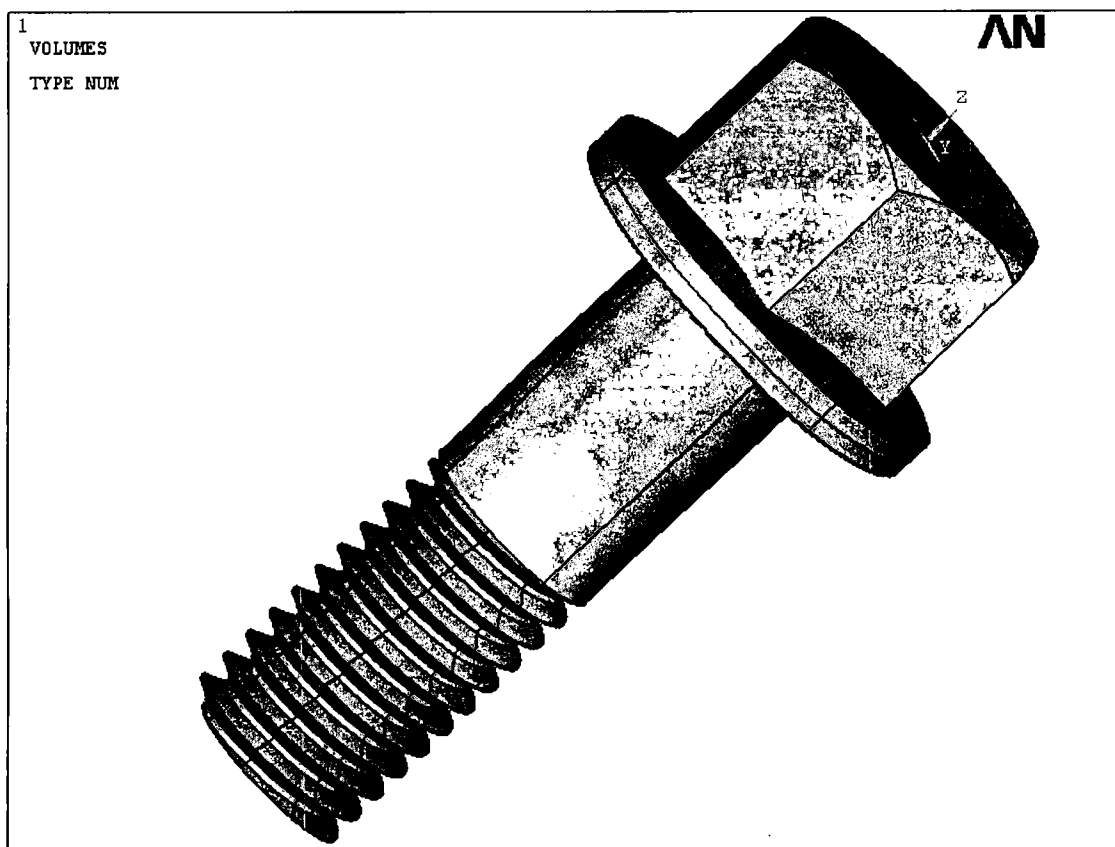


Figure 3.9 ANSYS image of the bolt.

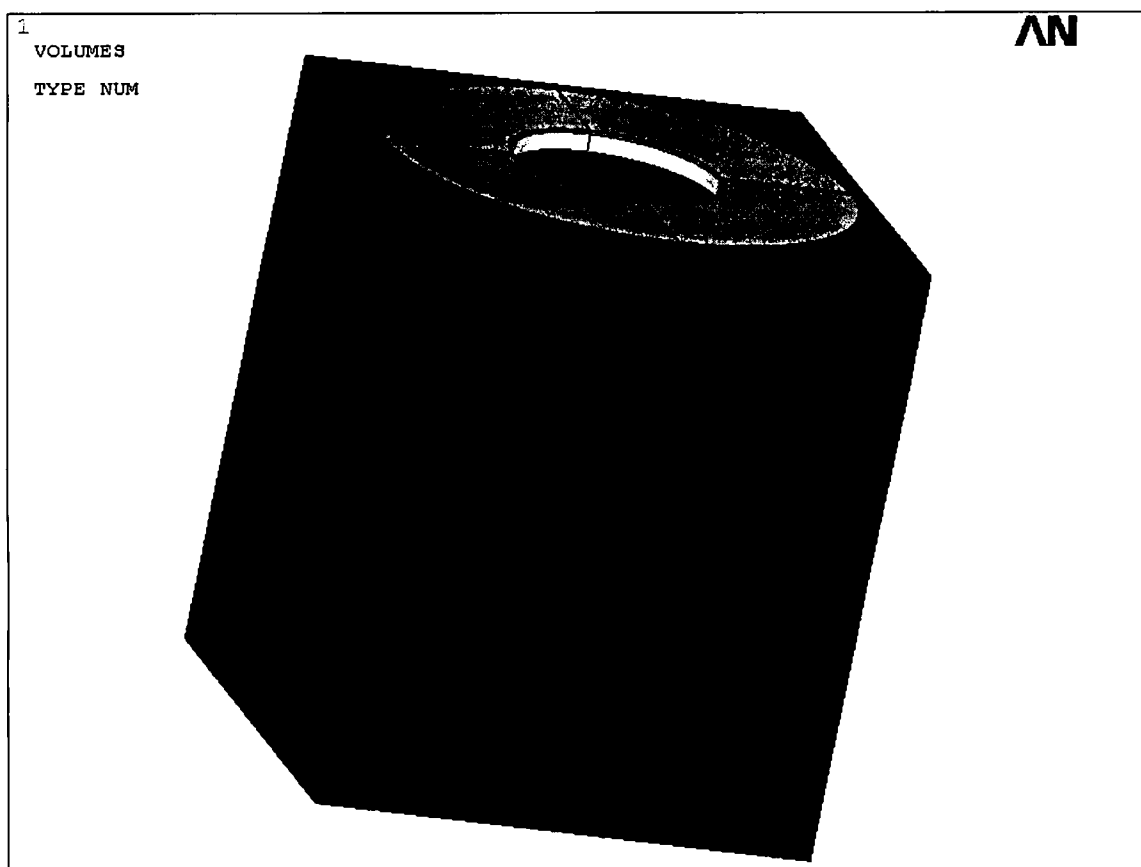


Figure 3.10 ANSYS image of the solids creating the entire nut-block assembly.

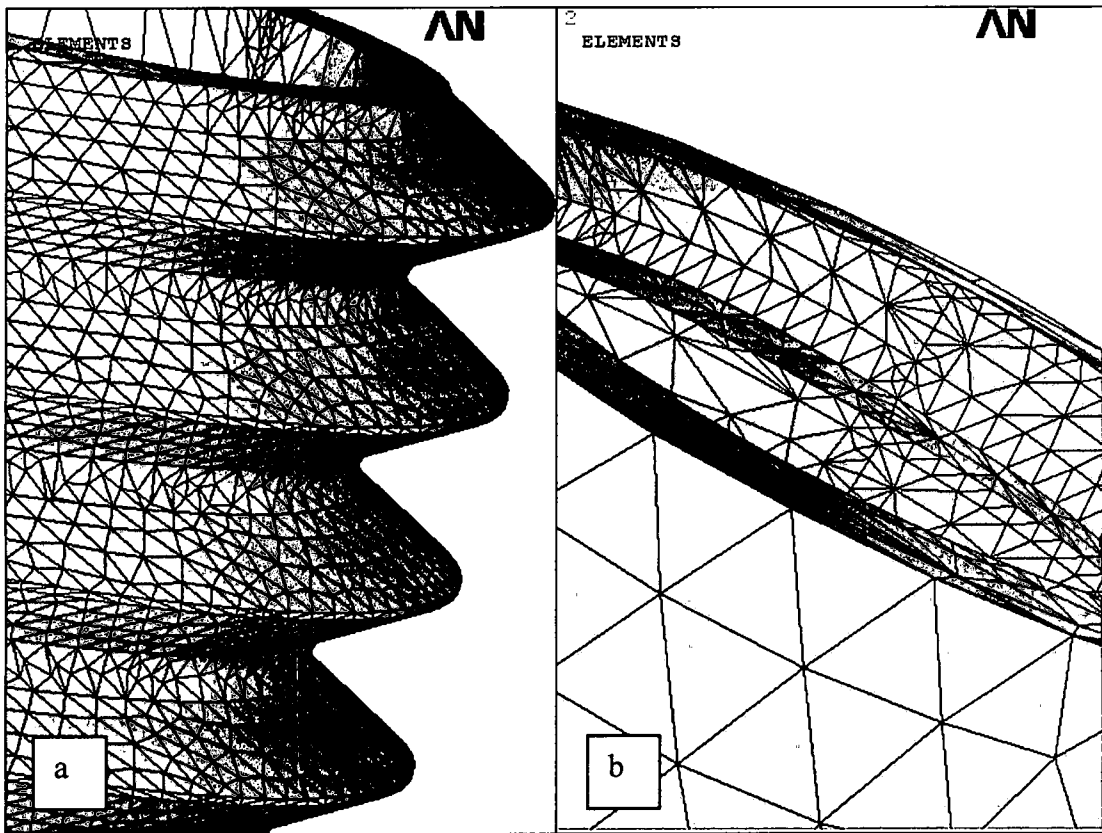


Figure 3.11 ANSYS FEA model of the external threads (a) and the internal threads(b) created using the SOLID186 elements.

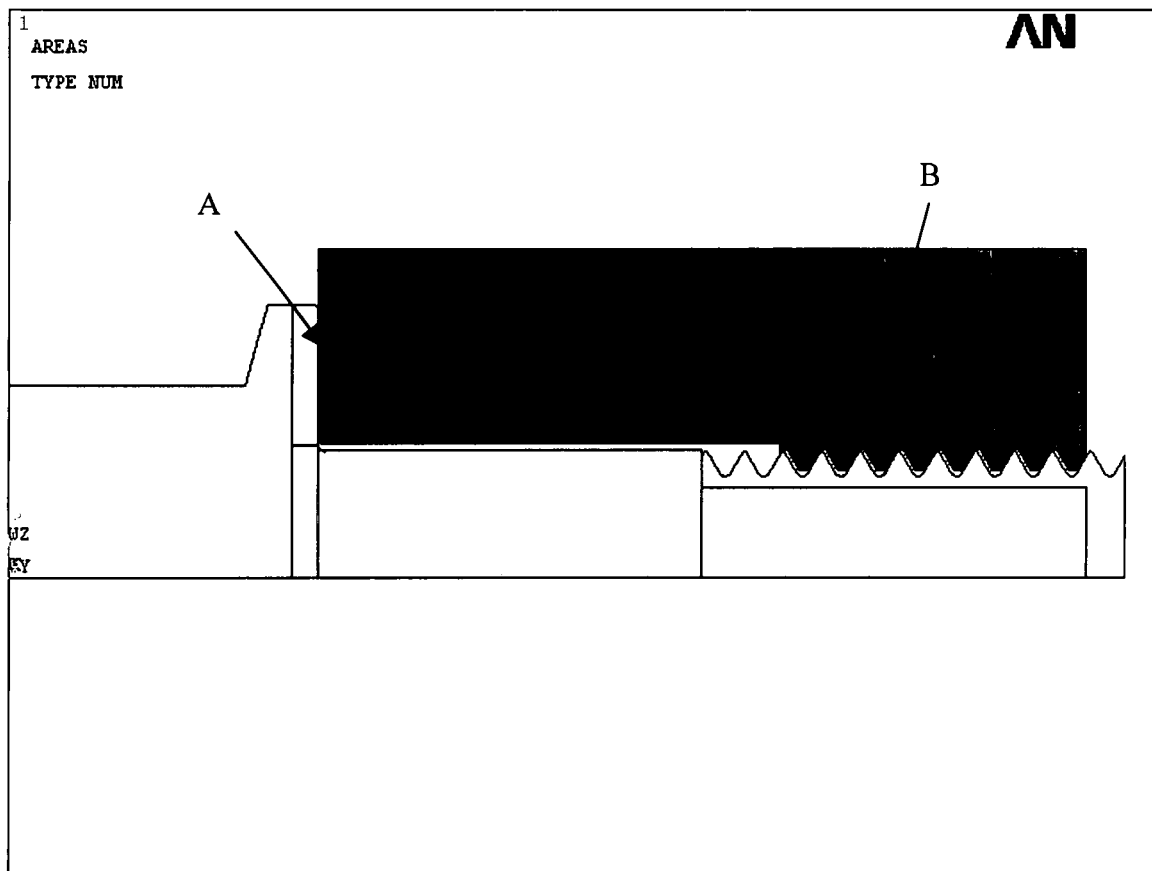


Figure 3.12 Axisymmetric image of the entire joint. Areas A and B indicate the contact regions of the model.

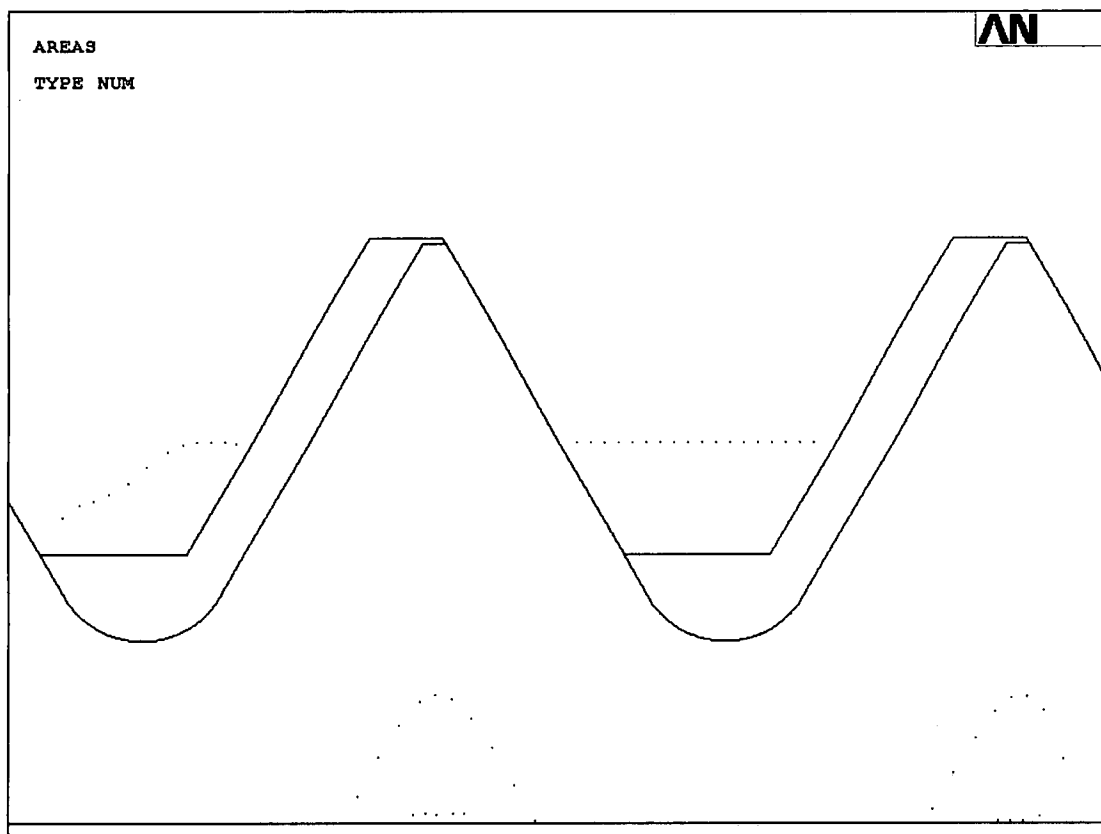


Figure 3.13 Axisymmetric image of the joint showing the contact between the internal and external threads. The upper portion of the image represents the internal thread.

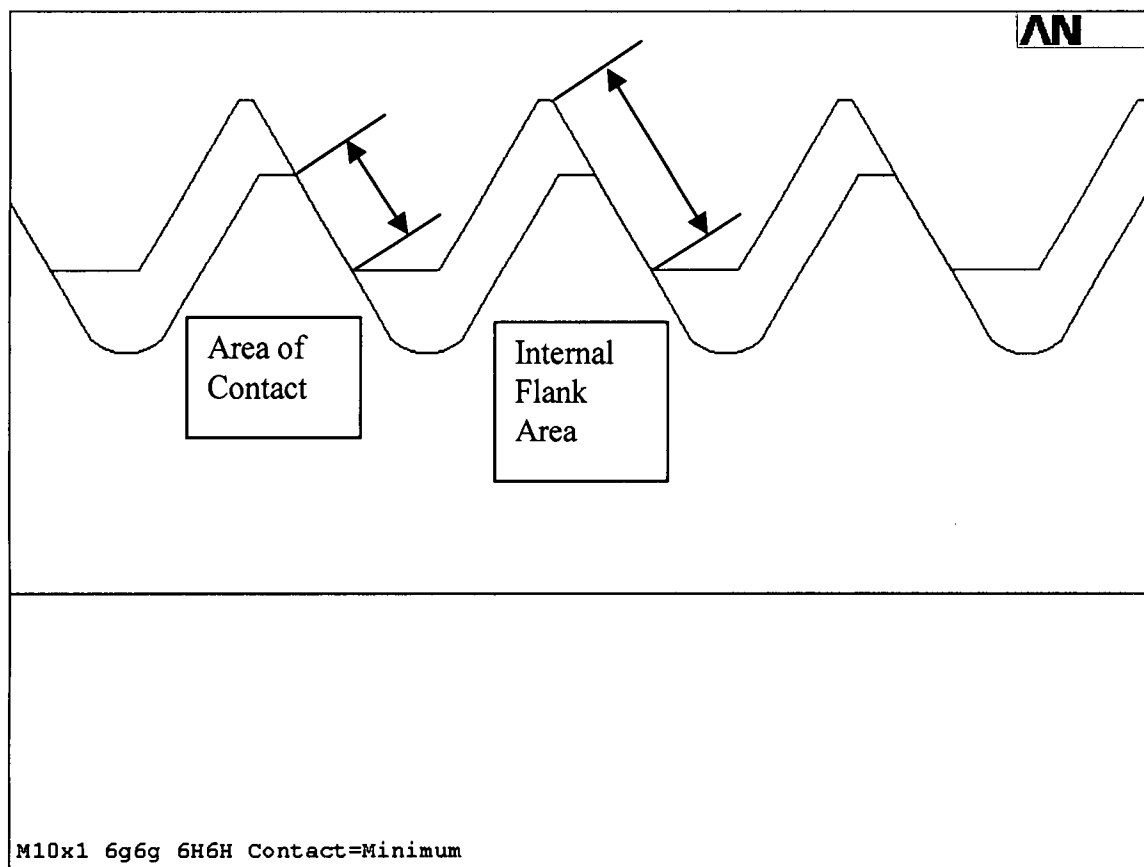


Figure 3.14 Axisymmetric image of the M10 x 1.0 minimum contact model. Note the difference between the flank area and the area of contact. The upper part of the image is the internal thread.

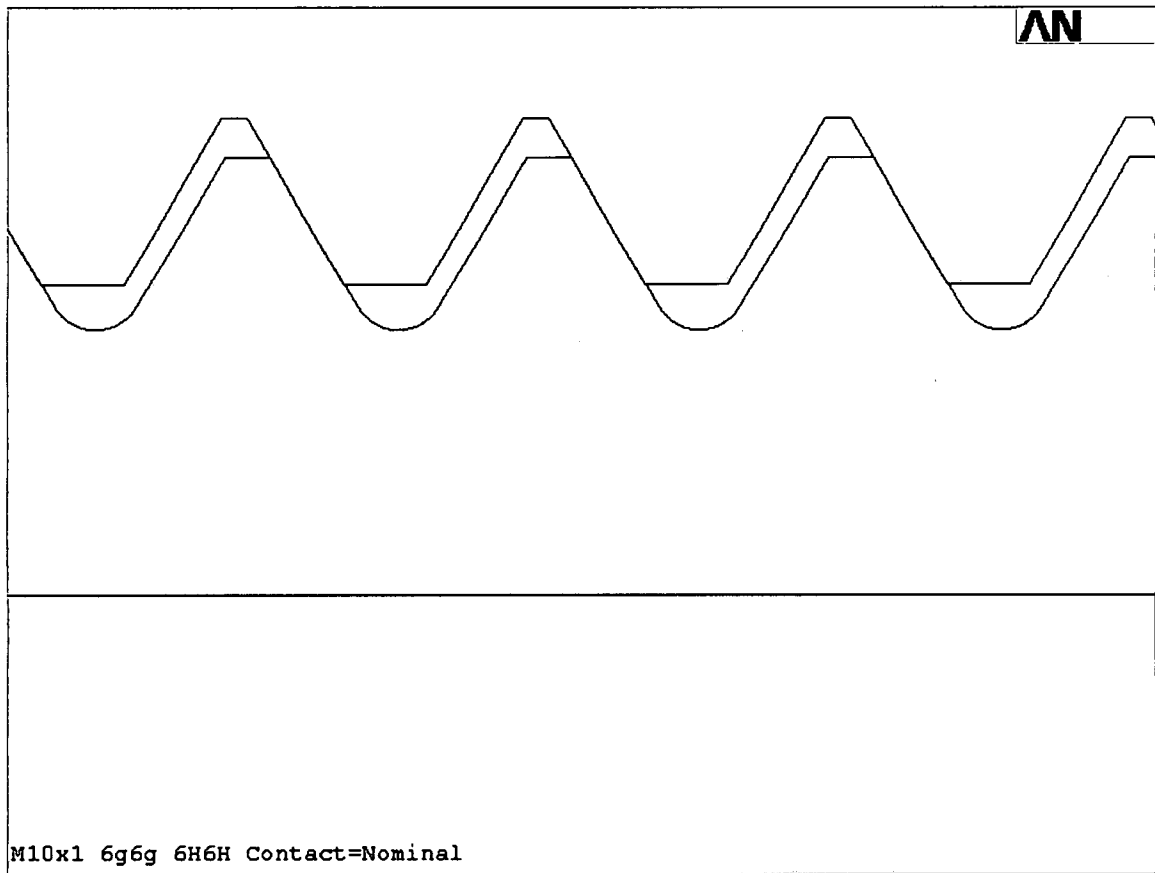


Figure 3.15 Axisymmetric image of the M10 x 1.0 nominal contact model. The upper area of the image is the internal thread.

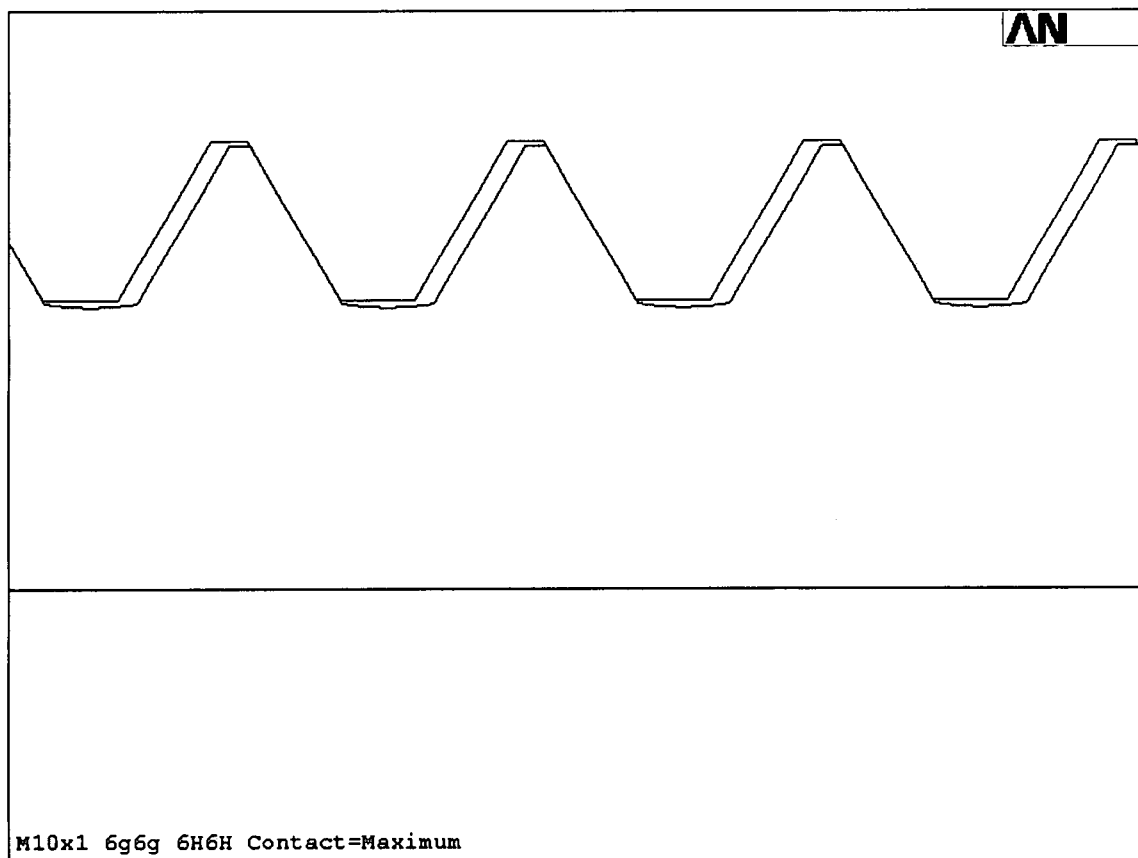


Figure 3.16 Axisymmetric plot of the M10 x 1.0 maximum contact model. Note that the root radius of the external thread has been altered. This was done so that no contact occurs between the root radius and the minor diameter of the internal thread (as happens in a real joint). The upper area of the image is the internal thread.

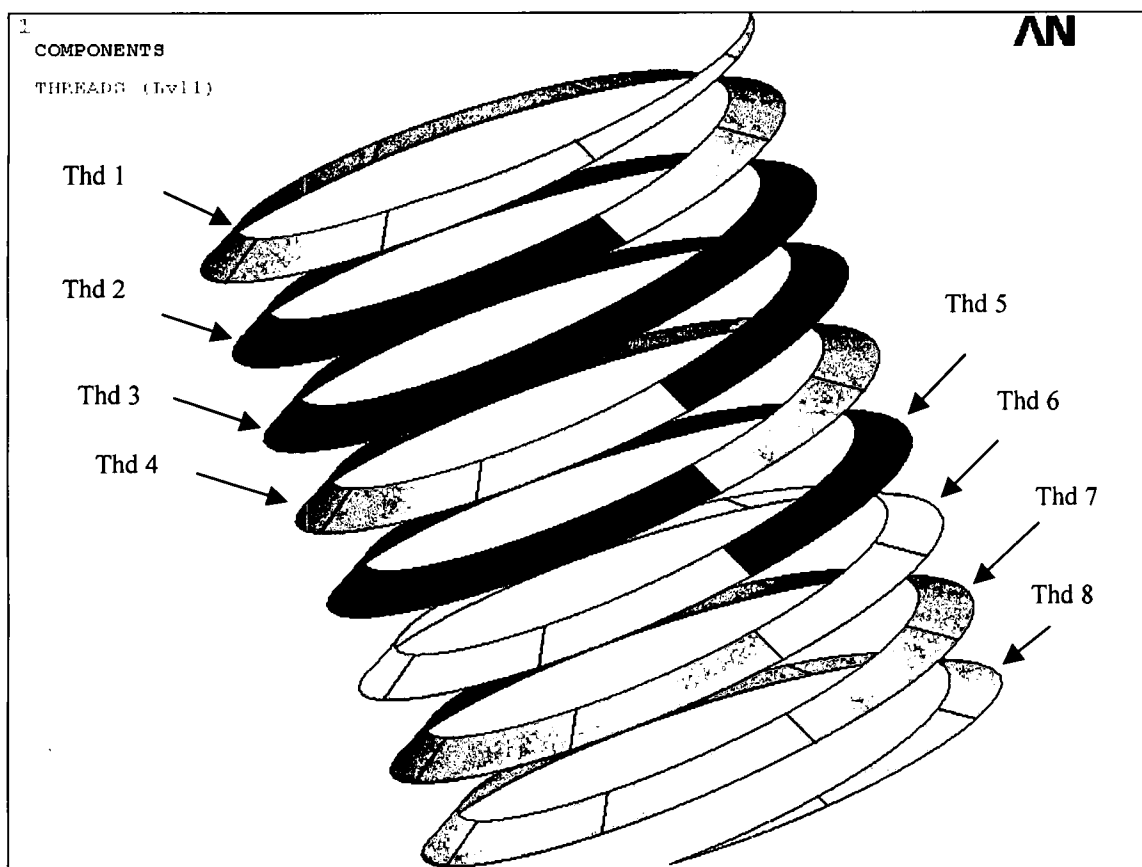


Figure 3.17 Areas of the flanks of the nut that were in contact with the flanks of the bolt. Area numbers correspond to those of Table 3.6. Thread No. 1 is closest to the head of the bolt. Threads shown are from the 1.5mm pitch at maximum contact level.

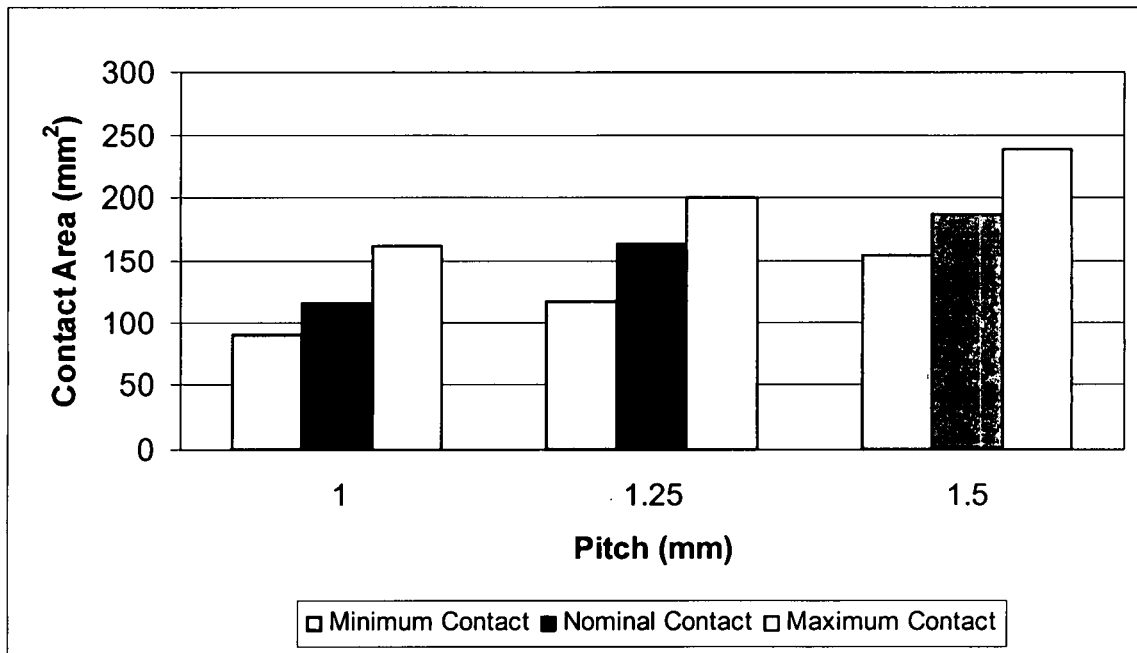


Figure 3.18 Total area of contact between the internal and external threads for the minimum, nominal, and maximum contact levels grouped by pitch size.

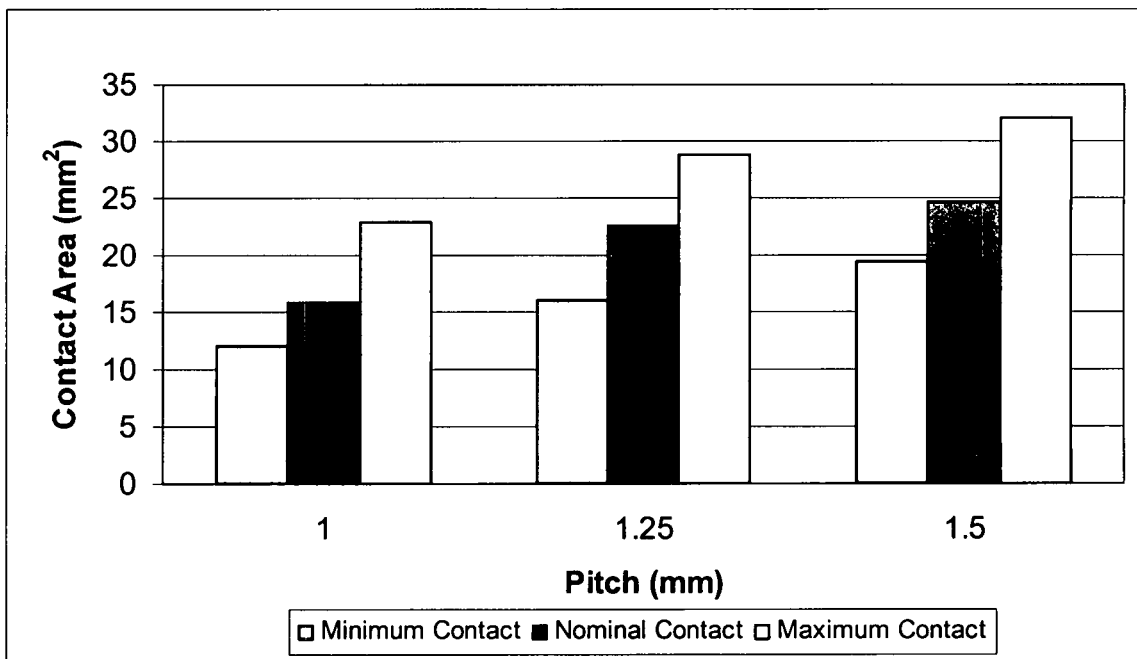


Figure 3.19 Area of contact between the internal and external threads for the 1st engaged thread for minimum, nominal, and maximum contact levels grouped by pitch size.

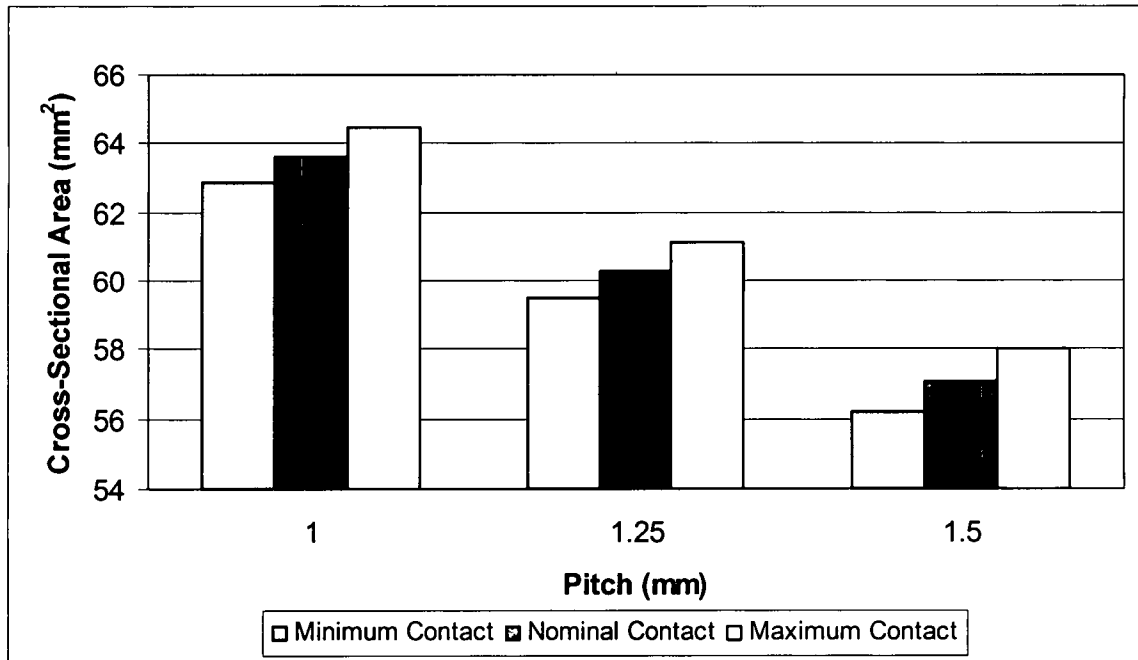


Figure 3.20 Cross-sectional areas of the bolt for the models created for the minimum, nominal, and maximum contact levels grouped by pitch size.

Table 3.1 Element and Node Data for the Model of Section 3.1			
Volume	Element Type	Number of Elements	Number of Nodes
Bolt's Threads	SOLID186	107,362	176,273
Bolt's Shank	SOLID187	9,384	15,910
Bolt's Flange	SOLID186	43,223	76,511
Bolt's Head	SOLID187	32,045	47,454
Bolt's Thread Solid Volume	SOLID187	22,530	32,255
Nut-Block's Threads	SOLID186	43,133	69,628
Nut-Block's Bearing Surface	SOLID186	6,811	12,994
Nut-Block	SOLID187	16,751	27,030

Table 3.2 Thread and under-head CoF values for the model of Section 3.1		
Torque Level (N-m)	Thread CoF	Under-Head CoF
15	0.177	0.141
30	0.165	0.137
45	0.159	0.134

CHAPTER IV

Results and Discussions

4.0 Results and Discussions

This chapter presents the results of the research performed for this dissertation. The results are presented in three sections, experimental, finite element analysis (FEA), and the combination of both the FEA and the experimental work.

The experimental research addressed the relationship amongst the applied torque, clamp-load, and the friction developed in the thread and under-head regions of a bolted joint. The individual investigations were focused on: 1) the effect of length of thread engagement and the bolt flange diameter on both the developed clamp-load and friction, 2) the influence of tightening speed on under-head and thread coefficient of friction (CoF), 3) the effect of material hardness on thread and under-head CoF, and 4) measurement of thread torque developed on each engaged thread of a seven thread engagement.

The FEA work consisted of the creating the model of a bolted joint, which allowed for the dynamic tightening of a bolt into a nut. This model was developed to replace the existing static models in which or load was placed onto the nut or bolt to create the clamp-load in the joint. The current model generated the clamp-load by the application of a torque to the bolt head. The work combines the results of both the experimental and FEA work and has the ability to determine the CoF on each individual thread for a seven thread engagement. Statistical Analysis of the experimental results included the

computation of the Probability Value (P-Value) as shown in Table 4.1. P-Value analysis allows for an understanding of which variable has a dominant effect on either the CoF or clamp-load values.

4.1 Experimental Research

4.1.1 Effect of Under-Head Area and Length of Engagement on Clamp-Load

This investigation examined the effect of the flange diameter and the length of thread engagement on the of thread and under-head CoF and clamp-load. The flange diameter varied from 18 to 21 mm and the length of engagements varied from 5.5 to 13 mm. Both experiments were conducted simultaneously to determine the effects of each dimension. Moly-Lit anti-seize lubricant was used in both cases to minimize friction variations. This lubricant was used due to its ability to maintain a lubricant film under pressure and provide a low CoF. All the fasteners were torqued to 40 N-m with the aid of an electronic torque gun running at 100 rpm into a torque-tension load-cell.

Table 4.2 lists the average values of thread and under-head CoF, under-head pressure, thread and under-head torque, clamp-load, and applied torque. The results were averaged for three replications with respect to the flange diameter and three runs for each of the nut heights. The results indicate that as the flange diameter increased, the under-head CoF decreased which allowed more clamp-load to be developed. Note that the bolt with the largest flange diameter produced the lowest under-head torque, lowest under-head CoF value, and the highest average clamp-load. However, it also had the smallest average contact pressure. There was little change in the thread CoF values for all the flange diameters. Figures 4.1 and 4.2 show the variation of clamp-load as well as thread and under-head CoF with flange diameter, respectively. There is a 33% difference in the

under-head CoF values between the 21 mm and 18 mm flange diameters, 0.061 for the 21 mm flange and 0.091 for the 18 mm flange. There is a 14.2% difference in the clamp-load developed in these tests, 27,782 N for the 21 mm flange and 24,323 N for the 18 mm. However, the thread CoF is unaffected by the increase in flange diameter.

Table 4.3 shows the same results as above, but with respect to the nut height. The thread CoF tends to decrease with increasing length of engagement. At the same time, the pressure between the threads increases with decreasing nut height. Similarly, there appears to be a slight relationship between the length of thread engagement and the magnitude of clamp-load, thread torque, under-head torque, and under-head CoF. Figures 4.3 and 4.4 show a graphical representation of the clamp-load as well as thread and under-head CoF results with increasing length of nut engagement.

The data were entered into a statistical software package SAS using the general linear model (GLM) procedure and then executed. The data included the bolt tension, flange diameter, and length of engagement. The dependent parameter for the analysis was bolt tension and the independent variables were flange diameter and nut height. The data was analyzed using three different models: bolt tension and flange diameter, bolt tension and nut height, and bolt tension with both flange diameter as well as nut height.

According to the established probability value (P-value) convention, there appears to be strong evidence that the under-head area is more effective in increasing the bolt tension than the nut height. When both independent variables are used together to create an interaction model, again the flange diameter indicated a strong effect on the bolt tension. The interaction between the nut height and flange diameter indicated no strong evidence on tension because of the reason that their effects counteracted against each-other.

Thus, this set of experiments indicates that the flange size affects the tension more than the length of engagement. This statement agrees with the conclusion made by Fukuoka [22]. The above friction behavior could be linked to the pressure distribution at the bearing surface. As the size of the flange increases, the contact pressure decreases. The lower contact pressure allowed more lubricant to stay under the flange of the rotating bolt, which reduced the under-head CoF. This phenomenon might also be evident if a solid plating or coating were used on the bolt instead of the lubricant. At lower pressure, the coating remains intact and results in little or no metal-to-metal contact. Similarly, at high pressure, the lubricant is squeezed out resulting in a very thin film and probably metal-to-metal contact. This results in high CoF at high pressure for the small diameter flange. The same explanation can be used for the effect of nut height on the thread CoF. As the length of engagement increased, the thread pressure decreased, resulting in lower CoF values.

4.1.2 Effect of Tightening Speed on Clamp-Load

The second investigation examined the effect of varying the bolt tightening speed on the thread and under-head CoF as well as the clamp-load. Here, an electronic torque gun capable of varying the tightening speed was used. The actual tightening speeds achieved ranged from 12 rpm to 665 rpm. The programmed speeds ranged from 25 rpm to 1,200 rpm. The speed disparity is due to the algorithm within the gun's controller that physically slows the speed at which the gun is turning as the targeted torque value is reached, e.g., a programmed run-down speed of 900 rpm equates to an actual speed of 390 rpm at the target torque. Three different lubricants, as well as the plain or dry condition, were used in this portion of the investigation. The 1st lubricant was Moly-Lit:

moly-disulfide/graphite based, the 2nd lubricant was N-5000: nickel/graphite based, and the 3rd lubricant was TS-74: sulfur based. The plain or dry condition was used to establish a base-line to determine the effect of the lubricants. The investigation used a bolt, nut, and washer that were assembled into a torque-tension load-cell.

Figures 4.5 and 4.6 show the variation of the thread and under-head CoF, respectively with tightening speed for the three lubricants of this section. The speeds listed in these figures are the speeds measured at a torque level of 28 N-m. Examination of the data shows that both CoF values decreased as speed increased. The thread CoF values for the TS-74 lubricant has a larger scatter than the other two lubricants. Figure 4.7 shows the results of the same experiments but with respect to clamp-load. The clamp-load increased with increasing speed. This was due to the drop in the CoF values; a lower CoF value means that a larger clamp-load can be generated for a given applied torque compared to that for a higher CoF value. Figure 4.8 shows the variation of the thread and under-head CoF with respect to actual tightening speed under dry conditions. Figure 4.9 show the variation of clamp-load with respect to actual tightening speed for the dry fasteners. It may be observed from these figures that there is a slight decrease in both the thread and under-head CoF values which increased the clamp-load values with increasing speed.

The SAS code, using the GLM procedure, was used to analyze the data obtained in this series of experiments. There were three different analyses performed on each of the four experiments. The dependent variable was always clamp load while the independent variables were speed, under-head CoF, and thread CoF. The Moly-Lit experiments show that all three independent variables have a very strong affect on

tension with speed being the most dominant variable. The experiments with the N-5000 lubricant showed that both speed and under-head CoF had a strong affect on bolt tension while thread CoF had only a moderate affect. The results of the TS-74 experiment indicated that speed and under-head CoF had a very strong affect on tension while the thread CoF did not. The data from the dry experiment showed significantly different results when compared to those with the three lubricated experiments. The dry data indicate that the thread CoF affected tension while the speed and under-head CoF did not. In all cases, the increase in bolt tension with increasing speed may be attributed to the decrease in both the thread and under-head CoF with sliding speed.

4.1.3 Effect of Bolt, Washer, and Nut Hardness on Thread and Under-Head CoF

In this section, each of the three parts of a joint, i.e. bolt, nut, and washer had three levels of hardness: 24-28HRC (soft), 34-38HRC (medium), and 44-48HRC (hard). Moly-Lit, was used as the lubricant in this experiment to minimize the influence of friction. The washer, bolt, and nut were assembled into a torque-tension load-cell and torqued to a value of 40 N-m.

Table 4.4 shows the results of the experiment after the data was analyzed at a torque of 35 N-m. The tests that developed the largest amount of clamp-load used the medium hardness bolt (34-38HRC). The top three clamp-load generators included the hard washer (44-48HRC), along with the medium hardness bolt. The hardness of the nut does not appear to affect the clamp-load. The data was analyzed using SAS and the GLM procedure, using only one model which included interactions amongst all three components. According to the established P-Value conventions, there is very strong evidence that one of the three bolt and washer hardness values have dominant effect on

the bolt tension. This model also indicated that there was no evidence of the nut hardness on the bolt tension.

The above results indicate that the hardness of the parts in a bolted joint does have an effect on the under-head CoF and therefore the magnitude of clamp-load developed. There appears to be little change in the thread CoF however. The lubricant used has an affect on the results.

4.1.4 Effect of Minimizing the Under-Head CoF on Thread CoF

The effect of varying the under-head CoF on the clamp-load is investigated in this section. In the 1st case, a thrust bearing was placed under the bolt head, which significantly reduced the under-head CoF. In the 2nd case, a standard washer was used and a lubricant was applied in the under-head region of the bolt. The threads were lubricated in both the cases. N-5000 was used as the lubricant and the joints were assembled in a torque-tension load-cell and torqued to 45 N-m.

Table 4.5 shows the results of the 1st experiment. With the thrust bearing, clamp-load showed an increase of 42%, 28,323 N to 40,200 N, when compared to the standard test washer as the bearing surface. The thread torque increased by 45%, 21 N-m to 30.4 N-m, and the under-head torqued decreased by 50.0%, 19 N-m to 9.6 N-m, when compared to the standard test washer. However, the thread CoF remained same for both the under-head configurations. This indicates that there is no interaction between the thread and under-head CoF, but only an interaction between the thread and under-head torque. The total tightening torque is equal to the sum of both the thread and under-head torques. Since the load-cell physically measures the under-head torque and the applied torque is known; thread torque is then computed as the difference between the two.

Therefore, if under-head torque decreases and applied torque remains the same, thread torque would increase resulting large values of clamp load. .

A 2nd investigation was conducted using the same fastener, which was used above, but with the exception of no thrust bearing. This investigation examined the relationship between thread and under-head CoF when one area was lubricated and the other kept dry. These were then compared to the cases when both regions were either lubricated or kept dry. These results are shown in Table 4.6.

The lubricated thread and dry under-head produced a clamp-load value of 24,466N. This clamp-load was 57% greater than that for the dry/dry combination of 15,590 N. However, it was 24% less than that for the lubricated/lubricated combination of 32,318 N. The thread CoF value for the lubricated thread/dry under-head showed a 25% decrease to that of the dry/dry condition, 0.141 to 0.106. However, the under-head CoF decreased by 47% compared to that of the dry/dry condition 0.228 to 0.121.

The dry thread/lubricated under-head produced a clamp-load of 31,305N which is 3.1% less than that of the lubricated/lubricated condition. However, it was 100% greater than that of the dry/dry condition, 15,590 N. The under-head CoF value for the dry thread/lubricated under-head condition was 82% less than that of the dry/dry condition, 0.228 to 0.041. However, the dry thread/lubricated under-head had a thread CoF value actually 4.1% more than that of the dry/dry condition, 0.141 to 0.147.

The results suggest that changes made to the under-head CoF had little affect on the thread CoF; however, changes made to the thread CoF did have an effect on the under-head CoF. In most cases, the under-head CoF was smaller than that of the thread CoF. But this was not the case in the dry/dry condition. When a plating or coating has

low frictional values, the under-head CoF were lower compared to those of the thread CoF values.

4.2 FEA Model Joint Experiment

This portion of the research generated two experimental bolted joints which were used to conduct the FEA modeling. First, the models were used to determine the values of the thread and under-head CoFs, which were then inputted into the model. In the second case, the results of the FEA model were verified with those of the experimental results. A Teflon based lubricant was used in both the under-head region as well as at the threads.

The 1st joint, Figure 2-18, (which consisted of a bearing surface, internal threads, and a bolt) was used to measure the thread and under-head CoF via a torque-tension load-cell. The friction values were determined corresponding to the applied torques of 15 N-m, 30 N-m, and 45 N-m. Figure 4.10 shows the variation of applied torque, thread torque, and under-head torque with tightening time. Figure 4.11 shows the clamp-load and thread and under-head CoF. A total of six tests were performed at 45 N-m and the thread and under-head CoF and the clamp-loads were obtained at 15, 30, and 45 N-m torque from these plots. Tables 4.7, 4.8, and 4.9 list the results for these torque values, respectively.

The 2nd experimental joint, had a bolt that contained an ultrasonic sensor (a piezoelectric device that measures both bolt stretch and clamp-load, Figure 2-19). The joint consisted of a nut, which was attached to an 18 mm long counter-bored nut-block, and the bolt. The bolt was torqued to 45 N-m. Clamp-load and bolt elongation data were measured at the same three torque levels as discussed above, Table 4.10. These results were used to verify the results from the FEA model.

4.3 Thread Torque Measurement

This experiment was conducted to determine the amount of thread torque on each thread, for a seven-thread engagement. A test fixture, as described in Section 2.6, was used to measure the amount of torque produced by each full engaged thread of a nut.

An M10 x 1.5mm bolt was torqued into the created test fixture to a value of 15 N-m. This applied torque gave a thread torque of 4.5 N-m to the fixture. This was the target value for the strain gauges on the fixture. There were two run-downs or tightening performed with all seven threads assembled and the average strain values recorded and then translated into thread torques.

The experiment was first conducted with seven threads, then with six threads, etc. The experiment was stopped when only one thread was engaged. The results of the testing are shown in Tables 4.11 through 4.17. Note that the corrections to the 1st washer have been accounted for and that the error or deviation from the known 4.5N-m thread torque is also shown. Figures 4.12 through 4.18 show the resulting measured thread torque from the blades of the fixture for seven threads of engagement through one thread of engagement. Note that the 1st thread always supports most of the developed thread torque and the last engaged thread tends to support the least. The tabularized thread data should sum to 4.5 N-m, using Equation 2.21.

$$T_{Thd} = \sum_1^7 T_{Thread.n} \quad (2.21)$$

This summed thread torque value should equal the thread torque value obtained from the torque-tension load-cell. The percent difference range was found to be -4.2% to +7.8% for all seven experiments, one engaged thread to seven engaged threads. The reason for

the discrepancy is probably due to imperfect threads on both the threaded washers and the bolt.

4.4 Finite Element Analysis

4.4.1 Finite Element Analysis of the Bolted Joint

The 1st FEA model was executed three times, each at a different torque level: 15 N-m, 30 N-m, and 45 N-m. This was done to examine the variation of clamp-load and the bolt elongation with torque and its comparison with the experimental results. Figure 4.19 compares the FEA model with the experimental one for the clamp-load and bolt elongation. Both the clamp load and elongation values computed by FEA are higher than the experimental ones. This difference may be attributed to the numerical errors. There was an 8.4%, 5.8%, and 5.2% difference between the computed and the experimental clamp-load for the 15N-m, 30N-m, and 45N-m torques, respectively. A 13.6%, 15.1%, and 10.6% difference was found between the computed and experimentally measured elongation on the 15 N-m, 30 N-m, and 45 N-m torques, respectively.

4.4.2 Load Distribution

The model's algorithm from Section 3.3 was used to examine the load distribution on the engaged threads of the nut following the dynamic tightening to 45 N-m. The nominal diameter of the joint remained at 10 mm, but three pitches were used: 1.0 mm, 1.25 mm, and 1.5 mm. Also, three different flank-to-flank contact levels were created: minimum, nominal, and maximum. The contact levels indicate how much area of contact was established between the flanks of the external and internal threads. The contact areas were changed by adjusting the size of the major and minor diameters of both the internal and external threads within the maximum and minimum limits for the M10 x 1.5 6g6g and 6H6H sizes, the series of letter and numbers indicate the fit and allowance between

these threads.

Figure 4.20 shows the magnitude of the total developed clamp-load for the three models. The clamp-load decreases with increasing pitch. This was to be expected since the CoF in the threads decreases as the pitch increases. Recall that the contact area also increases with increasing pitch and contact level. Figure 4.21 shows the clamp-load, as a percent of the total load, on the 1st thread. The load on the 1st thread increased with increasing pitch, which is an opposite trend than that shown in the previous plot. This is supported by Figure 4.22 which shows that the contact area at the 1st threads increases with increasing pitch. Since the load is proportional to the contact area, large load on the first thread is in order.

Figures 4.23 through 4.25 show plots of clamp load carried by different threads as a percent of total clamp load for the minimum, nominal, and maximum contact levels for the three pitches, respectively. The percent of clamp load decreases as the thread number increases; note that the 1st thread is the one closest to the head of the bolt and witnesses the onset of the load first. Furthermore, as the contact level increases, the % of total load carried by the first thread increases. A smaller pitch coupled with a smaller contact area resulted in a more uniform or a better distribution of the developed clamp-load among all eight engaged threads. The plots show that the load carried by the 3rd/4th thread is same for all the contacts and is around 14% of the clamp-load.

The results from this section indicate that the first three threads supported 45% to 56% of the total load. The results are based not only on the pitch of the threads but on the contact level as well. The lowest load ratio is the M10 x 1.0mm thread with minimum

contact level and the highest ratio is the M10 x 1.5mm thread with maximum contact level.

The results of the nine FEA models also showed that as the pitch decreased, the magnitude of pressure developed on the flanks increased, Figures 4.26 through 4.28. The abscissa is the flank area along the helix. The area calculation starts from the head of the bolt, or top of the nut. In the automotive manufacturing sector, the fine pitch thread is typically used when a steel bolt is threaded into aluminum. The yield stress of typical cast aluminum (A356) is about 179 MPa; the average contact pressure of the 1.0 mm pitch at minimum contact is 284 MPa which would indicate that the 1st thread would have plastically deformed.

The magnitude of both the clamp-load and contact pressure developed on the 1st engaged thread was related to the amount of thread contact between the internal and external threads. This can be illustrated by the two ANSYS area plots of the 1st thread's flanks that are in contact with each-other, for the 1.25mm pitch thread at both the maximum and minimum contact levels, Figures 4.30 and 4.31 respectively. The model's nut has been cut, which is similar to what is normally done in the manufacturing process (Figure 1.8). The flank of the internal thread for the minimum contact does not meet the flank of the external thread for about 90° at the start of the thread. Therefore, the size of the thread or the amount of contact between the internal and external threads is an important matter. For the maximum contact case, the contact between the internal and external threads starts right away. It is for this reason that the load carried by the first thread for the minimum contact case is smaller than that for the second thread.

4.4.3 Direct Comparison to Static Research

The 3rd FEA model was created with the purpose of performing a direct comparison of this work with the previous research that was conducted under static loading conditions using both analytical and FEA methods. Chen et al. [15] examined the load distribution for 1in diameter fastener with three different pitches: 8 threads/inch (tpi), 12tpi, and 16tpi which are defined as coarse, fine, and super fine for this size fastener. The analysis performed in the current research used a M10 x 1.75mm coarse thread, a smaller diameter and finer thread compared to the 1 in 8threads/inch fastener used by Chen et al [15]. It is unclear if the contact between the internal and external threads was at the maximum, minimum, or nominal condition in the static model research of Chen et al.? Axisymmetric plots of the internal and external threads do show a good deal of flank contact, however. The analysis of this research used a coarse thread at maximum flank-to-flank contact area between the internal and external threads.

Figure 4.32 shows the comparison of the % of clamp-load carried by different threads for the static and dynamic models (2nd and 3rd created models). Four pitches, 1.0 mm, 1.25 mm, 1.5 mm, and 1.75 mm, have been used from the current research. The dynamic load data for the 1st thread does not match with that of the static work. This can be explained by the contact area between the internal and external threads. Since the 1 inch threads had a much larger contact area, it would generate a higher load on the 1st thread. The dynamic model data supports this conclusion. Since no contact area was reported in the static model research, no further conclusions can be made. In addition, the shape of the 1st thread also had a significant effect on the load distribution. As the pitch of

the thread decreases and the contact area at the 1st thread diminished, the load that the 1st thread supports decreases as well.

4.5 Thread CoF

The results from the tests that were conducted to measure the thread torque on an individual thread basis are discussed here. The thread torque data was inputted into an FEA model (the 4th FEA model). This FEA model consisted of a bolted joint, similar to that presented in Figure 3-10, but with one exception; there were only seven engaged threads instead of the usual eight. Equation 2.18 that was used to determine the thread CoF had thread torque and clamp-load as independent variables.

$$\mu_{thd} = \frac{\left(\frac{T_{thd}}{P} \right) - 0.159 p}{0.578 d_m} \quad (2.18)$$

The thread CoF was analyzed at 4.5 N-m of developed thread torque from the test fixture (Figure 2.11). The clamp-load for each engaged thread (4th model) was obtained after the model's bolt was torqued to a value of 9.6 N-m. The thread torque and clamp-load data from each thread was then placed into Equation 2.18. The resulting data as well as the calculated thread CoF values are shown in Table 4.18. The thread CoF data can also be seen in Figure 4.32. The results show that the 1st thread has a higher CoF than the remaining six. The thread CoF decreases from the first thread through the fifth thread. The CoF on the 6th thread increased. This increase corresponded to the jump in thread torque for the sixth thread as well. This trend for the thread CoF is in order because the clamp-load and thread torque decreases as the distance of the thread increases. It is unclear, however, why the thread CoF started to increase at the end. It could be due to the

increase of pressure as the contact area of the thread starts to decrease. There was a 2.8% and 5.8% difference in the calculated Vs measured thread torque and thread CoF was respectively.

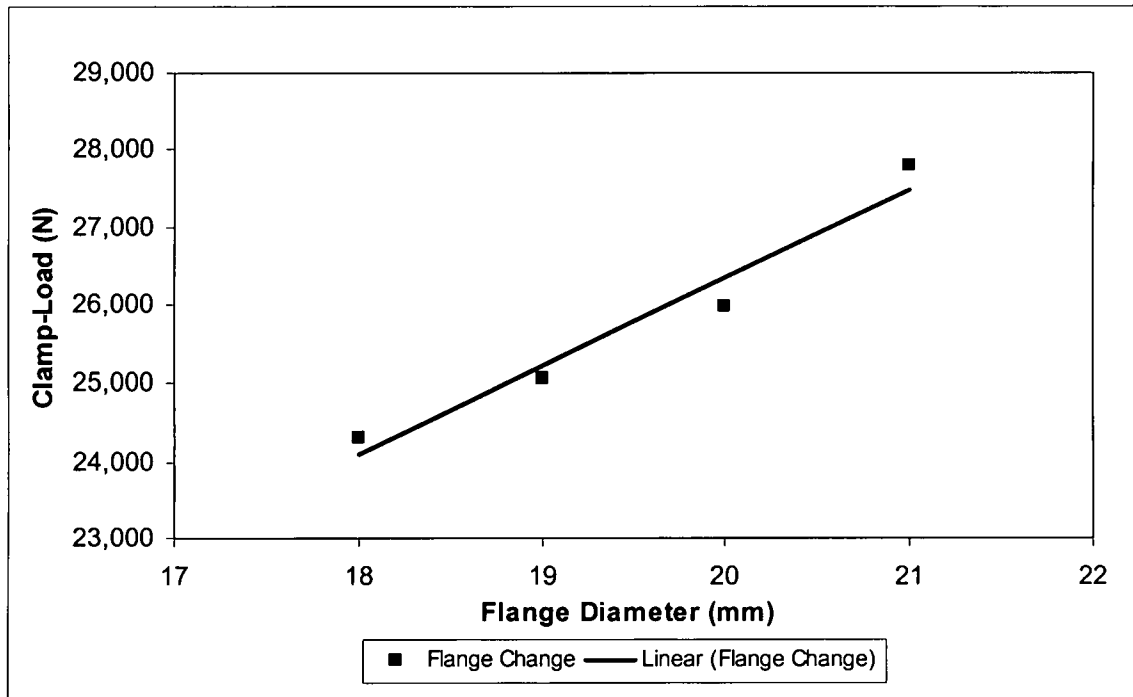


Figure 4.1 Plot of clamp-load Vs flange diameter. Data includes all nut heights.

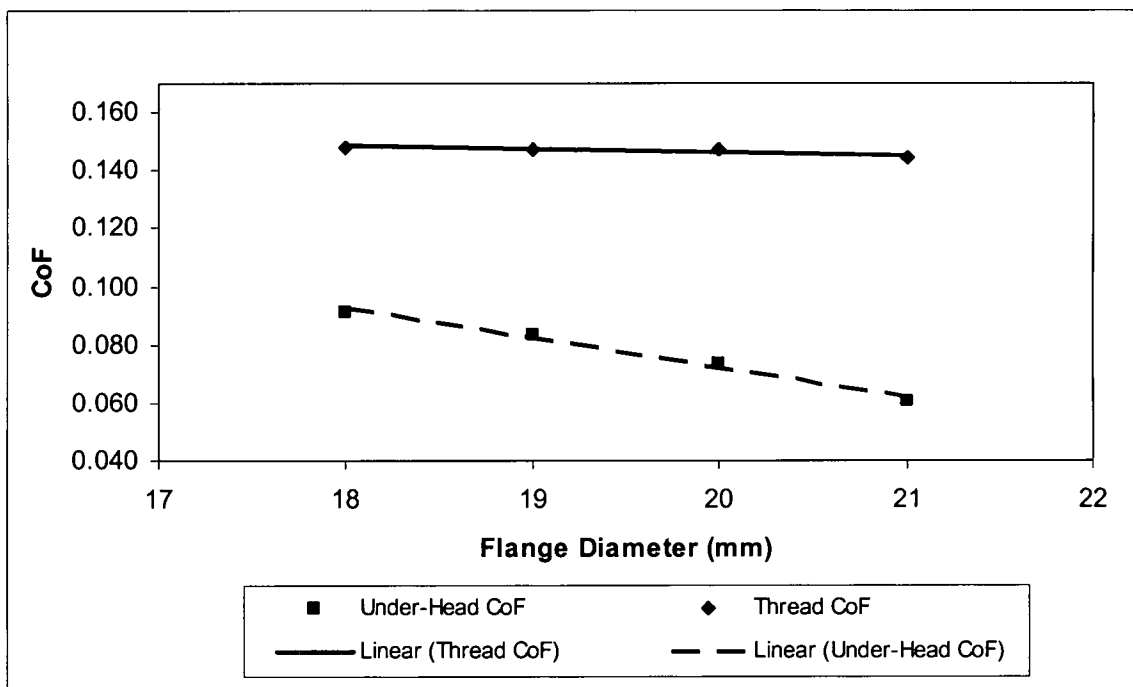


Figure 4.2 Plot of under-head and thread CoF Vs flange diameter. Data includes all nut heights.

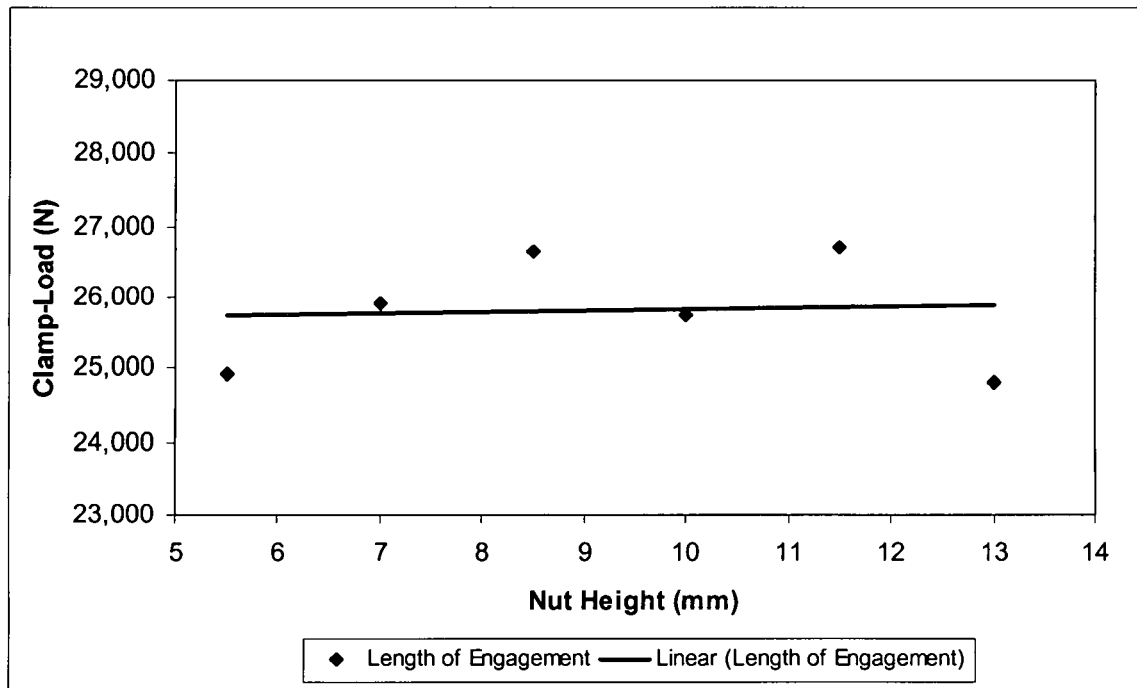


Figure 4.3 Plot of clamp-load Vs length of engagement. Data includes all flange diameters.

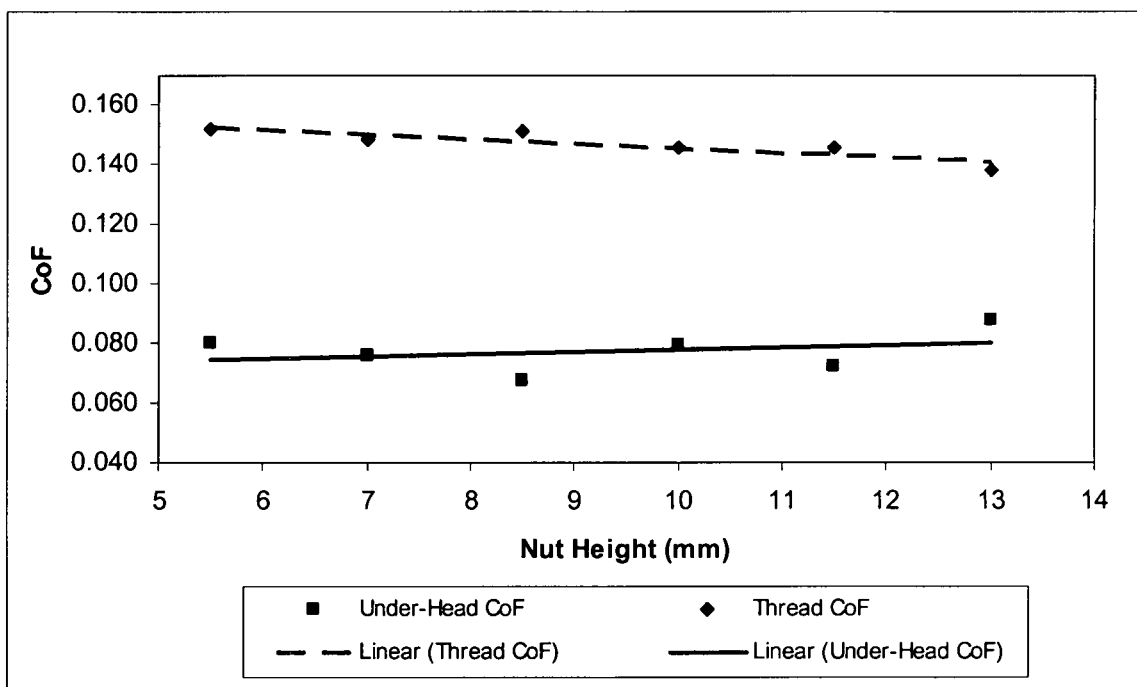


Figure 4.4 Plot of under-head and thread CoF Vs nut height. Data includes all flange diameters.

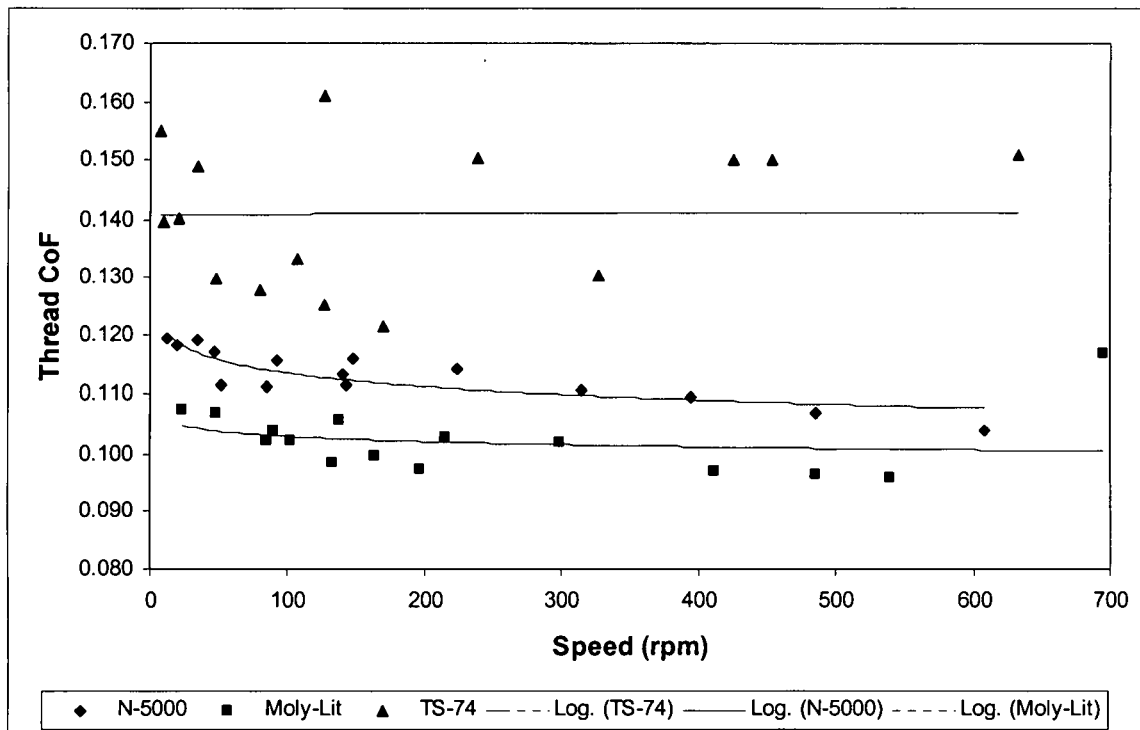


Figure 4.5 Thread CoF Vs tightening speed. A logarithmic trend line was fitted to the data.

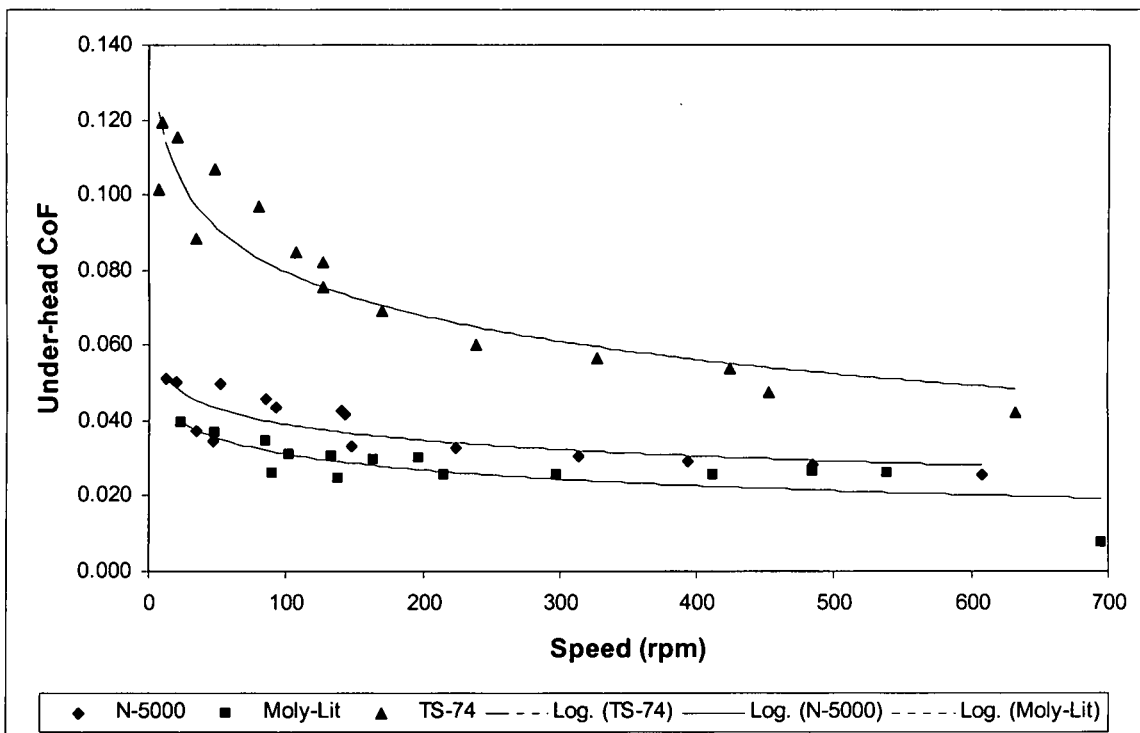


Figure 4.6 Under-Head CoF Vs tightening speed. A logarithmic trend line was fitted to the data.

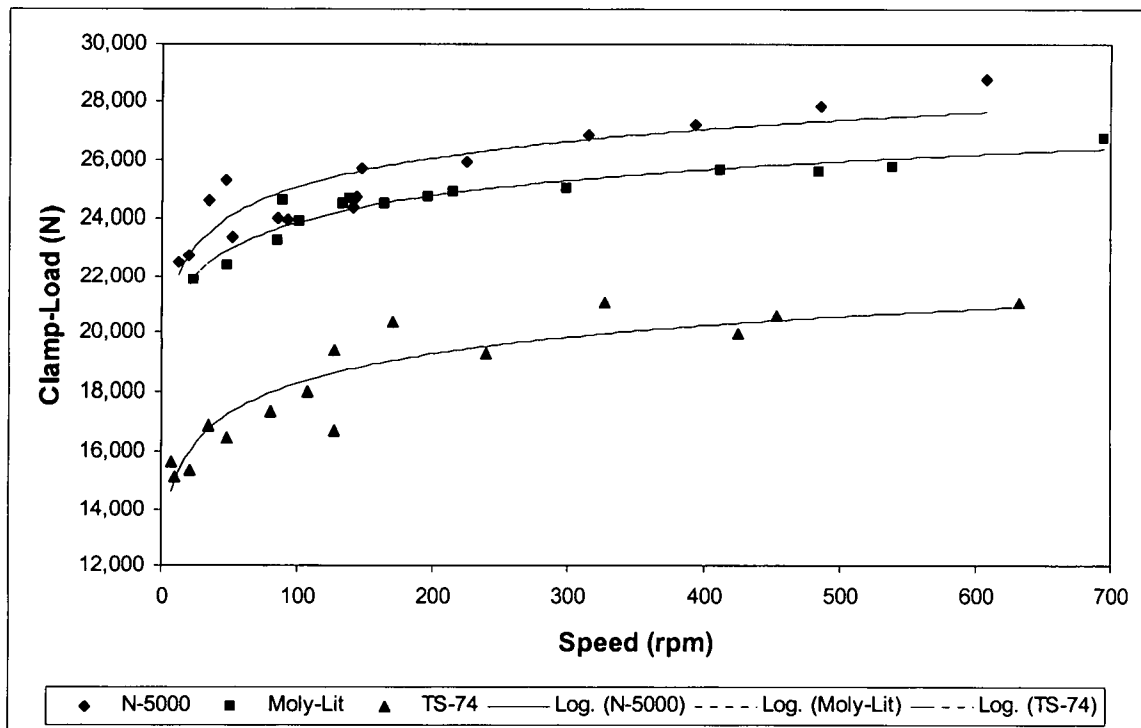


Figure 4.7 Clamp-load Vs tightening speed. A logarithmic trend line was fitted to the data.

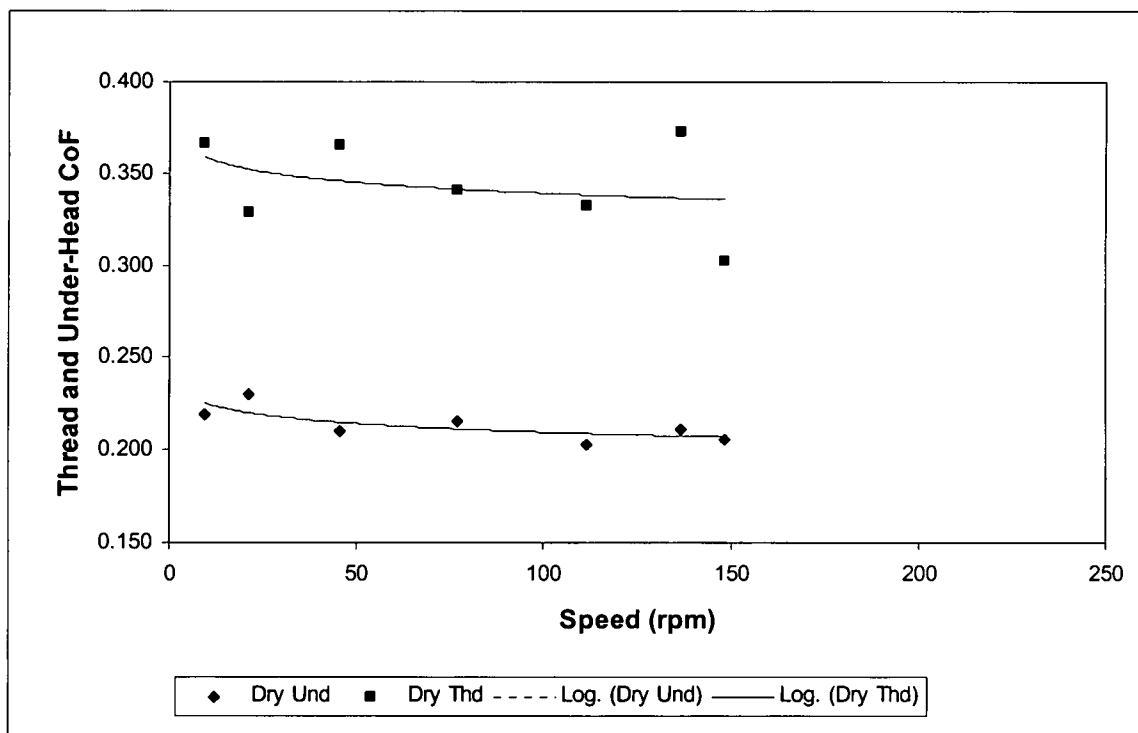


Figure 4.8 Thread and under-head CoF Vs tightening speed for dry experiment. A logarithmic trend line was fitted to the data.

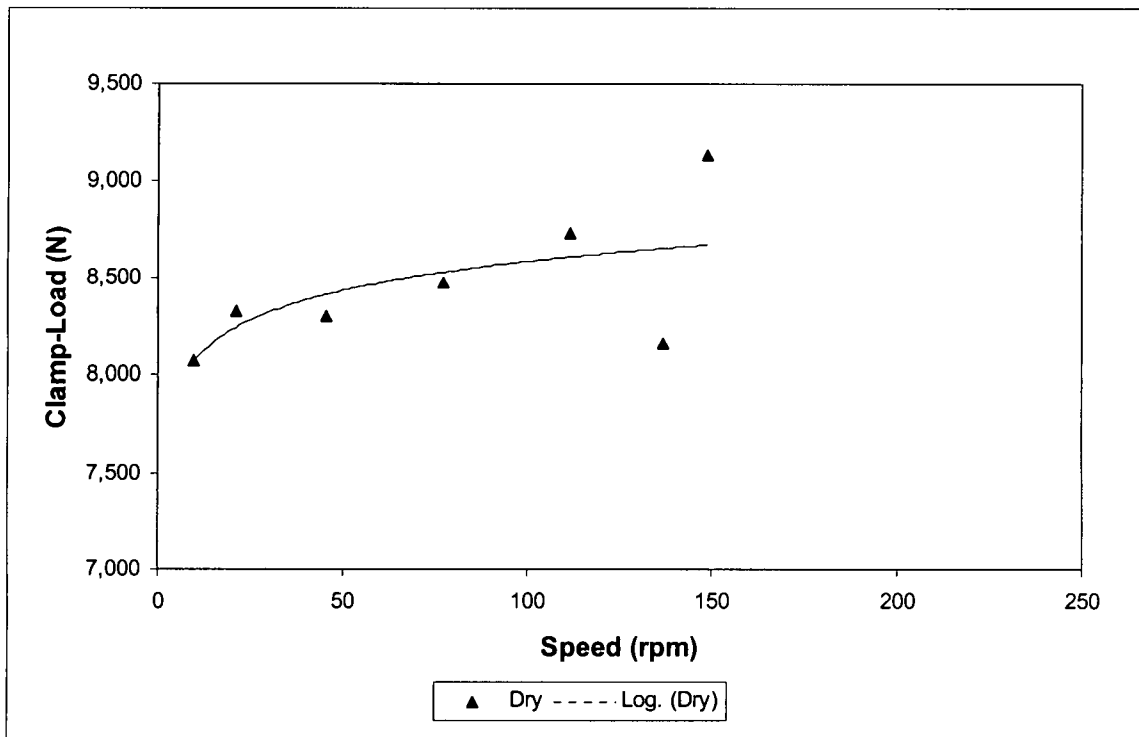


Figure 4.9 Clamp-Load Vs tightening speed for dry experiment (no lubrication was present). A logarithmic trend line was fitted to the data.

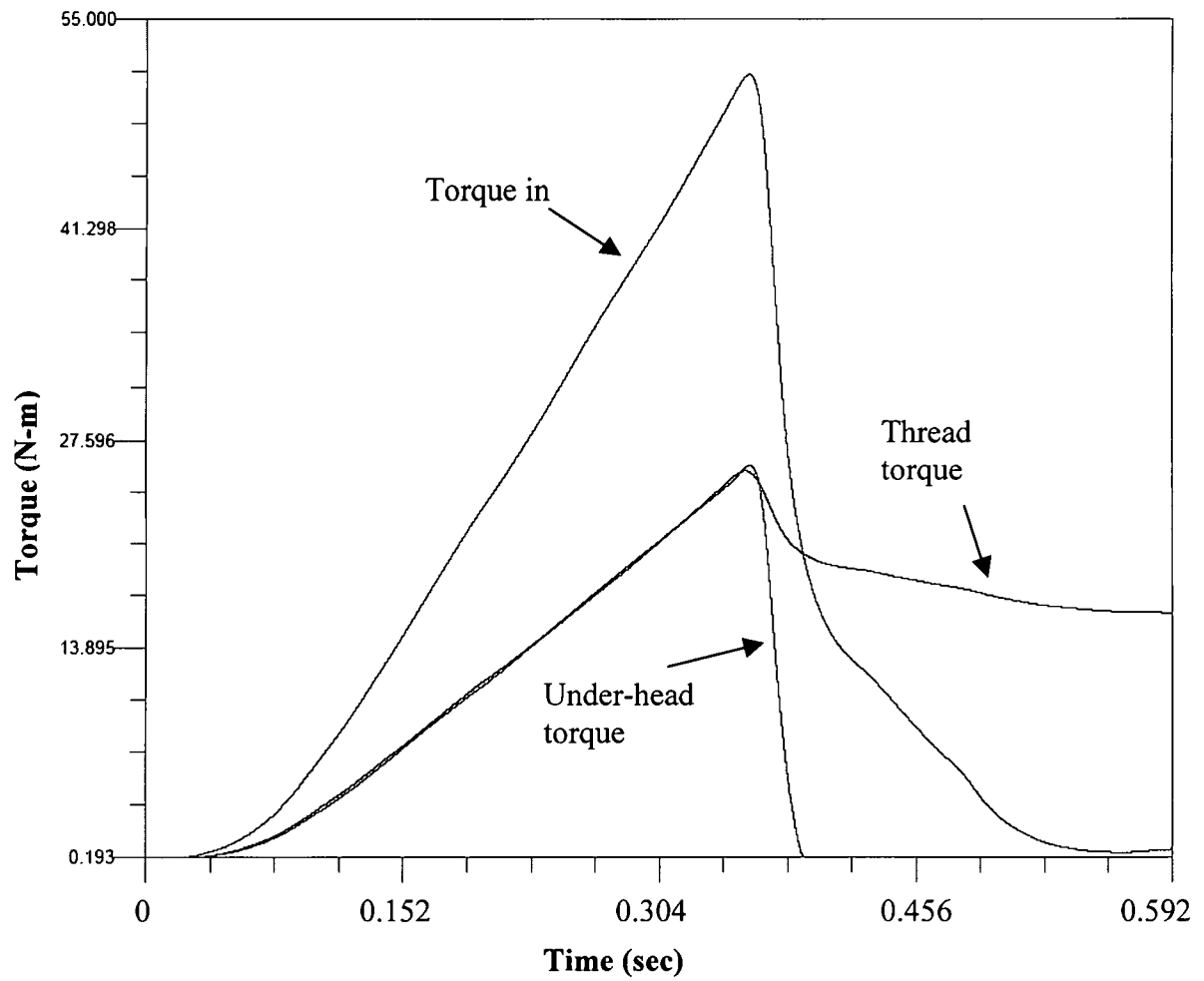


Figure 4.10 Run-down plot of applied torque, under-head, and thread torque Vs time. Applied torque: 45 N-m.

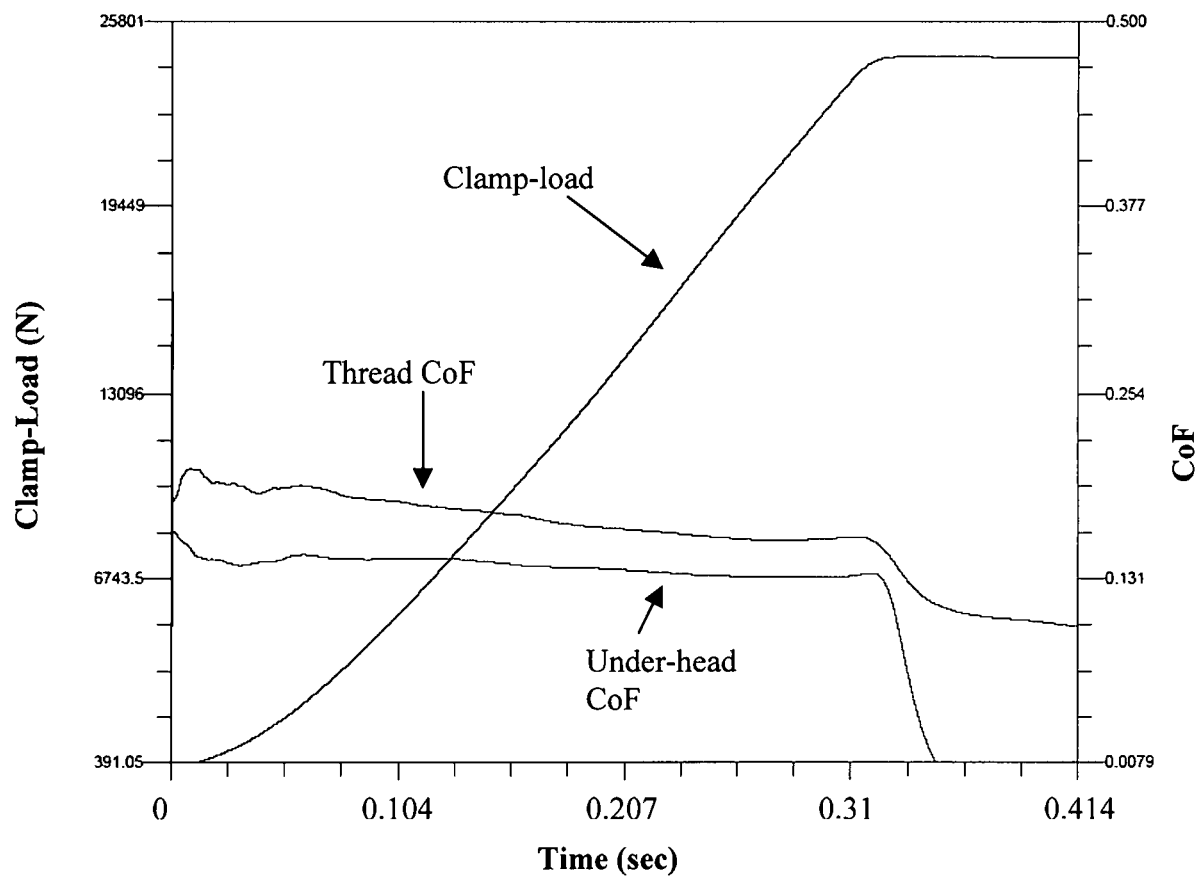


Figure 4.11 Run-down plot of clamp-load, thread and under-head CoF Vs time.
Applied torque: 45 N-m.

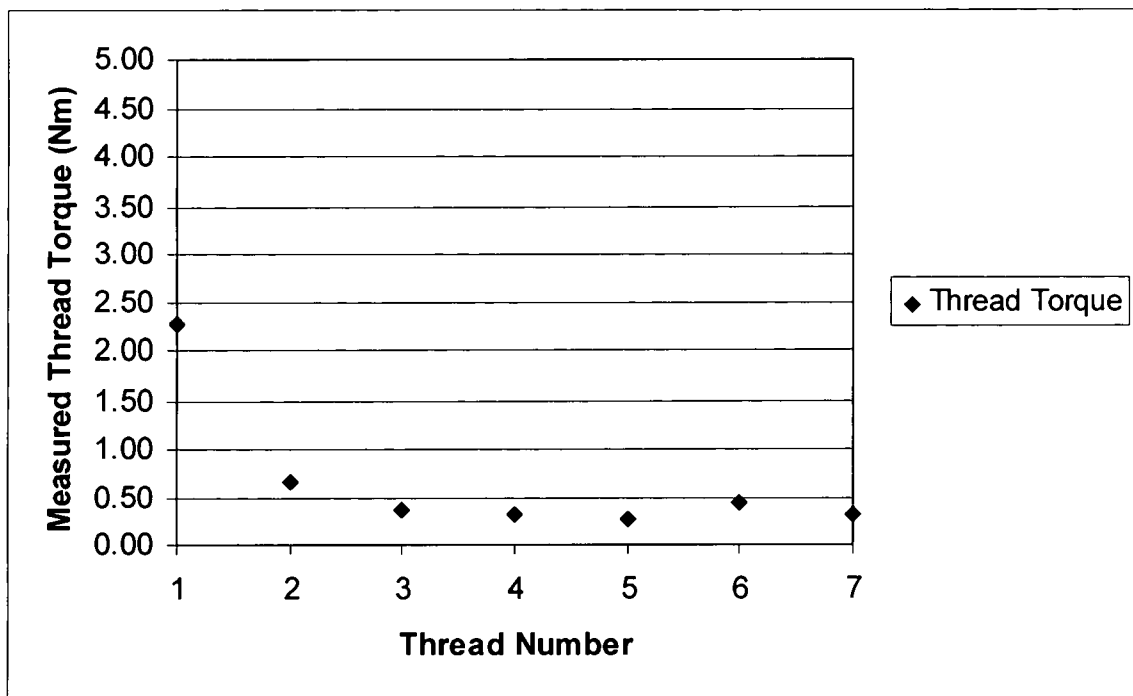


Figure 4.12 Plot of thread torque Vs seven engaged threads.

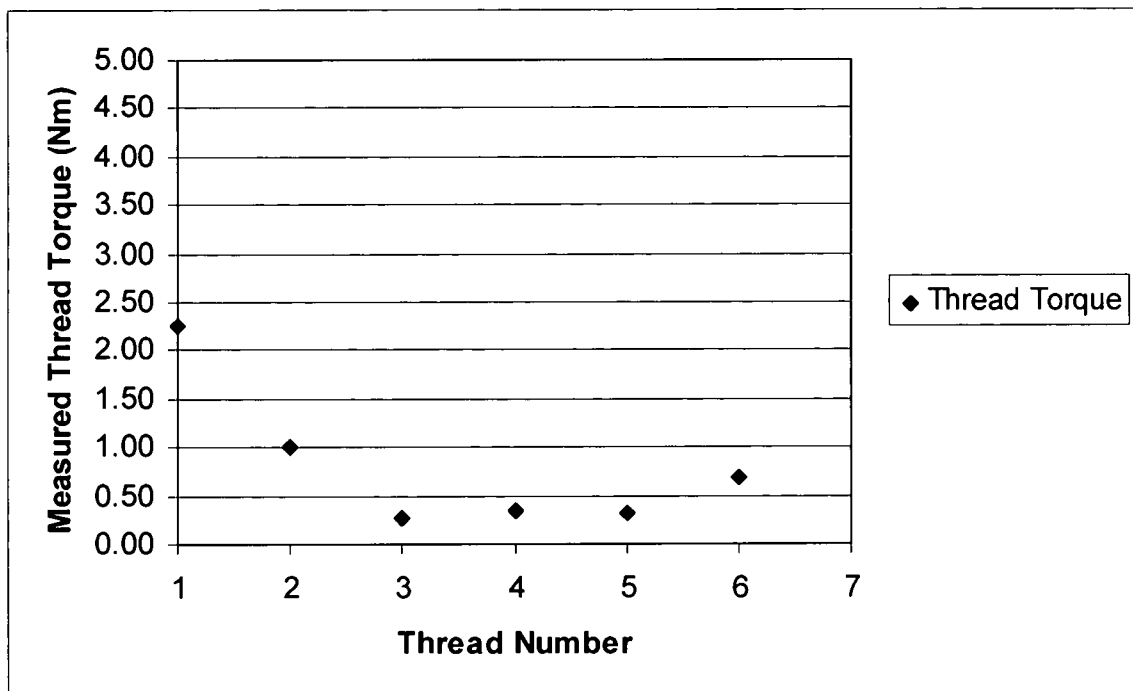


Figure 4.13 Plot of thread torque Vs six engaged threads.

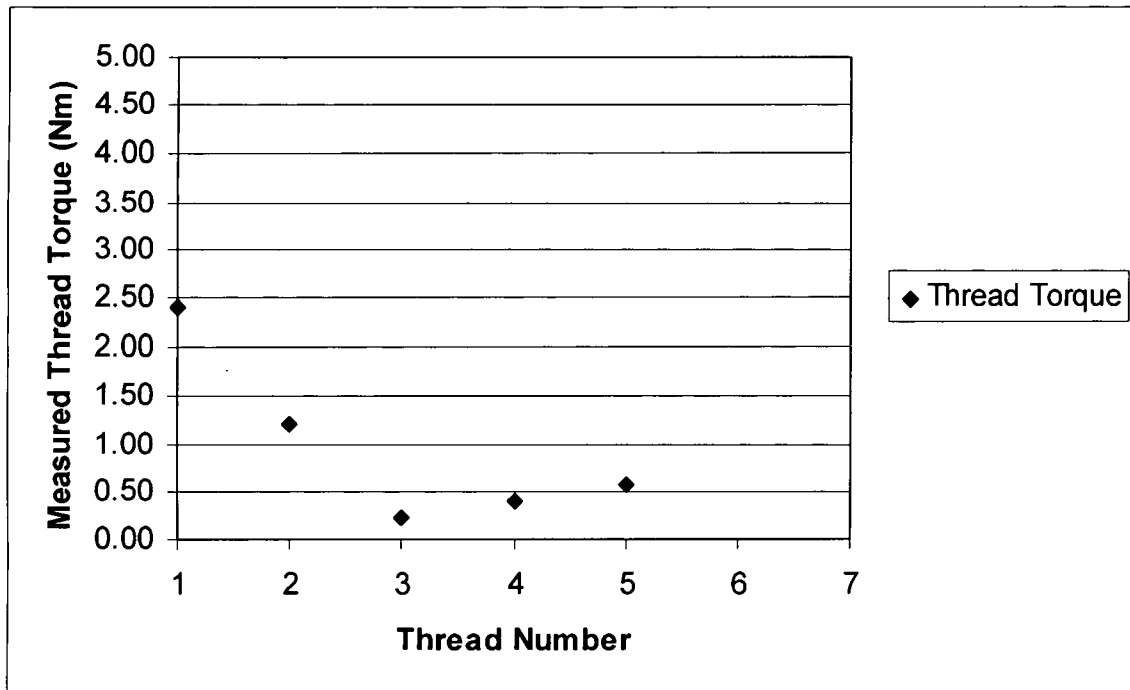


Figure 4.14 Plot of thread torque Vs five engaged threads.

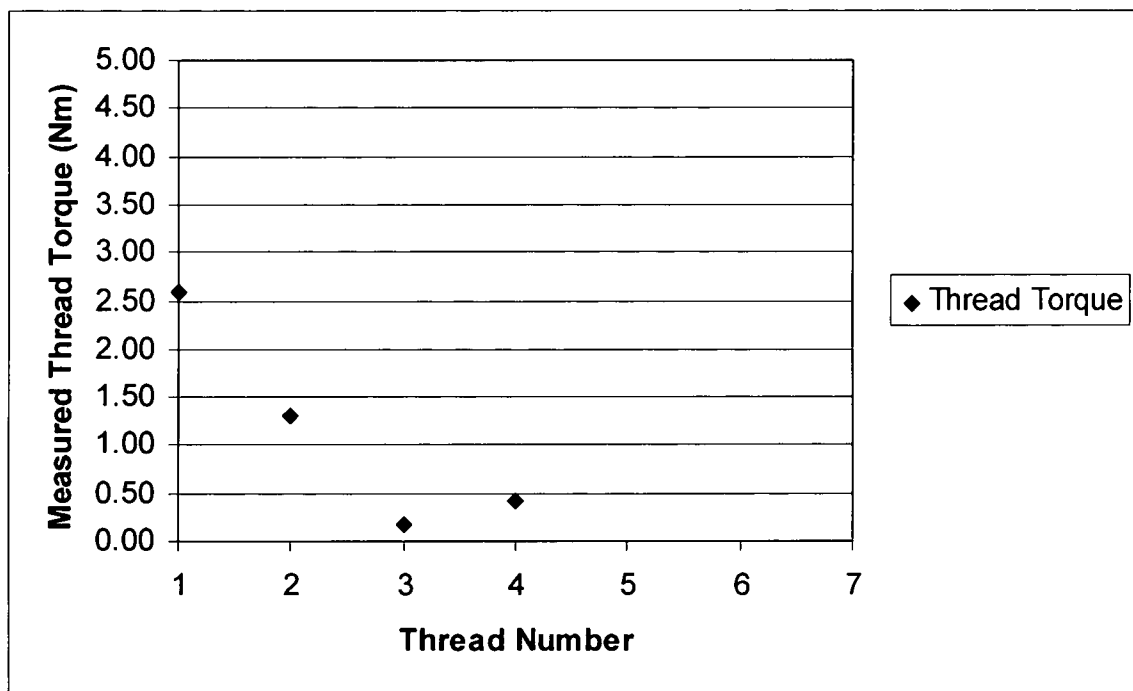


Figure 4.15 Plot of thread torque Vs four engaged threads.

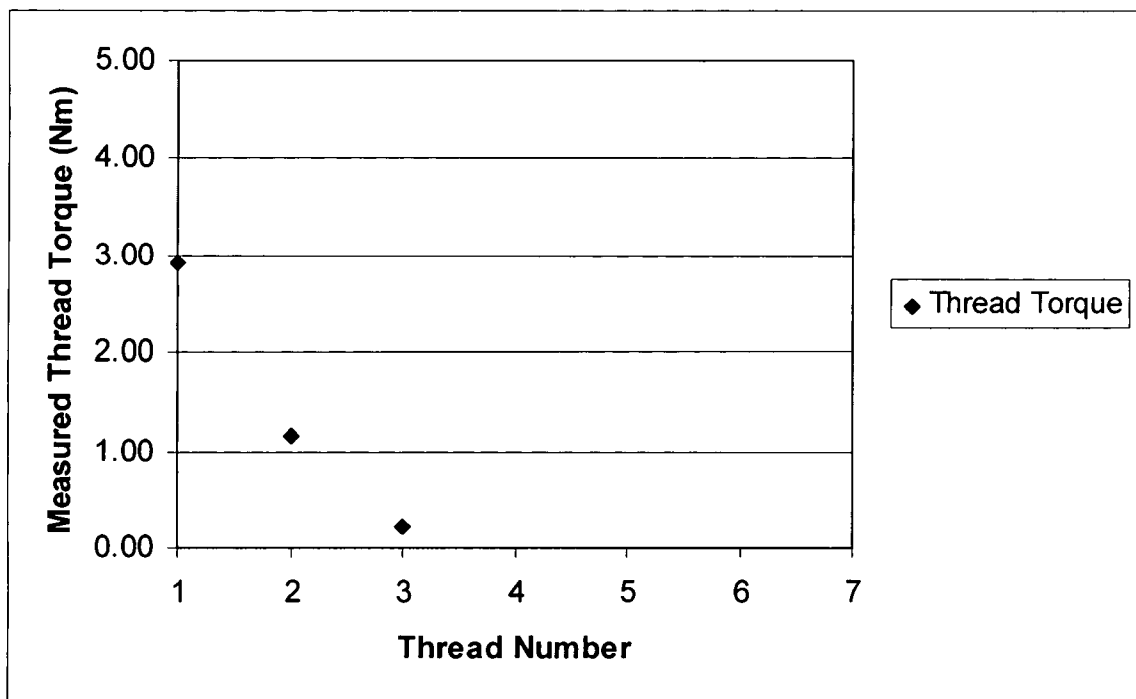


Figure 4.16 Plot of thread torque Vs three engaged threads.

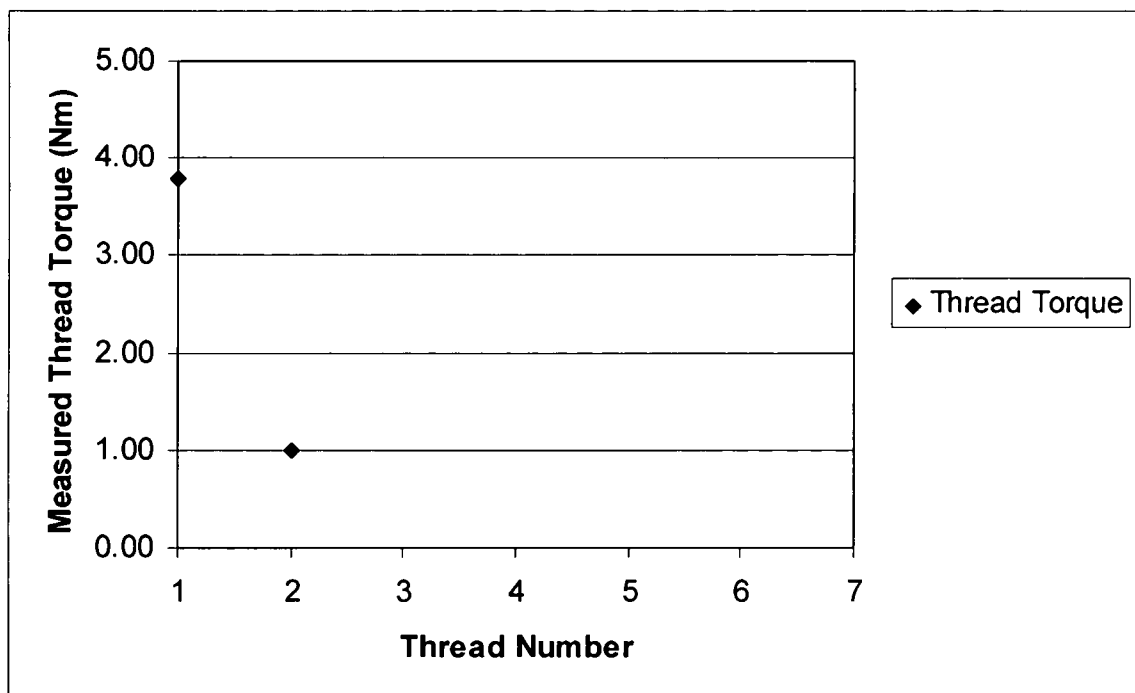


Figure 4.17 Plot of thread torque Vs two engaged threads.

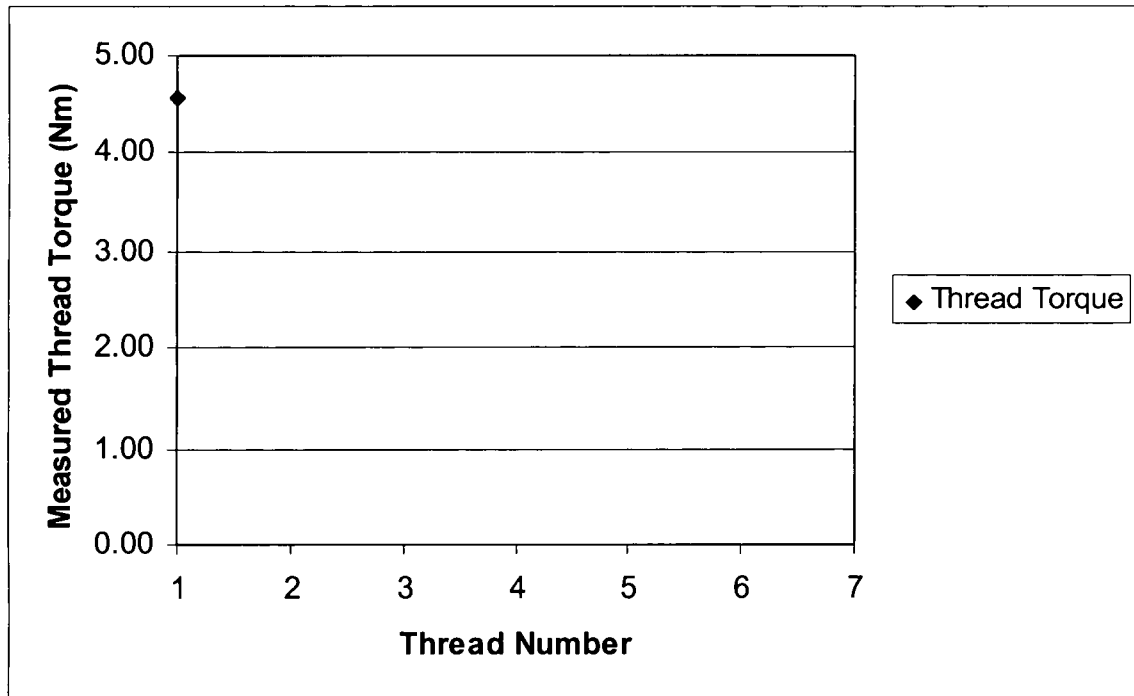


Figure 4.18 Plot of thread torque Vs one engaged threads.

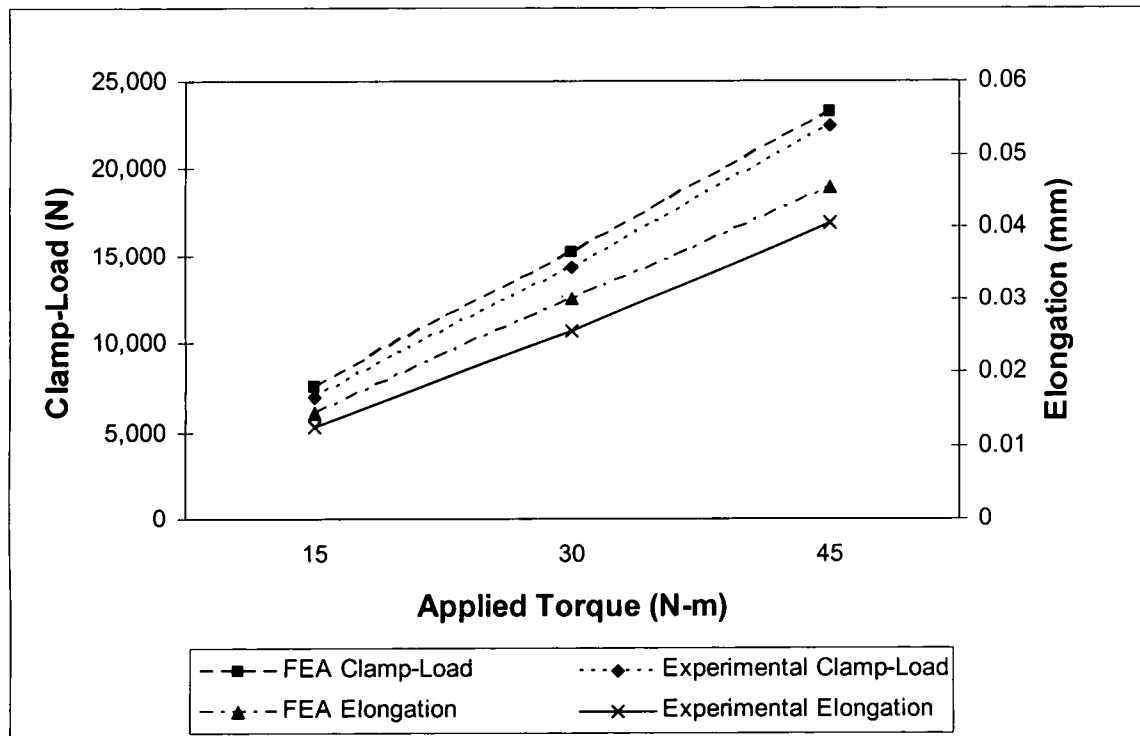


Figure 4.19 Plot of results from both the FEA modeling and the experiment for clamp-load and bolt elongation.

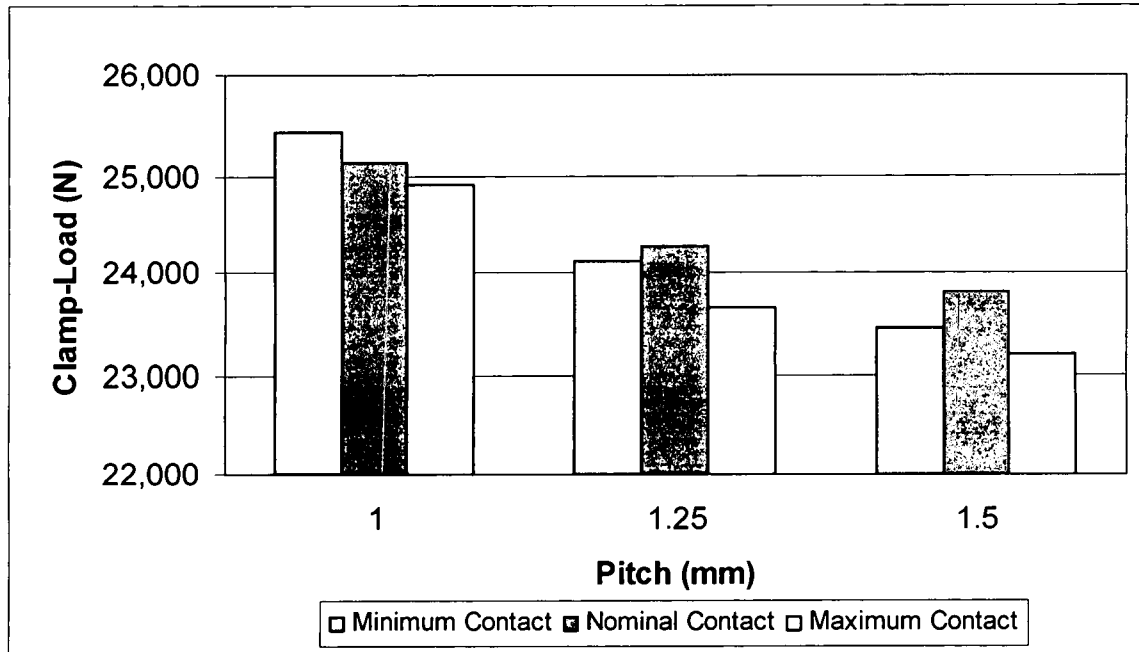


Figure 4.20 Bar chart showing the clamp-load for the minimum, nominal, and maximum contact levels, grouped by thread pitch.

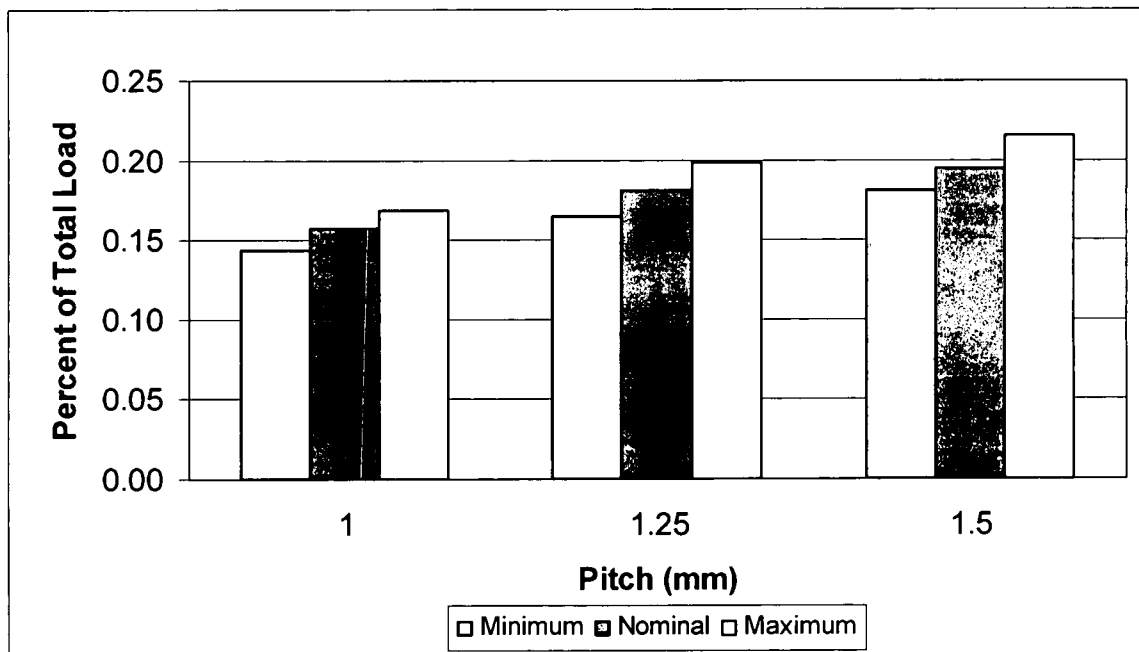


Figure 4.21 Bar chart showing the % of total clamp load on the 1st thread for the minimum, nominal, and maximum contact levels, grouped by pitch.

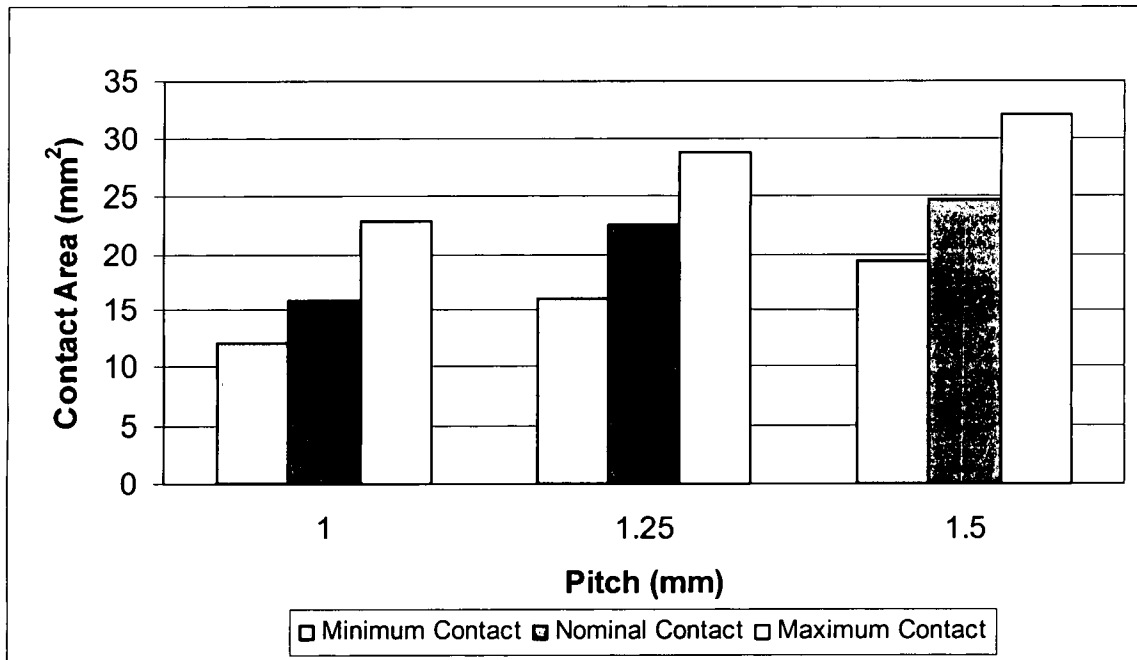


Figure 4.22 Bar chart showing the contact area at the 1st thread for the minimum, nominal, and maximum contact levels, grouped by pitch.

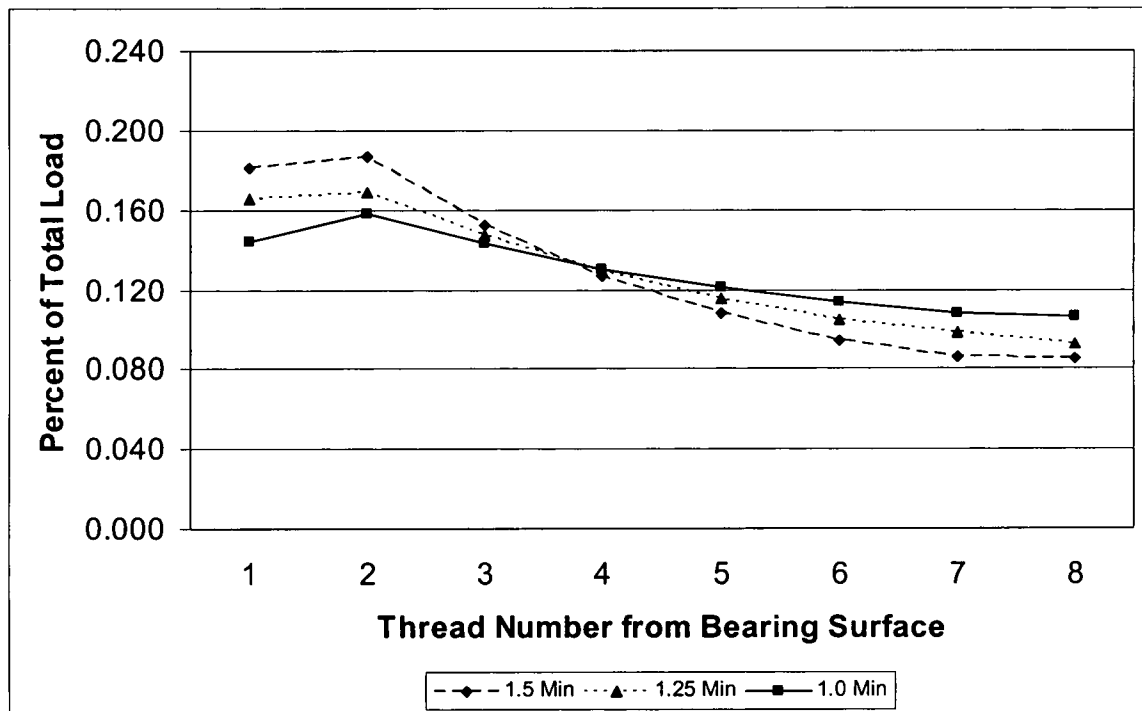


Figure 4.23 Plot of the load carried by different threads for an eight-thread engagement for the minimum contact level, grouped by pitch.

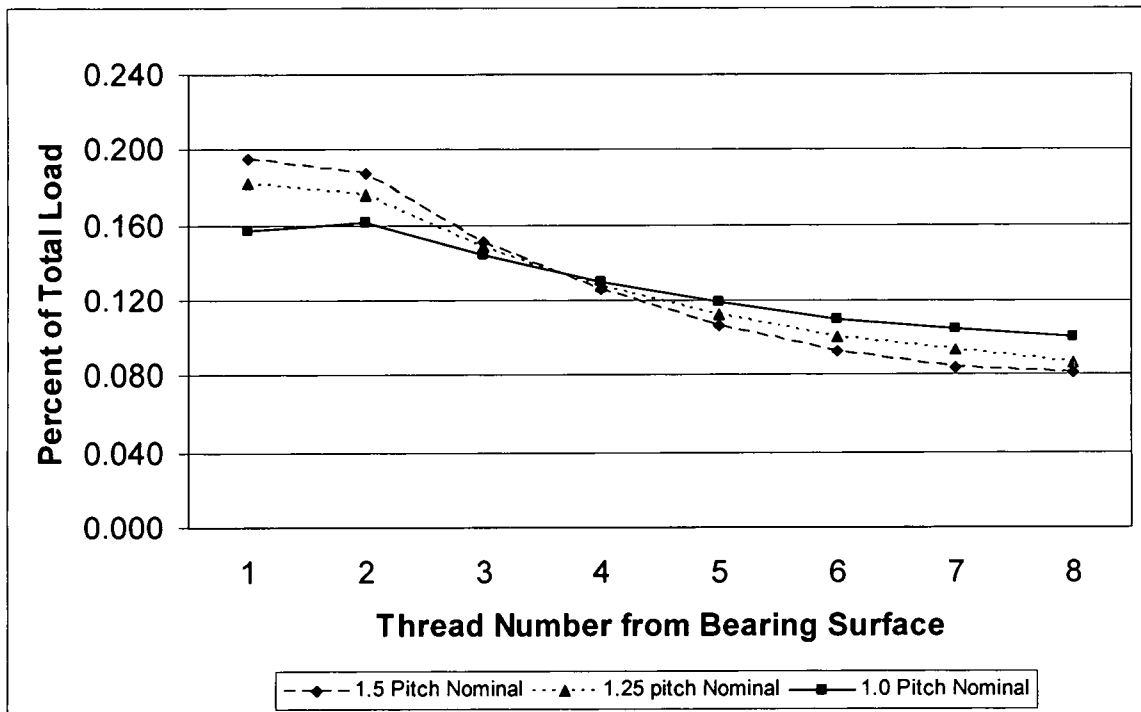


Figure 4.24 Plot of the load carried by different threads for an eight-thread engagement for the nominal contact level, grouped by pitch.

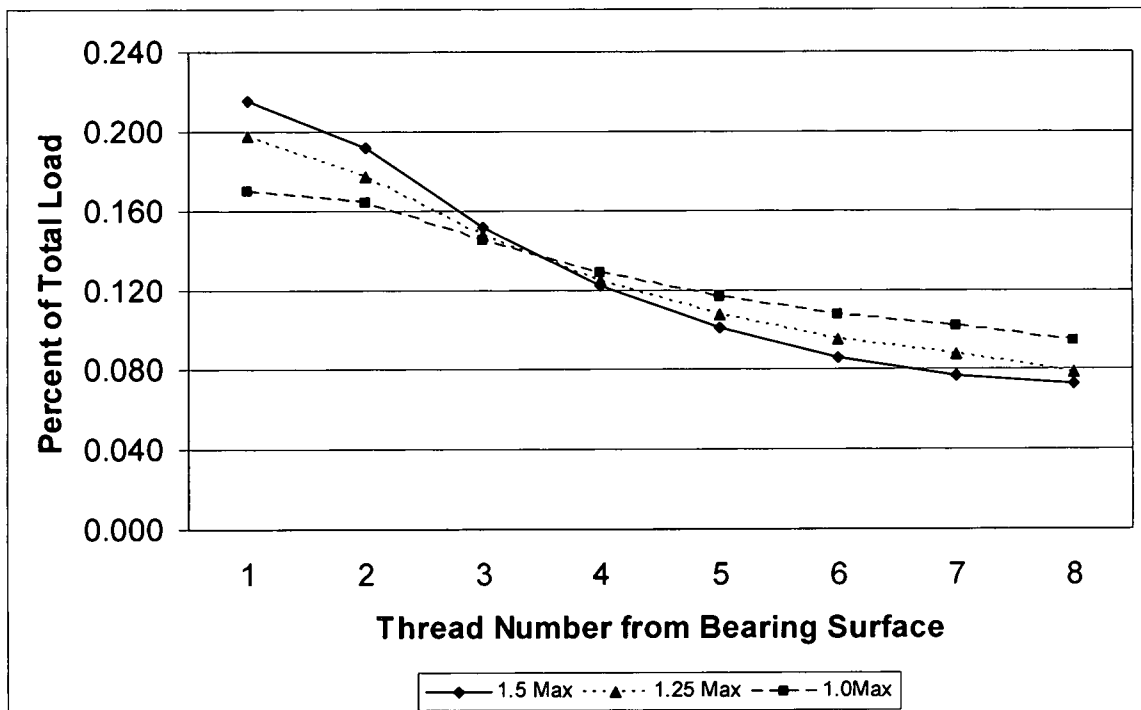


Figure 4.25 Plot of the load carried by different threads for an eight-thread engagement for the maximum contact level, grouped by pitch.

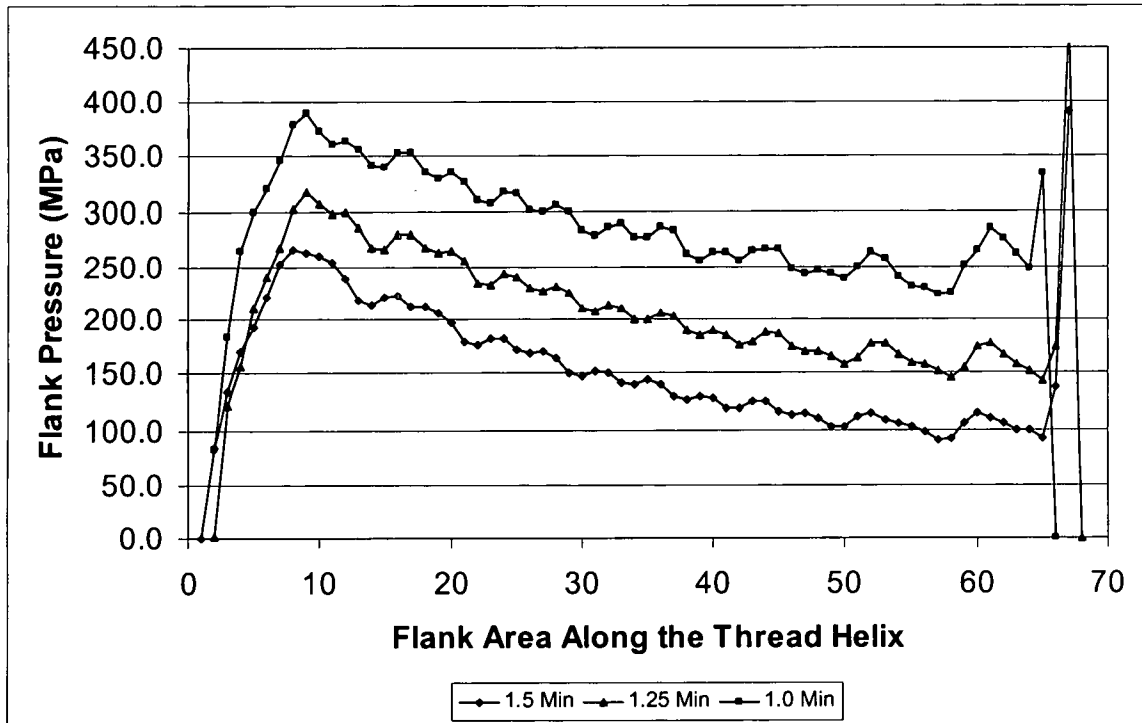


Figure 4.26 Plot of the contact pressure distribution across eight thread-engagement for the minimum contact level, grouped by pitch.

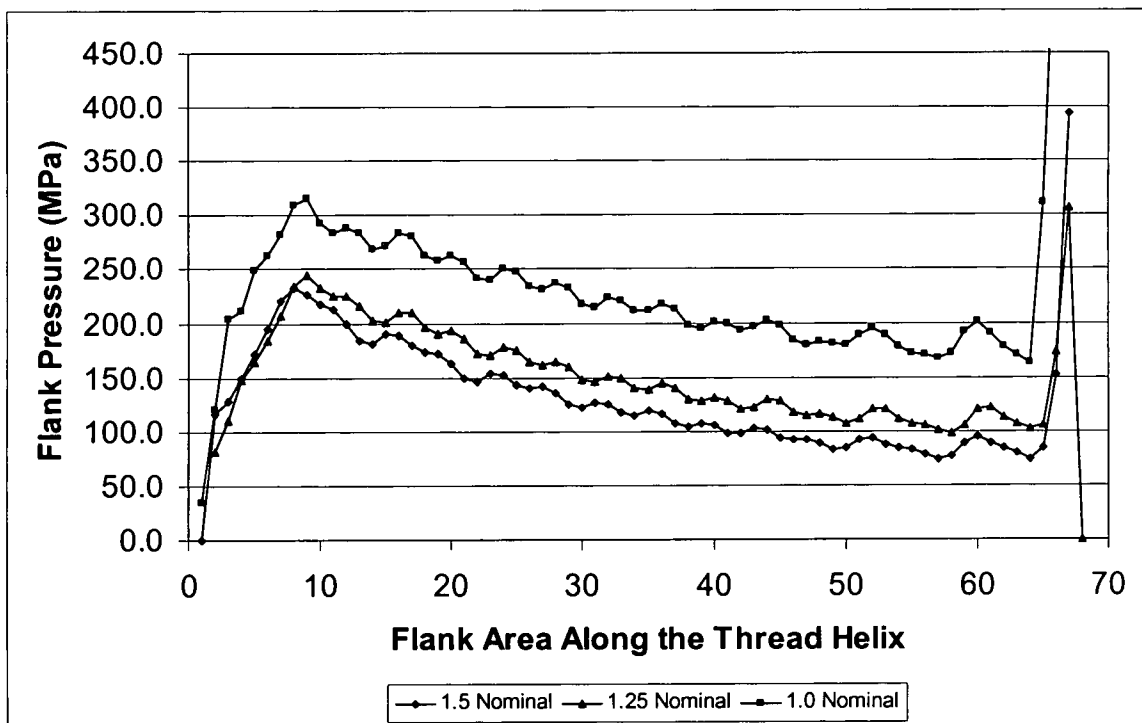


Figure 4.27 Plot of the contact pressure distribution across eight-thread engagement for the nominal contact level, grouped by pitch.

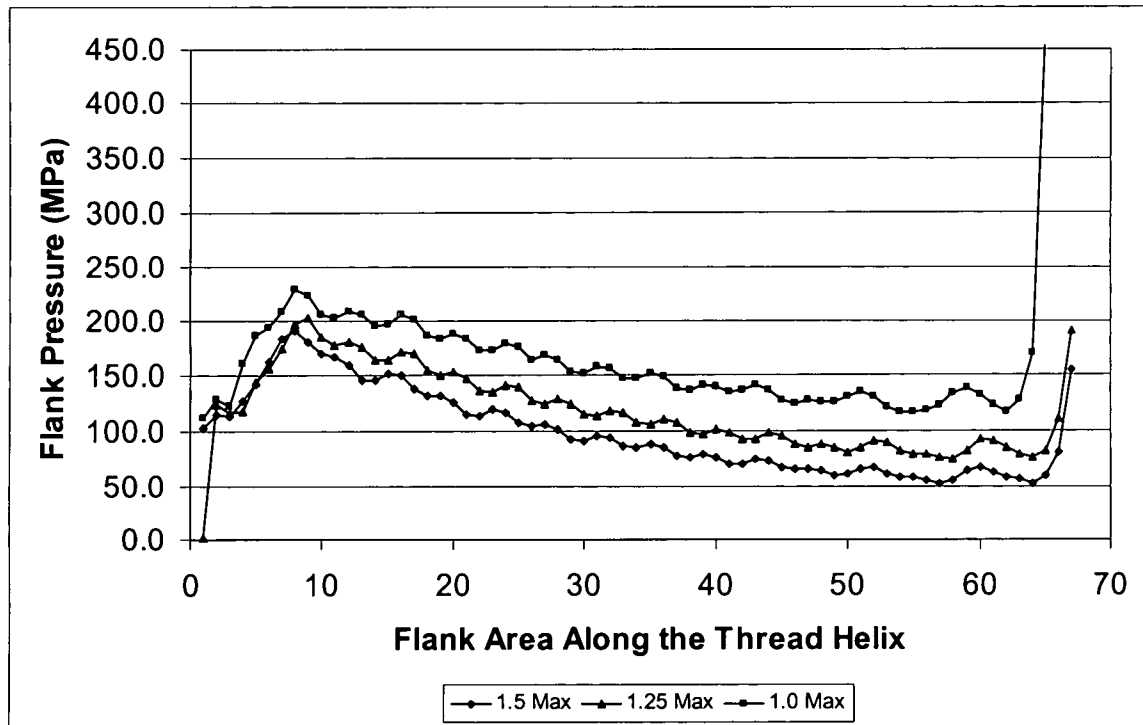


Figure 4.28 Plot of the contact pressure distribution across eight-thread engagement for the maximum contact level, grouped by pitch.

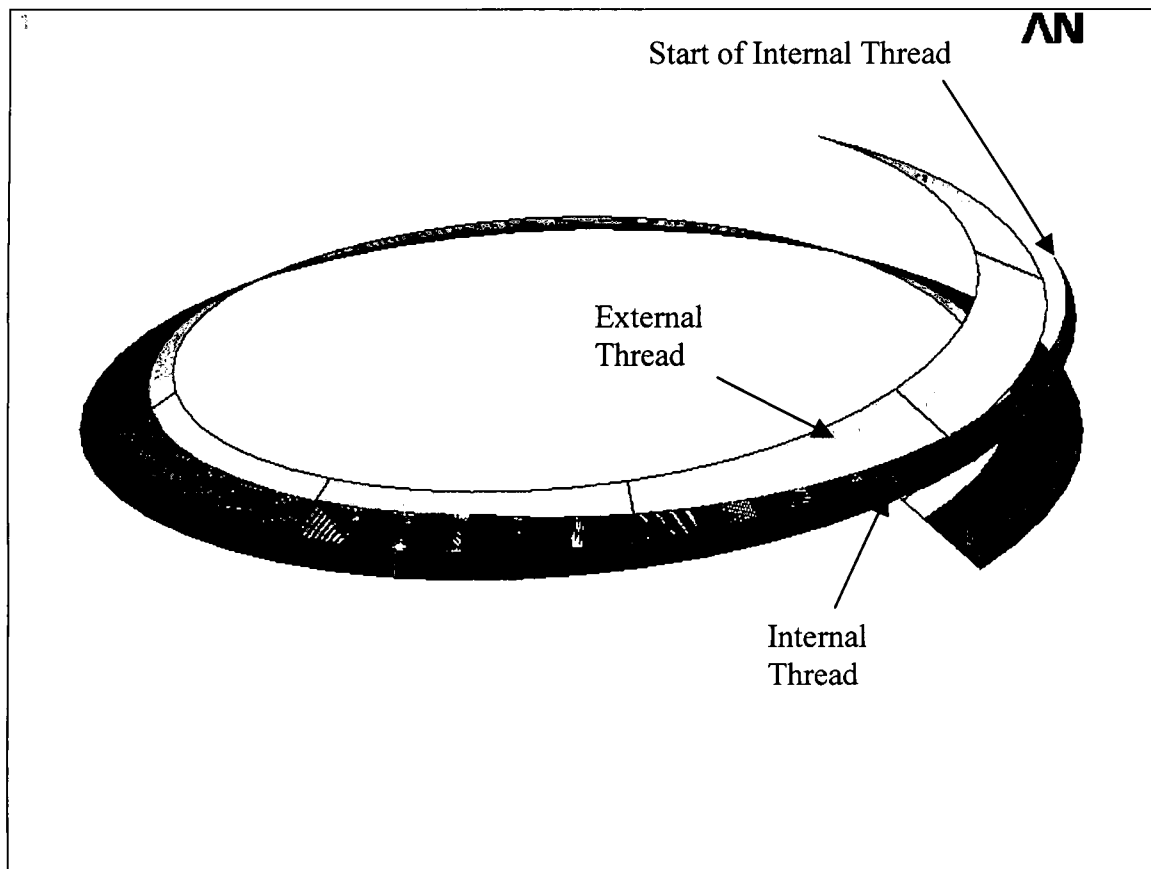


Figure 4.29 Plot of the contact area for the 1st thread on the 1.25mm pitch, minimum contact.

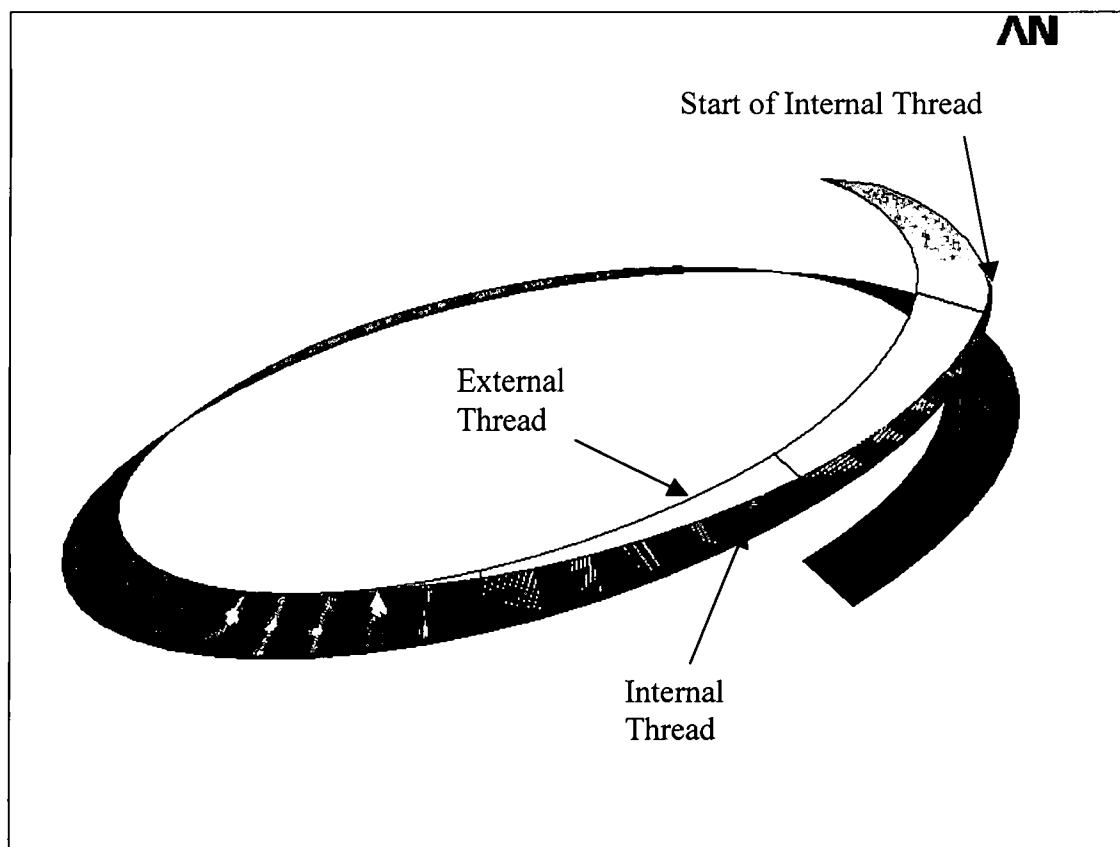


Figure 4.30 Plot of the contact area for the 1st thread on the 1.25mm pitch, maximum contact.

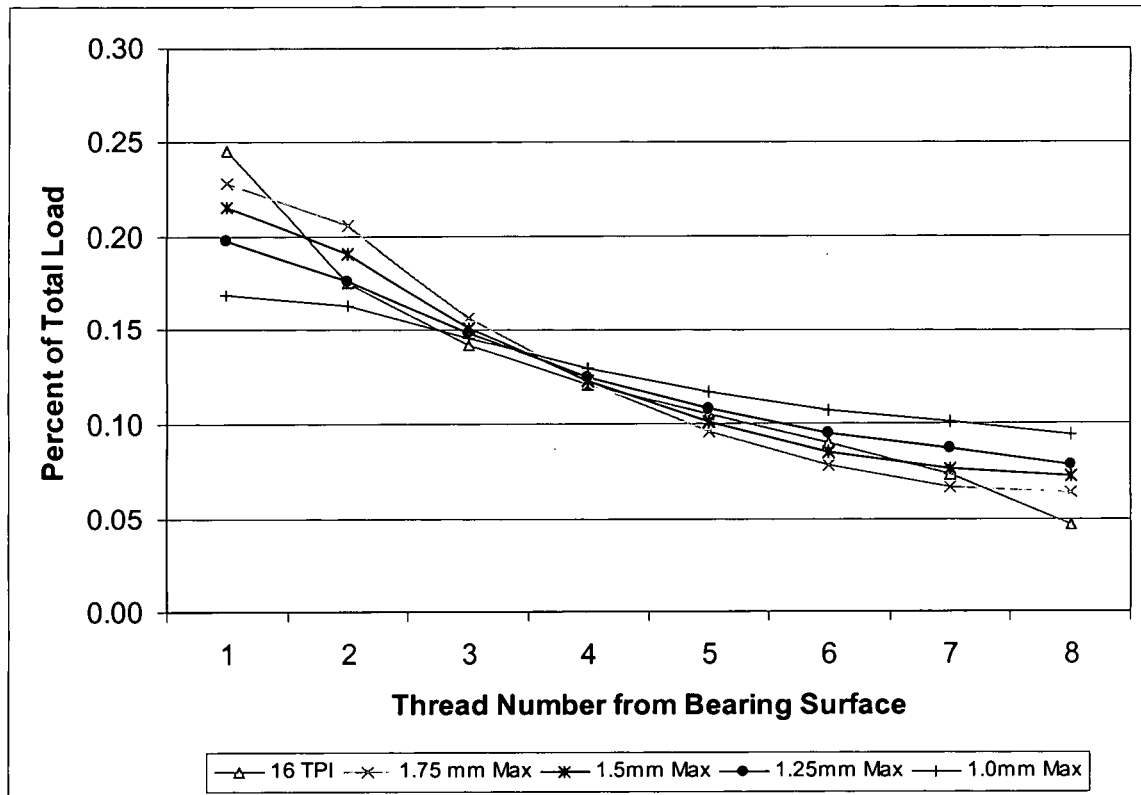


Figure 4.31 Plot of the load distribution for a 1 in 16 TPI bolt from Chen et al [15] using a static 3D model as well as the maximum contact level for the 1.0mm, 1.25mm, 1.5mm, and 1.75mm pitch.

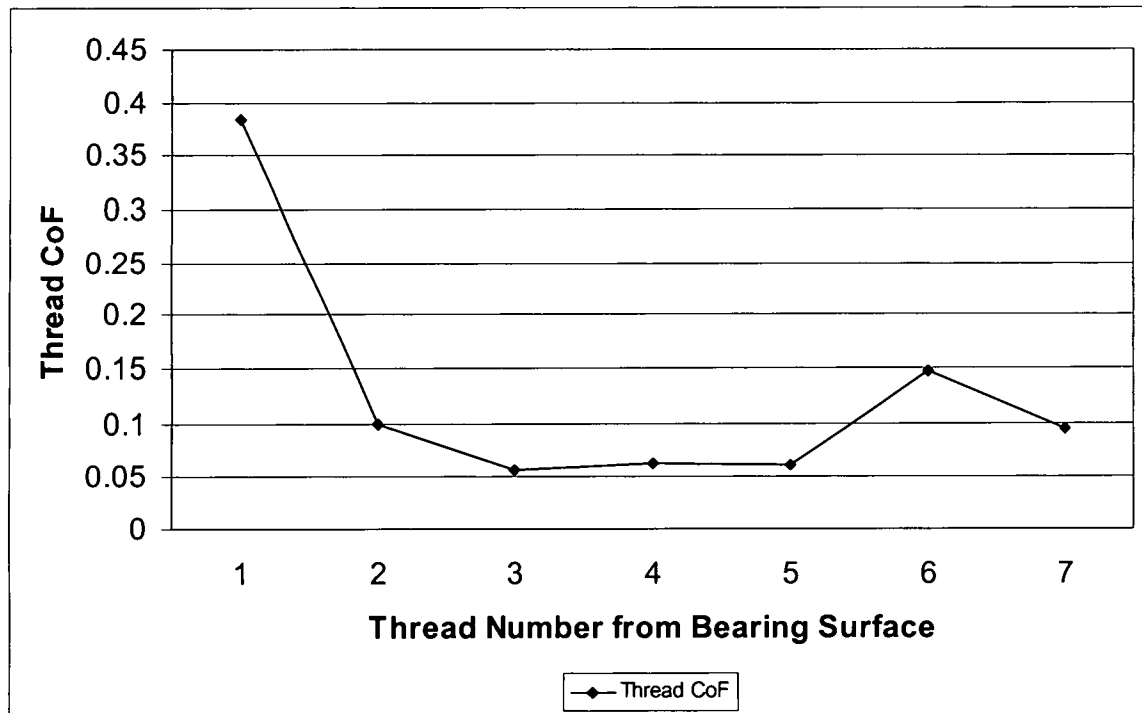


Figure 4.32 Plot of the thread CoF based on experimental thread torque data and FEA based clamp-load results.

Table 4.1 P-value convention	
Range	Description
P-Value > 0.1	No strong evidence that the independent variable affects the dependent variable
0.05 < P-Value < 0.1	Moderate evidence that the independent variable affects the dependent variable
0.01 < P-Value < 0.05	Strong evidence that the independent variable affects the dependent variable
P-Value < 0.01	Very strong evidence that the independent variable affects the dependent variable

Table 4.2 Averages of three replications on each of the six nut heights and four flange diameters with respect to flange diameter							
Head Size (mm)	Applied Torque (N-m)	Tension (N)	Under-Head Torque (N-m)	Thread Torque (N-m)	Thread CoF	Under-Head CoF	Under-Head Pressure (MPa)
21	40	27,782	12.7	27.3	0.145	0.061	346.8
20	40	25,981	14.2	25.8	0.147	0.073	399.5
19	40	25,065	15	25	0.147	0.083	486.4
18	40	24,323	15.6	24.4	0.148	0.091	614.4

Table 4.3 Averages for three replications on each of the six nut heights and four flange diameters with respect to nut height							
Nut Height (mm)	Applied Torque (N-m)	Tension (N)	Under-Head Torque (N-m)	Thread Torque (N-m)	Thread CoF	Under-Head CoF	Thread Flank Pressure (MPa)
13	40	24,818	16.4	23.6	0.138	0.088	188.9
11.5	40	26,711	13.6	26.4	0.146	0.072	229.8
10	40	25,738	14.6	25.4	0.146	0.079	254.7
8.5	40	26,633	12.9	27.1	0.151	0.067	310.1
7	40	25,893	14.1	25.9	0.148	0.076	366
5.5	40	24,933	14.6	25.4	0.152	0.080	448.6

Table 4.4 Effect of material hardness on clamp load parameters

Bolt	Washer	Nut	Applied Torque (N-m)	Clamp- Load (N)	Under- Head Torque (N-m)	Thread Torque (N-m)	Thread CoF	Under- Head CoF
Soft	Medium	Soft	35.0	26,290	13.0	22.0	0.116	0.064
Soft	Medium	Hard	35.0	26,517	12.4	22.5	0.119	0.061
Hard	Soft	Soft	35.0	26,541	11.8	23.1	0.123	0.058
Hard	Medium	Hard	35.0	26,602	11.6	23.4	0.125	0.057
Soft	Soft	Hard	35.0	27,027	12.0	22.9	0.119	0.058
Soft	Medium	Medium	35.0	27,036	12.7	22.3	0.114	0.061
Soft	Soft	Soft	35.0	27,082	12.5	22.5	0.115	0.061
Hard	Medium	Medium	35.0	27,171	11.1	23.9	0.125	0.053
Hard	Soft	Medium	35.0	27,192	10.5	24.5	0.128	0.050
Soft	Hard	Hard	35.0	27,476	10.9	24.1	0.124	0.052
Soft	Soft	Medium	35.0	27,568	12.3	22.7	0.113	0.058
Soft	Hard	Medium	35.0	27,612	12.2	22.7	0.114	0.058
Hard	Hard	Medium	35.0	28,092	9.9	25.1	0.127	0.046
Hard	Medium	Soft	35.0	28,110	11.0	23.9	0.119	0.051
Soft	Hard	Soft	35.0	28,145	11.7	23.3	0.115	0.054
Hard	Soft	Hard	35.0	28,176	10.7	24.3	0.121	0.050
Hard	Hard	Soft	35.0	28,562	11.0	24.0	0.117	0.050
Hard	Hard	Hard	35.0	28,606	10.1	24.8	0.122	0.046
Medium	Medium	Soft	35.0	29,527	10.1	24.9	0.117	0.045
Medium	Medium	Hard	35.0	29,622	9.7	25.3	0.119	0.043
Medium	Soft	Hard	35.0	30,151	9.2	25.7	0.119	0.040
Medium	Soft	Soft	35.0	30,425	9.6	25.4	0.115	0.041
Medium	Medium	Medium	35.0	30,455	9.6	25.4	0.115	0.041
Medium	Soft	Medium	35.0	30,603	8.9	26.1	0.119	0.038
Medium	Hard	Hard	35.0	31,131	8.1	26.9	0.121	0.034
Medium	Hard	Medium	35.0	31,433	8.2	26.8	0.119	0.034
Medium	Hard	Soft	35.0	32,585	8.6	26.4	0.111	0.034
Hardness Levels: Hard = 44 - 48HRC Medium = 34 - 38HRC Soft = 24 - 28HRC								

Table 4.5 Effect of minimizing under-head CoF on clamp load parameters

Bearing Surface	Clamp-Load (N-m)	Under-Head Torque (N-m)	Thread Torque (N-m)	Thread CoF	Under-Head CoF	Under-Head Pressure (MPa)	Thread Flank Pressure (MPa)
Thrust Bearing	40,200	9.6	30.4	0.101	0.037	482.3	198.9
Standard Washer	28,325	19	21	0.097	0.104	367.2	140.2

Table 4.6 Effect of thread and under-head CoF on clamp load parameters

Test	Thread Condition	Head Condition	Tension (N)	Under-Head Torque (Nm)	Thread Torque (Nm)	Thread CoF	Und CoF
1	Dry	Lubricated	31,305	9.2	30.8	0.147	0.041
2	Lubricated	Dry	24,466	20.8	19.2	0.106	0.121
3	Dry	Dry	15,590	25.0	15.0	0.141	0.228
4	Lubricated	Lubricated	32,318	14.3	25.7	0.108	0.063

Table 4.7 Clamp-load and CoF data for 15 N-m of applied torque for FEA model joint

Run-Down	Applied Torque (N-m)	Clamp-Load (N)	Under-Head CoF	Thread CoF
1	15	6,564	0.144	0.176
2	15	6,511	0.145	0.178
3	15	6,571	0.141	0.18
4	15	6,576	0.142	0.178
5	15	6,656	0.14	0.176
6	15	6,794	0.136	0.173
Averages	15	6.612	0.141	0.177

Table 4.8 Clamp-load and CoF data for 30 N-m of applied torque for FEA model					
Run-Down	Applied Torque (N-m)	Clamp-Load (N)	Under-Head CoF	Thread	CoF
1	30	13,740	0.137	0.167	
2	30	13,866	0.137	0.164	
3	30	13,687	0.138	0.167	
4	30	13,762	0.137	0.166	
5	30	13,820	0.138	0.162	
6	30	13,958	0.135	0.163	
Averages	30	13.806	0.137	0.165	

Table 4.9 Clamp-load and CoF data for 45 N-m of applied torque for FEA model joint					
Run-Down	Applied Torque (N-m)	Clamp-Load (N)	Under-Head CoF	Thread	CoF
1	45	21,267	0.135	0.158	
2	45	21,480	0.132	0.157	
3	45	21,250	0.134	0.159	
4	45	21,129	0.135	0.16	
5	45	20,992	0.136	0.162	
6	45	21,592	0.131	0.157	
Averages	45	21.285	0.134	0.159	

Table 4.10 Clamp-load and bolt elongation at various torques						
Run-Down	Tension @ 15N-m of Applied Torque (N)	Elongation @ 15N-m of Applied Torque (mm)	Tension @ 30N-m of Applied Torque (N)	Elongation @ 30N-m of Applied Torque (mm)	Tension @ 45N-m of Applied Torque (N)	Elongation @ 45N-m of Applied Torque (mm)
1	6,737	0.0124	13,947	0.0254	21,520	0.0406
2	7,036	0.0130	14,578	0.0279	22,181	0.0406
3	7,053	0.0130	14,764	0.0279	22,433	0.0406
Averages	6.942	0.0127	14.430	0.0254	22.045	0.0406

Table 4.11 Thread torque and adjustment for 7 engaged threads					
Number of Threads Engaged	Thread Number	Ave Strain @4.5Nm Thread Torque	Calculated Thread Torque (Nm)	Correction for 1st Thread	Adjusted Thread Torque (Nm)
7	1	92.2	2.69	0.42	2.27
	2	22.4	0.65		0.65
	3	20.7	0.37		0.37
	4	17.1	0.32		0.32
	5	23.2	0.27		0.27
	6	19.6	.044		0.44
	7	19.2	0.31		0.31
				Total	4.63

Table 4.12 Thread torque and adjustment for 6 engaged threads					
Number of Threads Engaged	Thread Number	Ave Strain @4.5Nm Thread Torque	Calculated Thread Torque (Nm)	Correction for 1st Thread	Adjusted Thread Torque (Nm)
6	1	91.7	2.68	0.41	2.26
	2	28.5	1.0		1.0
	3	14.7	0.26		0.26
	4	18.4	0.35		0.35
	5	26.3	0.32		0.32
	6	27.6	0.69		0.69
				Total	4.88

Table 4.13 Thread torque and adjustment for 5 engaged threads					
Number of Threads Engaged	Thread Number	Ave Strain @4.5Nm Thread Torque	Calculated Thread Torque (Nm)	Correction for 1st Thread	Adjusted Thread Torque (Nm)
5	1	96.8	2.8	0.39	2.41
	2	31.8	1.21		1.21
	3	12.2	0.22		0.22
	4	20.8	0.4		0.4
	5	37.3	0.56		0.56
				Total	4.8

Table 4.14 Thread torque and adjustment for 4 engaged					
Number of Threads Engaged	Thread Number	Ave Strain @4.5Nm Thread Torque	Calculated Thread Torque (Nm)	Correction for 1st Thread	Adjusted Thread Torque (Nm)
4	1	107.0	3.03	0.44	2.59
	2	33.2	1.31		1.31
	3	6.9	0.16		0.16
	4	22.1	0.43		0.43
				Total	4.5

Table 4.15 Thread torque and adjustment for 3 engaged threads					
Number of Threads Engaged	Thread Number	Ave Strain @4.5Nm Thread Torque	Calculated Thread Torque (Nm)	Correction for 1st Thread	Adjusted Thread Torque (Nm)
3	1	129.1	3.5	0.59	2.91
	2	31.2	1.18		1.18
	3	12.2	0.22		0.22
				Total	4.31

Table 4.16 Thread torque and adjustment for 2 engaged threads					
Number of Threads Engaged	Thread Number	Ave Strain @4.5Nm Thread Torque	Calculated Thread Torque (Nm)	Correction for 1st Thread	Adjusted Thread Torque (Nm)
2	1	142.6	3.78	0.37	3.41
	2	28.5	0.99		0.99
				Total	4.4

Table 4.17 Thread torque and adjustment for 1 engaged					
Number of Threads Engaged	Thread Number	Ave Strain @4.5Nm Thread Torque	Calculated Thread Torque (Nm)	Correction for 1st Thread	Adjusted Thread Torque (Nm)
1	1	184.5	4.58	0	4.58
Total					4.58

Table 4.18 Addition of measured thread torque values from Section 2.7.6 to the FEA results from Section 3.4 and discussed in Section 4.5

Thread Number	Measured Thread Torque per Thread (N-m)	FEA Clamp-Load per Thread (N)		Resulting Thread CoF
1	2.27	1,023.5		0.384
2	0.65	864.8		0.099
3	0.368	695.4		0.056
4	0.322	573.3		0.063
5	0.275	493.0		0.062
6	0.436	438.7		0.146
7	0.306	419.3		0.095
Total measured thread torque for seven thread engagement fixture	4.63		Average measured thread CoF for seven thread engagement fixture	0.129
Actual average calculated thread torque from load-cell	4.5		Actual average calculated thread CoF from load-cell	0.137

* The thread number indicates the position of the thread in relation to the head of the bolt (the 1st thread is closest to the head)

CHAPTER V

CONCLUSIONS AND RECOMMENDATIONS FOR FUTURE WORK

5.1. Conclusions

An investigation of the thread and under-head coefficient of friction in a bolted joint was conducted, which involved experimental, analytical, and finite element analysis (FEA) modeling to understand the effects of friction on the clamp-load.

In the experimental work, presented in this dissertation, the amount of thread torque developed on individual threads for a seven thread engagement was successfully measured for the first time. The analytical work established the equations, which are necessary to calculate the CoF values for the thread and under-head regions of the bolted joint. To derive these equations, a thread was considered as an inclined plane. The equation's independent variables included the clamp-load, thread pitch and nominal pitch diameter, thread and under-head CoF, as well as the included half angle of the thread. The FEA work consisted of successfully creating a working dynamic model capable of allowing a torque to be applied to the head of a bolt. This was a realistic representation of how the bolt is tightened, and no prior information is available on this type of the model.

The following are the specific conclusions from the research conducted for this dissertation.

1. The size of the under-head flange of the bolt has pronounced effect on the clamp load more than the length of engagement. It was shown that as the diameter of the flange increases, the magnitude of developed clamp-load also increases.

2. The thread and under-head CoF values decreased as the speed at which the fastener is tightened increased. The decreasing CoF allowed for an increase in the magnitude of the clamp-load. This trend was evident regardless of the presence of a coating, plating, or a lubricant on the fastener.
3. The relative hardness of the joint materials has an affect on the thread and under-head CoF values. The choice of material hardness can result in the both the thread and under-head CoF being equal or very different, as much as by a factor of 2-3. This disproves that accepted understanding that the two frictional values are always similar. The best results were obtained with medium bolt and high washer hardnesses.
4. The under-head CoF has more pronounced effect on clamp load than the thread CoF.
5. Changes made solely to the under-head CoF value had an effect on under-head CoF, clamp-load, and thread and under-head torque; however, it did not have any effect on thread CoF.
6. In most cases, the under-head CoF value is lower than the thread CoF. This relationship holds when both values are low and less than 0.1. When the under-head CoF value is greater then 0.1, the difference between the two frictional values increases dramatically.
7. When examining an eight thread engagement, the load carried by the 1st thread is maximum and minimum on the 8th thread, except that for the case of the minimal flank area. The first three threads support 45% to 56% of the total load developed in the threads.

8. A dynamic FEA model was created which allowed for the tightening of a bolt into a joint. The full 3D model was patterned after an actual bolted joint machined from 4140 steel. The critical parameters for the model, the thread and under-head CoF values were physically measured from the actual joint. There was a 5.2% difference between the model clamp-load and the experimental joint clamp-load.
9. The load is more evenly distributed for a fine pitch thread than for the coarse pitch threads. The standard deviation of the load on all eight engaged threads is smaller for the fine pitch bolt compared to all eight engaged thread of the coarse pitch bolt.
10. The pressure distribution is inversely proportional to the load distribution. As the thread pitch decreases, the amount of pressure on each engaged thread increases. This is due to the relative contact area between the internal and external threads. A fine pitch thread has a smaller contact area compared to that of a coarse pitch thread. The fine pitch thread had a higher level of pressure associated with it.
11. Thread torque generated on each individual thread was measured independent of each-other. The 1st engaged thread (one closest to the head of the bolt) had a higher level of thread torque associated with it compared to the remaining six threads for a seven thread engagement. The magnitude of thread torque decreased from the 1st thread to the 7th thread.
12. The thread CoF generated on each individual thread was calculated from the results of both experimental and FEA data. The thread CoF was found to be highest on the 1st engaged thread and then was found to diminish when examining the 2nd through the 7th thread.

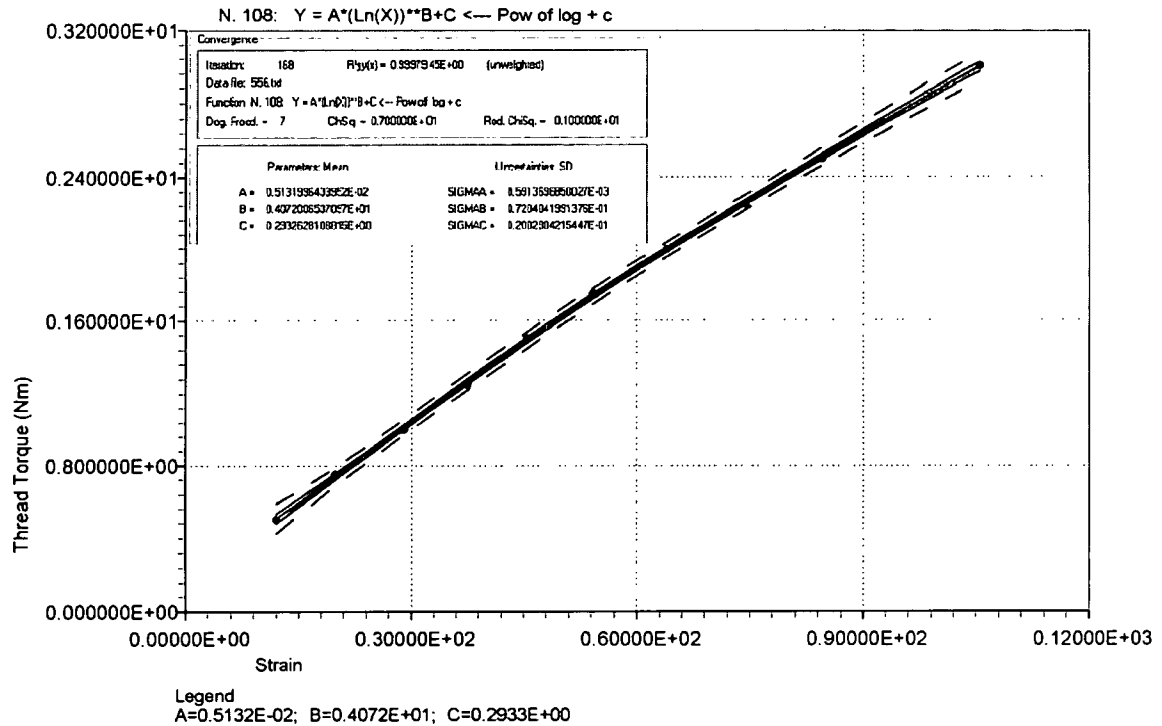
5.2 Future Research

Future research will involve the refinement of the dynamic FEA model of the bolted joint. The new model will interactively create any size threaded joint with a choice of several bolt head styles. This next generation model will be design tool capable of not only realistically determining the torque/clamp-load relationship, but also the effect of loading parameters on the developed clamp-load. The code will prompt the user to input material choice of the bolt, nut, and bearing surface, number of threads on both the nut and the bolt, the length of the shank of the bolt, the thread and under-head CoF values, and the class and tolerance of the internal and external threads. The code will also ask the user to input the target torque and solve the model. After all parameters are inputted, the clamp load and other corresponding parameters will be outputted.

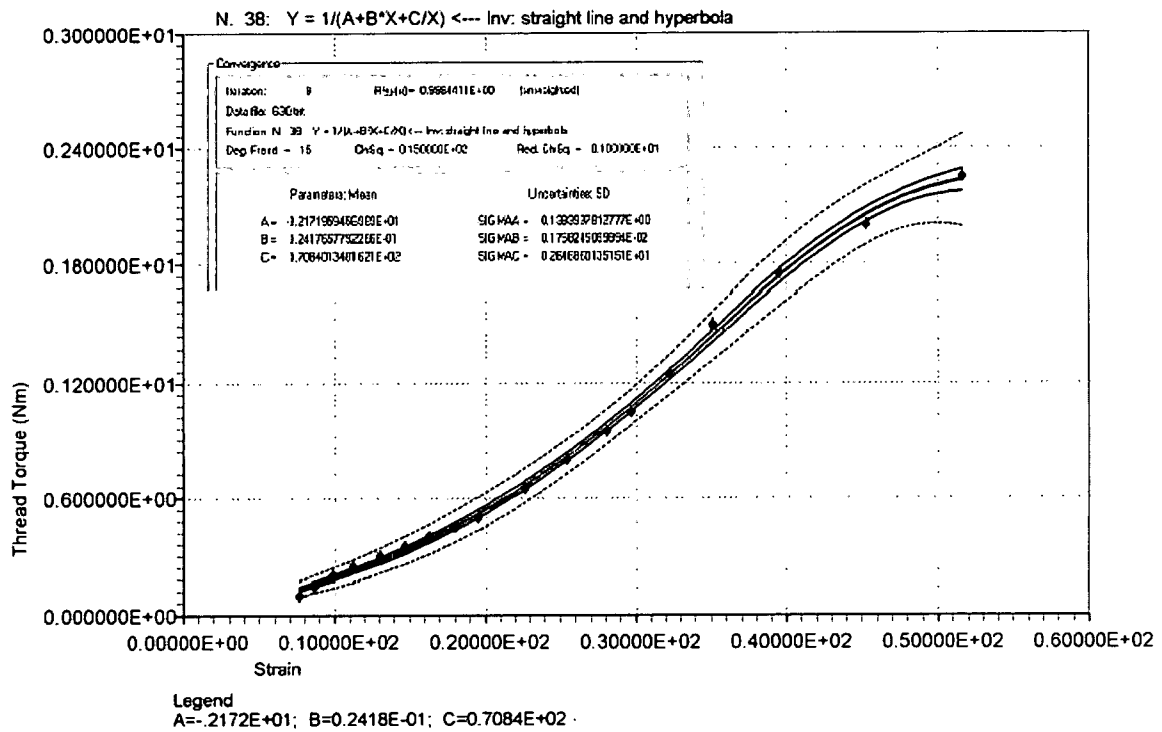
APPENDIX I

The following graphs are calibration curves for the thread torque development of Section 2.7.6.

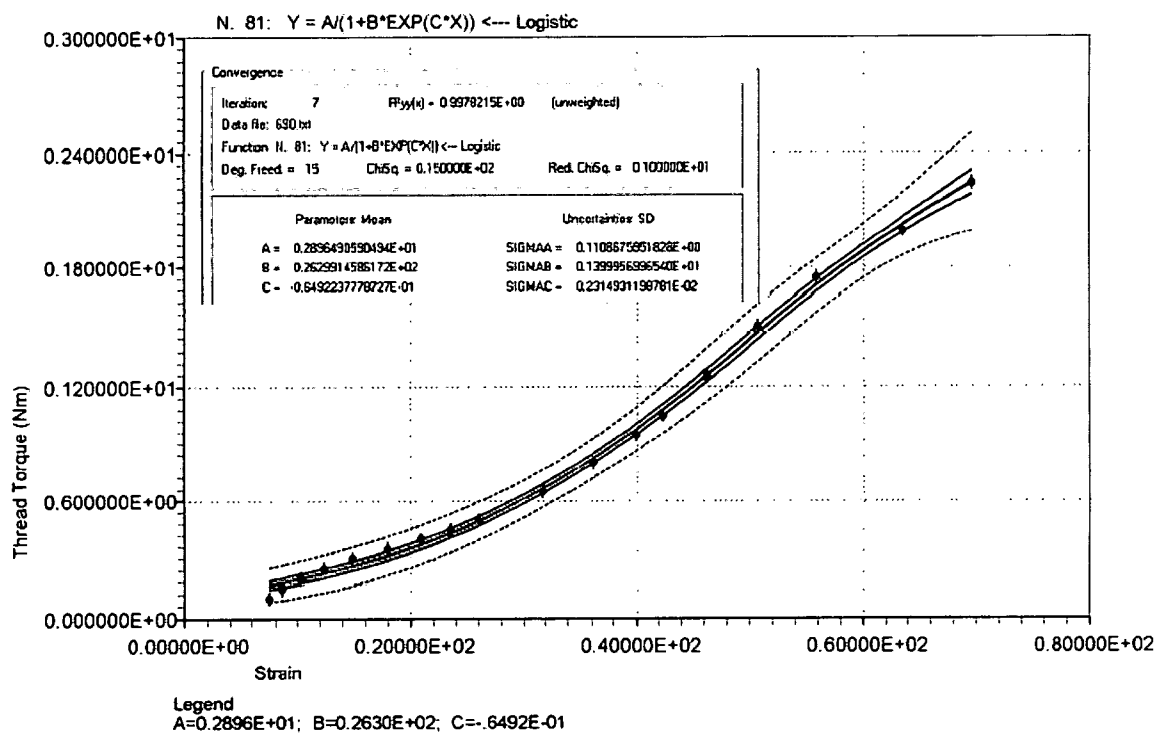
556



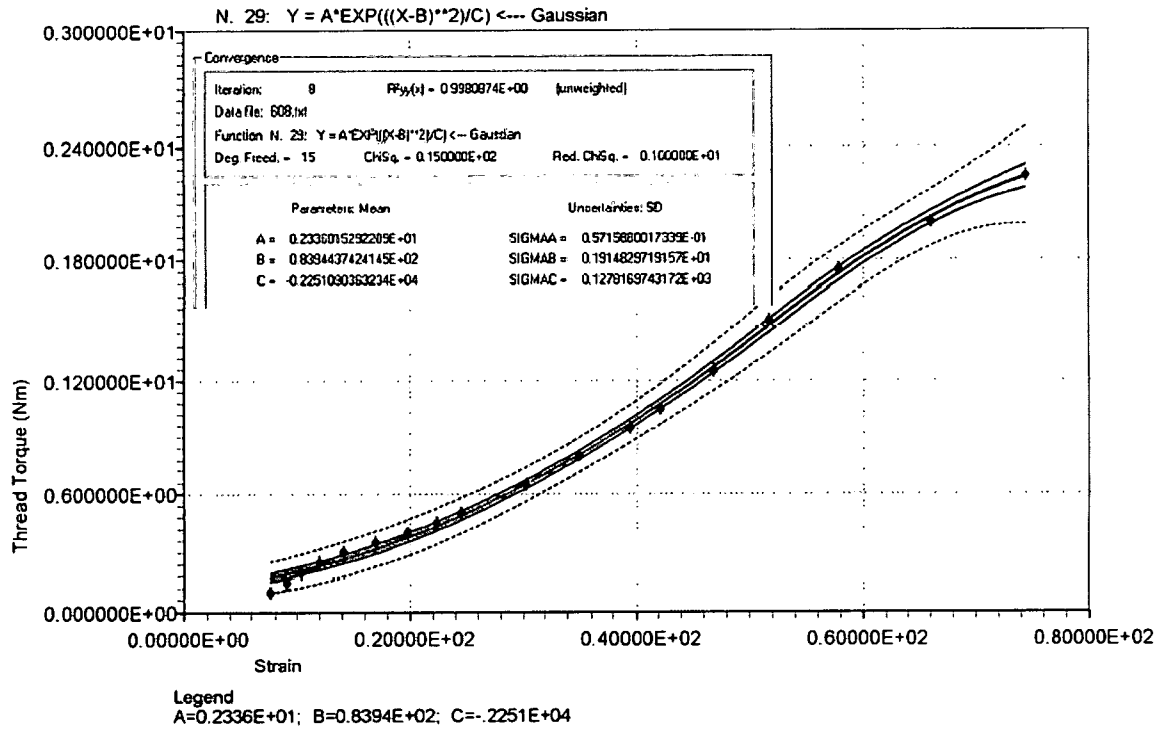
Calibration Curve for Thread #1



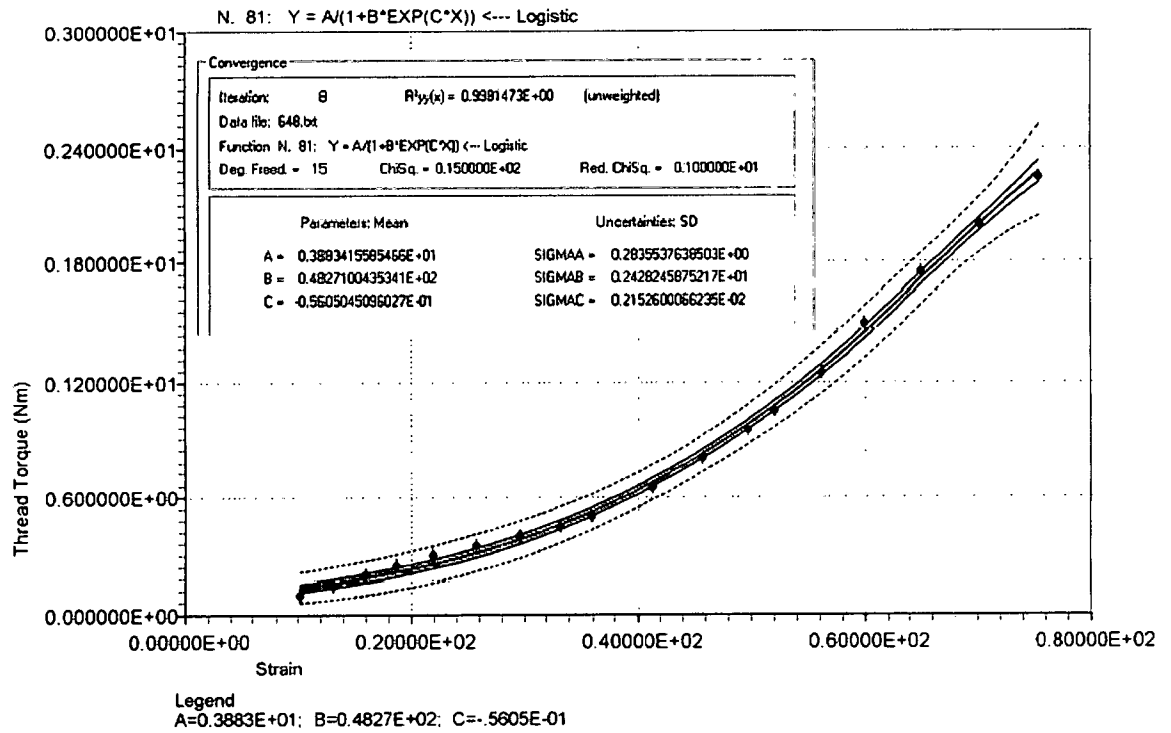
Calibration Curve for Thread #2



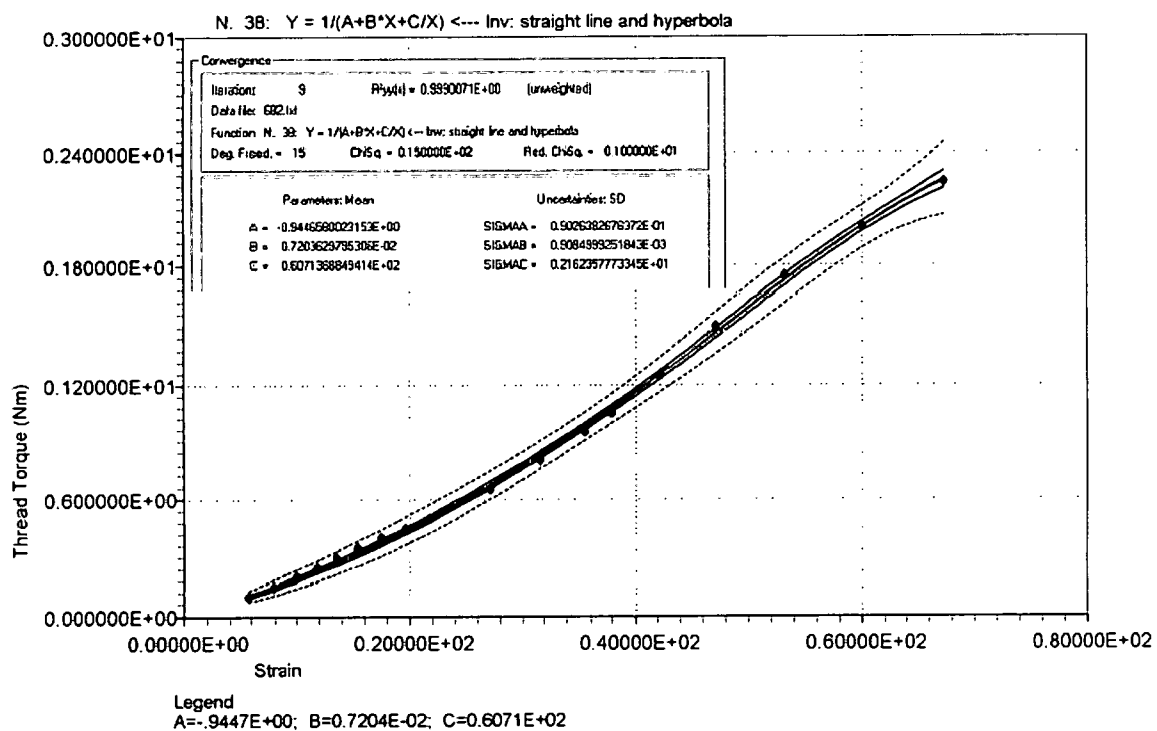
Calibration Curve for Thread #3



Calibration Curve for Thread #4

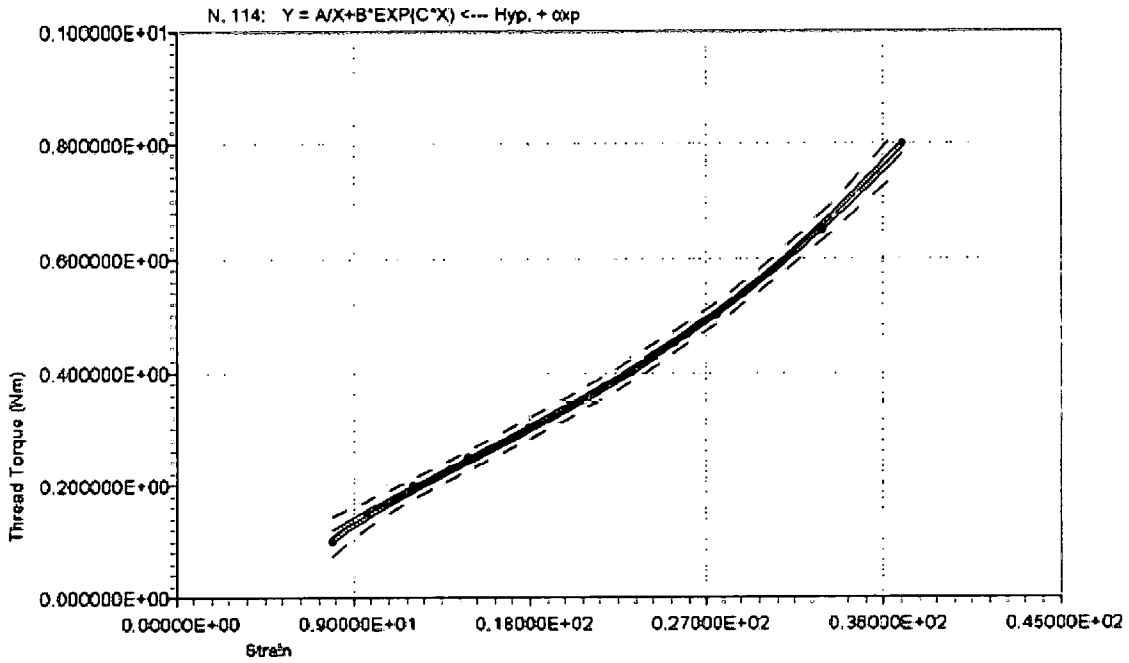


Calibration Curve for Thread #5



Calibration Curve for Thread #6

581 A



Legend
 $A = -0.9059E+00$; $B = 0.1562E+00$; $C = 0.4482E-01$

Convergence

Iteration: 7 $R^2_{xy}(x) = 0.9993827E+00$ (unweighted)
 Datafile: 581 A.txt
 Function N. 114: $Y = A/X + B \cdot \exp(C \cdot X)$ --- Hyp. + exp
 Deg. Freed. = 8 ChSq. = 0.800000E+01 Red. ChiSq. = 0.100000E+01

Parameters: Mean	Uncertainties: SD
$A = -0.9058710381473E+00$	$SIGMAA = 0.7052554325200E-01$
$B = 0.1562496859152E+00$	$SIGMAB = 0.4919564971019E-02$
$C = 0.4482153350530E-01$	$SIGMAC = 0.3005032237401E-03$

Calibration Curve for Thread #7

REFERENCES

- [1] Bolt Science Limited, (boltscience.com), 15 Isleworth Drive, Chorley, Lancashire, PR7 2PU, UK, 2005.
- [2] Probert Encyclopedia, (probertencyclopaedia.com), The Probert Encyclopedia, 87 Cheiriton Avenue, Southampton, Hampshire, SO18 5HN, UK, 2005.
- [3] "Thread Inspection," Power Point Presentation, Johnson Gage Company, 2005.
- [4] ANSI/ASME B1.13M 1983 Metric Screw Threads – M Profile Specification, 1983.
- [5] Speck, J., A., Mechanical Fastening, Joining, and Assembly, Marcel Dekker, New York, 1997.
- [6] "Private communication," Karl Kleinhardt, General Motors Fastener Engineer, Warren, MI, 2004.
- [7] "2 Vital Signs 2002," (worldwatch.org), Worldwatch Institute, 1776 Massachusetts Avenue, N.W., Washington, D.C., 2005.
- [8] Blendulf, B., "The Fundamentals of Fastening Technology and Bolted Joint Design," Seminar, Delphi, Dayton, OH, 2002
- [9] Sopwith, D. G., "The Distribution of Load in Screw Threads," Proc. of the Institution of Mechanical Engineers, Vol. 159, 373-383, 1948
- [10] Goodier, J. N., "The Distribution of Load on the Threads of Screws," Journal of Applied Mechanics, Vol. 62, A10-A16, 1940.
- [11] Yamamoto, A., "The Theory and Computation of Thread Connection," Youkendo, 39-54, 1980.
- [12] Kenny, B. and Patterson, E. A., "Stress Analysis of Some Nut-Bolt Connections with Modifications to the Nut Thread Form," Proc. of the Institute of Mechanical Engineers, 35-41, 1983.
- [13] D' Eramo, M. and Cappa, P., "An Experimental Validation of Load Distribution in Screw Threads," Experimental Mechanics, 70-75, 1991.

- [14] Englund, R. B., Johnson, D. H., and Sweeney, S. K., "Issues and Case Studies," *Journal of Mechanical Engineering Design Education*, Vol. 102, 73-79, 1999.
- [15] Chen, J. and Shih, Y., "A study of the Helical Effect on the Thread Connection by Three Dimensional Finite Element Analysis," *Nuclear Engineering and Design*, Vol. 191, 109-116, 1999.
- [16] Rabinowicz, E., Friction and Wear of Materials, 2nd Edition, John Wiley, New York, 1995.
- [17] Bhushan, B., Introduction to Tribology, John Wiley, New York, 2002.
- [18] Persson, B. N. J., Albohr, O., Mancosu, F., Peveri, V., Samoilov, V. N., and Sivegack, I. M., "On the Nature of the Static Friction, Kinetic Friction, and Creep," *Wear*, Vol. 254, 835-851, 2003.
- [19] Shi, Xi, Polycarpou and Andreas, A., "A Dynamic Friction Model for Un-lubricated Rough Planar Surfaces," *Transactions of the ASME*, Vol. 125, 788-796, 2003.
- [20] Rabinowicz, E., "The Nature of the Static and Kinetic Coefficients of Friction," *Journal of Applied Physics*, Vol. 22, 1,373-79, 1951.
- [21] Golubev, G. A. and Smirnov, V.A., "Calculation of the Effective Friction Radius on the Bearing Surface of a Nut," *Journal of Soviet Engineering Research*, Vol. 66, Issue 2, 14-17, 1986.
- [22] Fukuoka, T. and Takaki, T., "Mechanical Behaviors of Bolted Joint During Tightening using Torque Control," *JSME International Journal*, Ser. A, Vol. 41, 185-191, 1998.
- [23] Bickford, J. H., An Introduction to the Design and Behavior of Bolted Joints, 3rd Edition, (Revised and Expanded), New York, Marcel and Dekker, 1995.
- [24] Shoberg, R. S., "Mechanical Testing of Threaded Fasteners and Bolted Joints", R. S. Technology Seminar, Farmington Hills, MI, 2000.
- [25] Shigley, J. E., Mitchell, L. D., and Budynas, R. G., Mechanical Engineering Design, 7th Edition, McGraw-Hill, New York, 2004.
- [26] VDI 2230 Part 1, Systematic Calculation of High Duty Bolted Joint, Joints with One Cylindrical Bolt, Germany, August 1988.
- [27] DIN946 German Standards (CIN-Normen), Determination of Coefficient of Friction of Bolt/Nut Assemblies Under Specified Conditions, October 1991

R702032137

HECKMAN

BINDERY, INC

T 022382 F 14 00



1/5/2006

- [28] ISO16047, Fastener – Torque/Clamp Force Testing, ISO, Geneva, Switzerland, November, 2000.